Developmental and functional characteristics of hypothalamic Lhx6-positive neurons

By

Kai Liu

A dissertation submitted to Johns Hopkins University in conformity with the requirements for the degree of Doctor of Philosophy

Baltimore, Maryland

February, 2017

Abstract

My thesis has identified a subpopulation of inhibitory GABAergic neurons in the dorsolateral hypothalamus and zona incerta that express the LIM homeodomain transcription factor Lhx6, that are found in close proximity to wake-promoting hypocretin-expressing of the lateral hypothalamus (LH), which selectively degenerate in narcolepsy. Lhx6 is a master regulator of the development of GABAergic interneurons in telencephalic structures such as the cortex and hippocampus, but its function in the hypothalamus is unknown. Over the past several years, we have investigated the development and function of these neurons, and have found hypothalamic Lhx6-expressing neurons do not migrate but require Lhx6 for their survival, and are activated by sleep pressure, directly inhibit wake-active hypocretin cells in the LH. Conditional deletion of Lhx6 from the developing diencephalon leads to decreases in both NREM and REM sleep. Furthermore, selective activation and inhibition of Lhx6-positive zona incerta (ZI) neurons acutely and bidirectionally regulates sleep duration in adult animals. These studies identify a novel GABAergic subpopulation of ZI neurons that play a central role in promoting sleep.

Thesis advisor: Seth Blackshaw, Ph.D.

Thesis Committee:

Paul Fuchs, Ph.D. (Chair)

Jeremy Nathans, Ph.D.

Samer Hattar, Ph.D.

Marshall Shuler, Ph.D.

Acknowledgement

First, I would like to thank my thesis advisor Seth Blackshaw for his guidance, encouragement and tremendous support throughout my six years as his graduate student. With a physics and engineer background, I started my PhD education with limited knowledge about the biological system. Seth introduced me to the neuroscience field and helped me develop a critical mind for research. As a scientist, Seth is full of passion and curiosity, with vast knowledge and critical eyes. As my advisor, he is always open-minded, proposed great ideas and encouraged me to try new directions and novel techniques. At the beginning, I started my PhD thesis project from scratch and had a lot of hard times. With Seth's strong support, I was able to combine my multi-disciplinary background to explore many directions and finally made important scientific discoveries. Thank you, Seth, for giving me an invaluable PhD training and for being an influential advisor of my career and life.

I would like to thank my thesis committee members – Paul Fuchs, Jeremy Nathans, Samer Hattar and Marshall Shuler for giving me invaluable advice. I was learning a lot from you every time when we had a discussion during thesis committee meetings or personal communications. I would like to thank all my great collaborators, especially Samer Hattar, Solange Brown, Juan Song, Stephanie Zhang, Juhyun Kim, Dong Won Kim, Hechen Bao, for your devotion and indispensable contribution to our work. Vassilis Pachinis and Daniel Lee gave great suggestions on my manuscript. In addition I hope to thank the professors in our program for their dedicated education on students, especially King-Wai Yau for giving me great advice on my career. I was also

very lucky to be among a collaborative and supportive environment of Blackshaw lab, and I would like to thank all my colleagues in the lab and the Department of Neuroscience to share the passion of research.

Finally, I would love to thank my family – my parents, my wife and my parents-in-law, for their endless support and love.

Table of Contents

List of Figures

List of Abbreviations

DMH	dorsal medial hypothalamus
DR	dorsal raphe
Drd2	Dopamine Receptor D2
DREADDs	Designer Receptors Exclusively Activated by Designer Drugs
EEG	Electroencephalogram
EMG	Electromyography
GABA	gamma-Aminobutyric acid
HCRT	Hypocretin
LH	Lateral hypothalamus
Lhx6	LIM Homeodomain transcriptional factor 6
Nxph1	Neurexophilin1
PENK	Proenkephalin
PH	posterior hypothalamus
REM	rapid eye movement
SN	Substantia nigra

vlPAG	ventral lateral periaqueductal gray
VTA	Ventral tegmental area
ZI	Zona Incerta
ZT	Zeitgeiber Time

Background

1. Developmental characteristics of Lhx6 in telencephalon and diencephalon

The research focus in my thesis is about the developmental and functional characteristics of hypothalamic Lhx6 neurons. I will start of introducing this specific marker, Lhx6, a transcription factor with its known functions in the brain.

1.1 Lhx6 in telencephalon

LIM domains, which are now recognized as mediating selective protein-protein interaction, are known to be key components of the regulatory machinery in the cell [1]. There are approximately 55 amino acids with 8 highly conserved residues , mostly cysteine and histidine, comprising of individual LIM domains. Recent analysis of LIM domains from many different species, including human beings, has identified a slightly broader consensus sequence than the classical LIM consensus sequence, orginally defined as CX2CX16–23HX2CX2CX2CX16–21CX2(C/H/D) (where X denotes any amino acid) [2] (Figure 1.1.1 a) [3]. The LIM domain contains two zinc ions,which are bound by the eight most highly conserved residues are the zinc-binding residues. Residues 1–4 coordinate with the first zinc ion, and residues 5–8 coordinate the second zinc ion, which establishes the tandem zinc-finger topology [4] illustrated in Figure. 1.1.1 b. LIM domains are present in many proteins that have diverse cellular roles as regulators of gene expression, cytoarchitecture, cell adhesion, cell motility and signal transduction. The LIM homeodomain family of transcription factors has been reported to be involved

in many neuronal processes during brain development, including cell fate specification, neuronal migration and connectivity [3,5].

Lhx6, a LIM homeodomain factor originally termed Lhx6.1 (Figure 1.1.2), was found in several restricted regions in the developing CNS, mostly within the embryonic telencephalon [6] and diencephalon. Acting in part through LIM domain-medidated its protein-protein interaction function, Lhx6 may have a critical role in controlling cell differentiation and cell fate during development.

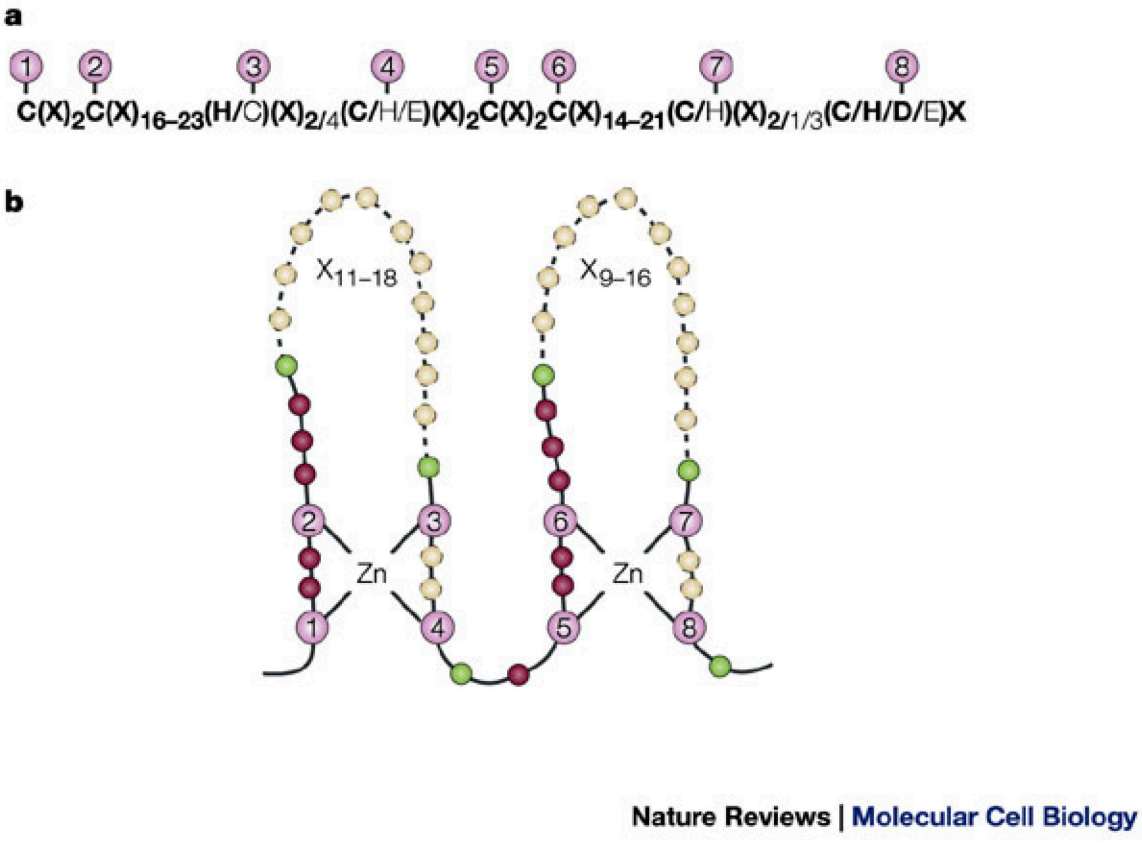

Figure B1.1.1 The sequence and topology of the LIM domain (a) analysis of 135 human LIM sequences showed eight zinc-binding residues (1–8) (b) zinc coordination. The zinc-binding residues are shown as purple circles. The green spheres indicate semi-conserved aliphatic/bulky residues. The magenta spheres represent Non-conserved residues with invariant spacing. A variable number of residues are shown by dashed yellow circles.[3]

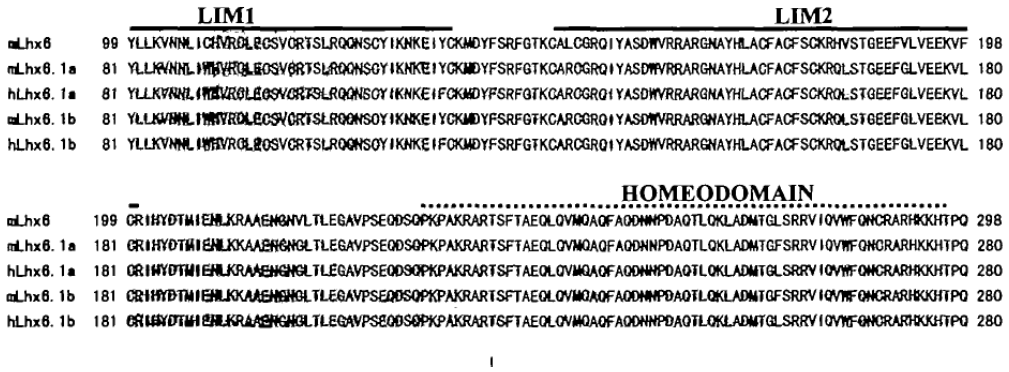

Figure B1.1.2 Human Lhx6.1, and mouse Lhx6 with multiple amino acid sequence alignment. There is difference between deduced amino acid sequences of mouse (m) and human (h) Lhx6.1. Solid lines indicate two LIM domains. The homeodomain is represented by dashed line. [6]

1.2 Lhx6 is required for the survival, migration and differentiation of GABAergic interneurons in the cerebral cortex

Thus far, most studies of Lhx6 function have focused on its role in migration and differentiation of cortical GABAergic interneurons. In rodents, inhibitory GABAergic interneurons, which constitute 20~30% of cortical neurons, are an extremely heterogeneous cell population, which are composed of multiple subtypes that are broadly distributed, and which display different morphologies, electrophysiolological and molecular properties [7, 8, 9, 10]. In contrast to pyramidal neurons, which are born in the dorsal telencephalon, the majority of cortical GABAergic interneurons originate in the medial ganglionic eminence (MGE) and caudal ganglionic eminence (CGE) of the ventral forebrain, are generated between embryonic day 12.5 (E12.5) and birth, and reach the cortex by tangential migration [11,12, 13, 14, 15, 16,17,18, 19, 20]. The homeodomain transcription factors, Nkx2.1 and Lhx6 are known to play essential roles in intitiating the cascades of gene expression that are required for MGE-derived cortical

interneuron development [21, 22, 23]. In addition, Nkx2.1 is a gene with both activator and repressor function. By means of its repressor function, it can attenuate the expression of CGE-specific genes, while its activator function induces the expression of Lhx6 [24]. During cortical development, Lhx6 transcripts were detected in the subventricular and mantle zones of the MGE , while a small number of Lhx6-expressing cells were also found in the LGE, and represent the tangentially migrating population of cortical interneurons (Figure 1.2.1) [25].

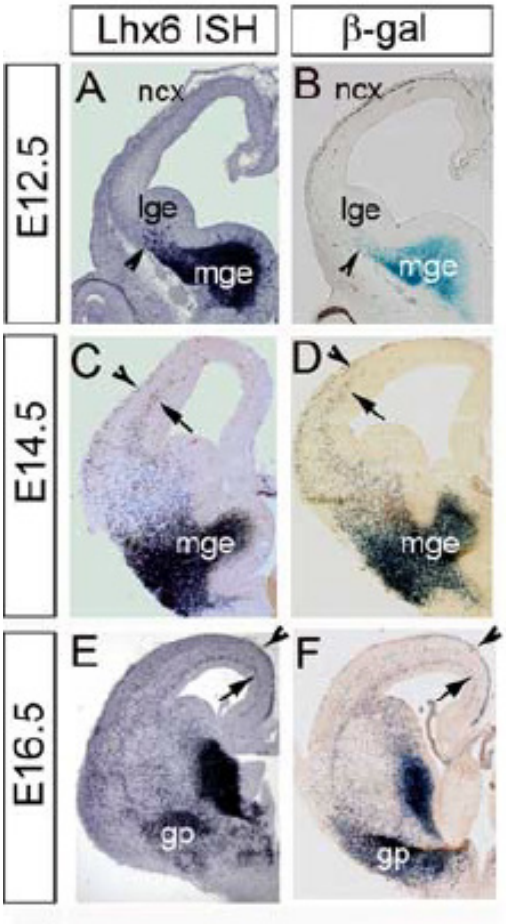

Figure B1.2.1 Expression of the Lhx6/LacZins allele recapitulates the pattern of expression of the wild-type Lhx6 locus. Coronal sections from the forebrain of E12.5 (A, B), E14.5 (C, D), and E16.5 (E, F) [25].

Cortical interneurons derived from MGE can be identified based on the expression of calcium-binding proteins parvalbumin (Pv), calbindin(Cb), calretinin(Cr) or the neuropeptide somatostatin (Sst) [26, 27, 28]. Nkx2.1 activates Lhx6, which in turn drives the expression of a series of factors including Sox6 and Satb1 whose actions selectively affect the development of both Pv- and Sst-expressing interneurons [29, 30].

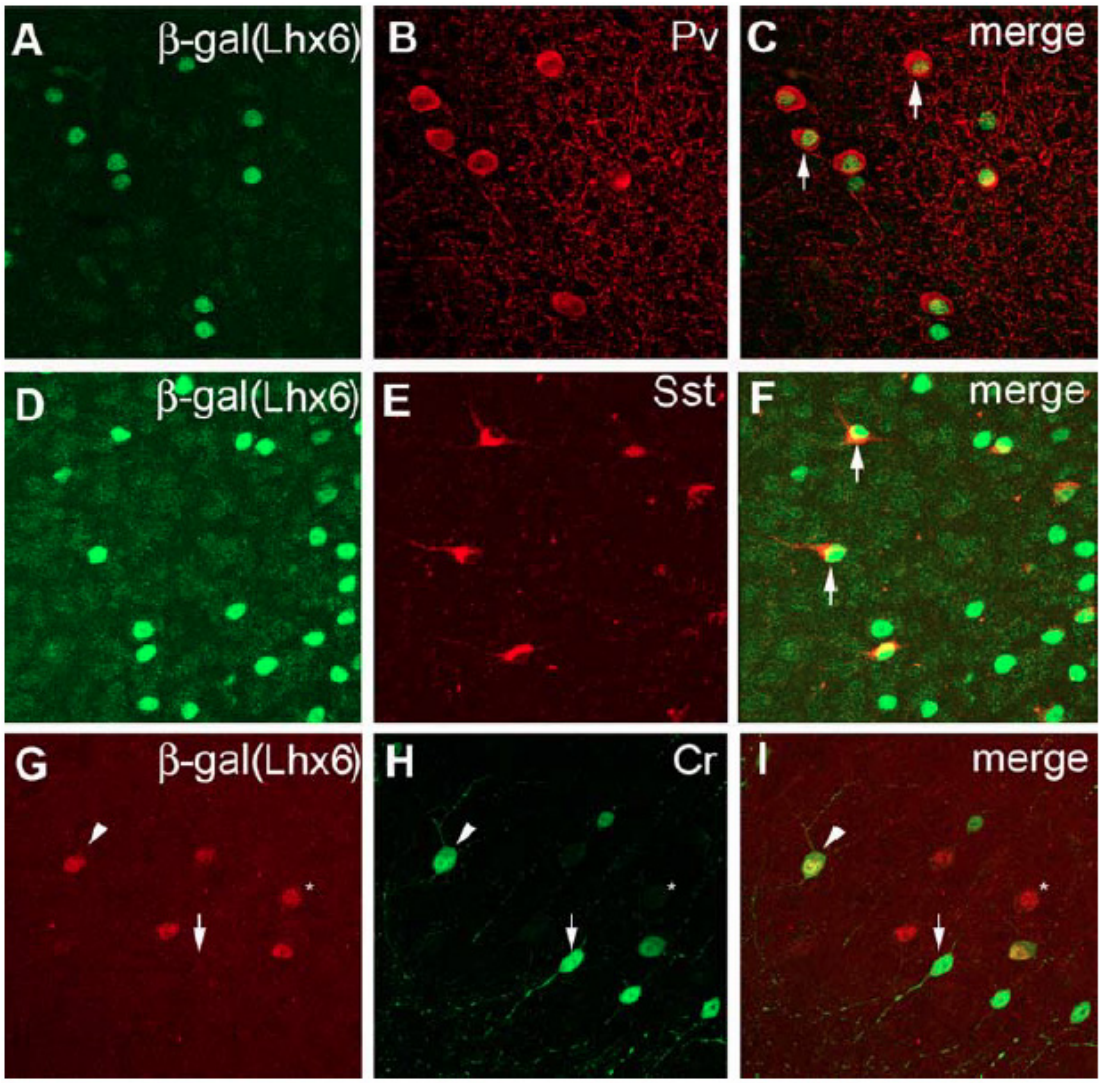

Figure B1.2.2 Lhx6 is expressed in the majority of Pv+ and Sst+ cortical interneurons. Confocal microscope images of cortical sections from Lhx6+/LacZins animals double immunostained for beta-gal and either Pv (A–C), or Sst (D–F), or Cr (G–I). As is evident from the merged images, virtually all Pv- and Sst-expressing interneurons

coexpress beta-gal (C, F, arrows) but was generally excluded from neurons of bipolar morphology that expressed high levels of Cr (G–I, arrows)[25].

Lhx6 is preferentially expressed in mature Pv+ and Sst+ cortical interneurons [25] (Figure 1.2.2). Functionally, Lhx6 mutants exhibit many phenotypes, including severe reduction of the number of Sst+ and Pv+ cortical interneurons, slowed or even failed tangential migration, and abnormal neocortical laminar position of interneurons [31, 32].

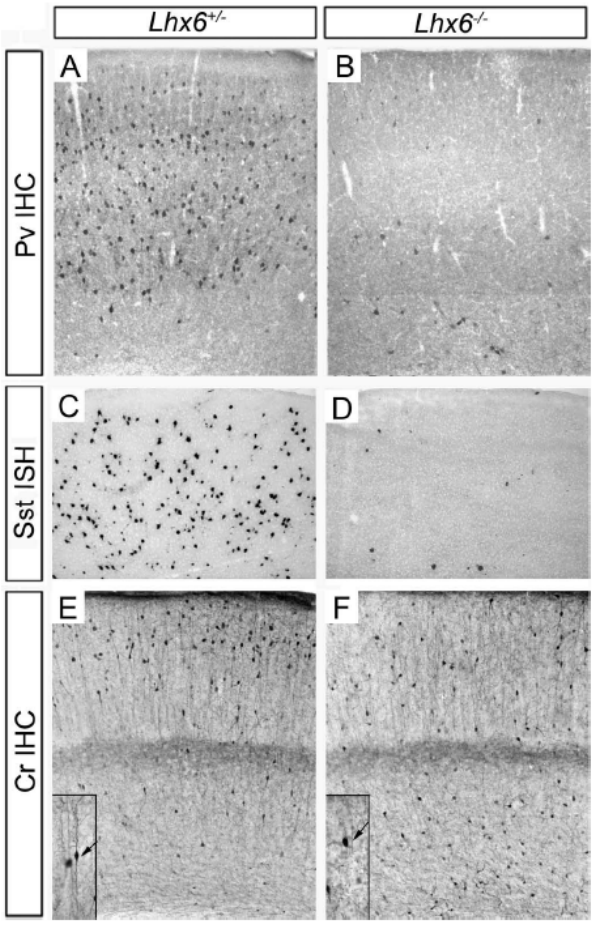

*Figure B1.2.3 Lhx6 knockout leads to dramatic reduction in the number of Pv- and Sst-expressing interneurons in the neocortex. Sections from the neocortex of 2-week-old animals heterozygous (**A**, **C**, **E**) or homozygous (**B**, **D**, **F**) for Lhx6 deletion were showed for Pv (**A**, **B**) or Cr (**E**, **F**) immunostaining or hybridized with an Sst-specific riboprobe (**C**, **D**). [25]*

Lhx6 is required for the specification of Pv+ and Sst+ cortical interneurons, while severe reduction in the number of Pv+ and Sst+ expressing interneurons was observed in Lhx6 null cortex (Figure 1.2.3). However, the effects are not only restricted to Pv+ and Sst+ cortical interneurons. Furthermore, Lhx6 deletion leaded to abnormal tangential migration of the great majority of cortical GABAergic interneurons (Figure 1.2.4) [25].

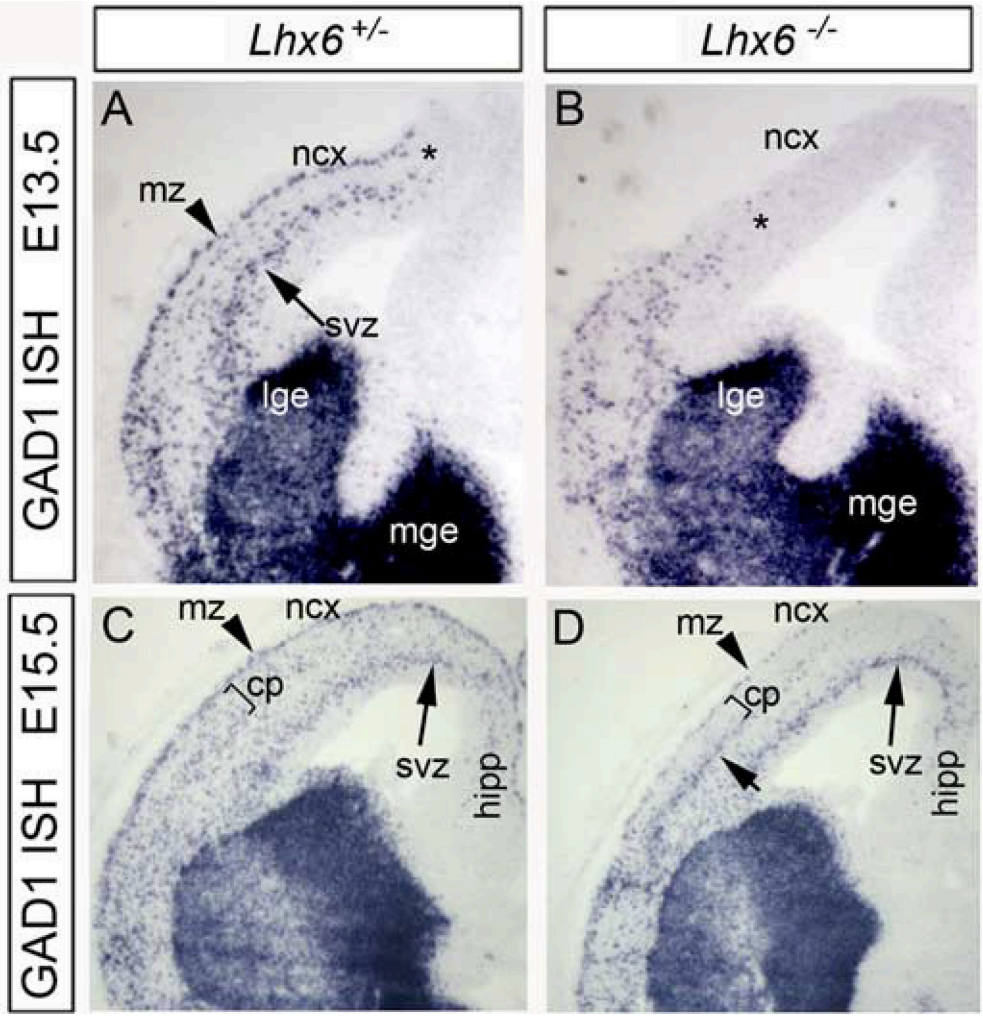

Figure B1.2.4 Lhx6 mutant embryos showed delayed tangential migration and abnormal distribution of GABAergic interneurons in the cortex. A–D, In situ hybridization of coronal brain sections from E13.5 (A, B) and E15.5 (C, D) embryos compared heterozygous controls (A, C) with homozygous (B, D) the Lhx6 straight knockouts.

Compared to controls, GAD67+ cells were restricted to the most ventrolateral region of E13.5 mutant cortex. [25]

At E13.5, a large number of GABAergic cells were observed in the MGE and LGE (Figure 1.2.4 A control). Tangentially migrating GAB67+ cells were located in a substantially more ventrolateral position in the E13.5 Lhx6 mutant cortex (Figure 1.2.4 B mutant). At a later stage, E15.5, although most of GAB67+ cells were present in the lower intermediate and subventricular zones (IZ/SVZ), many remaining cells were found in the subplate of the lateral cortex, with the MZ and the cortical plate containing very few GAD67+ neurons (Figure 1.2.4 D).

These data demonstrate the importance of Lhx6 in the development of cortical interneurons. However, Lhx6 is not required for the survival of the cortical interneurons, despitet the fact that they failed to migrate to the correct cortical laminar positions [25, 31, 32]. In contrast to the role of Lhx6 in cortex and other telencephalic regions, Lhx6 is required for the survival of Lhx6 neurons in hypothalamus, which will be discussed in Chapter 2.

1.3 Lhx6 in the developing hypothalamus

The vertebrate hypothalamus is known as a central homeostatic regulator of innate behaviors within the neuroendocrine system with physiological processes that are essential for survival. A number of transcription factors have been identified previously as markers that regulate the development of specific hypothalamic nuclei and neuronal subtypes [33,34,35,36,37,38,39]. However, we still lack extensive knowledge of the genes that control hypothalamic development. In 2010, our lab has published a paper

entitled "A genomic atlas of mouse hypothalamic development ", in Nature Neuroscience [40]. In this paper our lab identified hypothalamic markers that labeled each major developing hypothalamic nucleus, and generated in situ hybridization for 1,045 genes through the entire course of hypothalamic neurogenesis. Based on these *in situ* results, our lab constructed a detailed molecular atlas for the developing hypothalamus from which the hypothalamus developing stages can be characterized by various groups of gene populations. Among all the genes identified in our lab work, Lhx family genes were found to delineate discrete regions of the developing hypothalamus. Two-color ISH with Lhx6 and the inhibitory interneuron marker Gad67 was conducted to characterize the cell types of the intrahypothalamic diagonal and tuberomamillary terminal. As will be shown in the Results (Chapter 1), Lhx6 and Gad67 expression fully overlapped at all stages of hypothalamic development. Other Lhx family members including Lhx9, Lhx8, Lhx1 were also expressed in distinct domains in the intrahypothalamic diagonal (Figure 1.3.1) [40]. Lhx9 was found to be expressed immediately ventral to the Lhx6-positive zone of the intrahypothalamic diagonal (Figure 1.3.1a), and it has been reported that Lhx9 colocalizes with hypocretin (Hcrt) and is both necessary and sufficient to specify Hcrt-expressing neurons in the developing mouse and zebrafish hypothalamus (Figure 1.3.1 c,f,i)[41, 42]. Lhx8 was expressed immediately anterior to the Lhx6-positive region of the intrahypothalamic diagonal (Figure 1.3.1 d), while anterodorsal to Lhx9 at E12.5 (Figure 1.3.1g). The relative positions of each gene expression domain were maintained, even at E16.5 (Figure 1.3.1h). In adult, Lhx8 is expressed in dorsal medial hypothalamus, a region that has been reported to be important for feeding-dependent entrainment of circadian rhythms. Lhx1, which regulates terminal differentiation and circadian function

of the suprachiasmatic nucleus [43, 44], was coexpressed with Lhx8 at E12.5, but at later stages was expressed in a more posterior, non-overlapping region (Figure 1.3.1h).

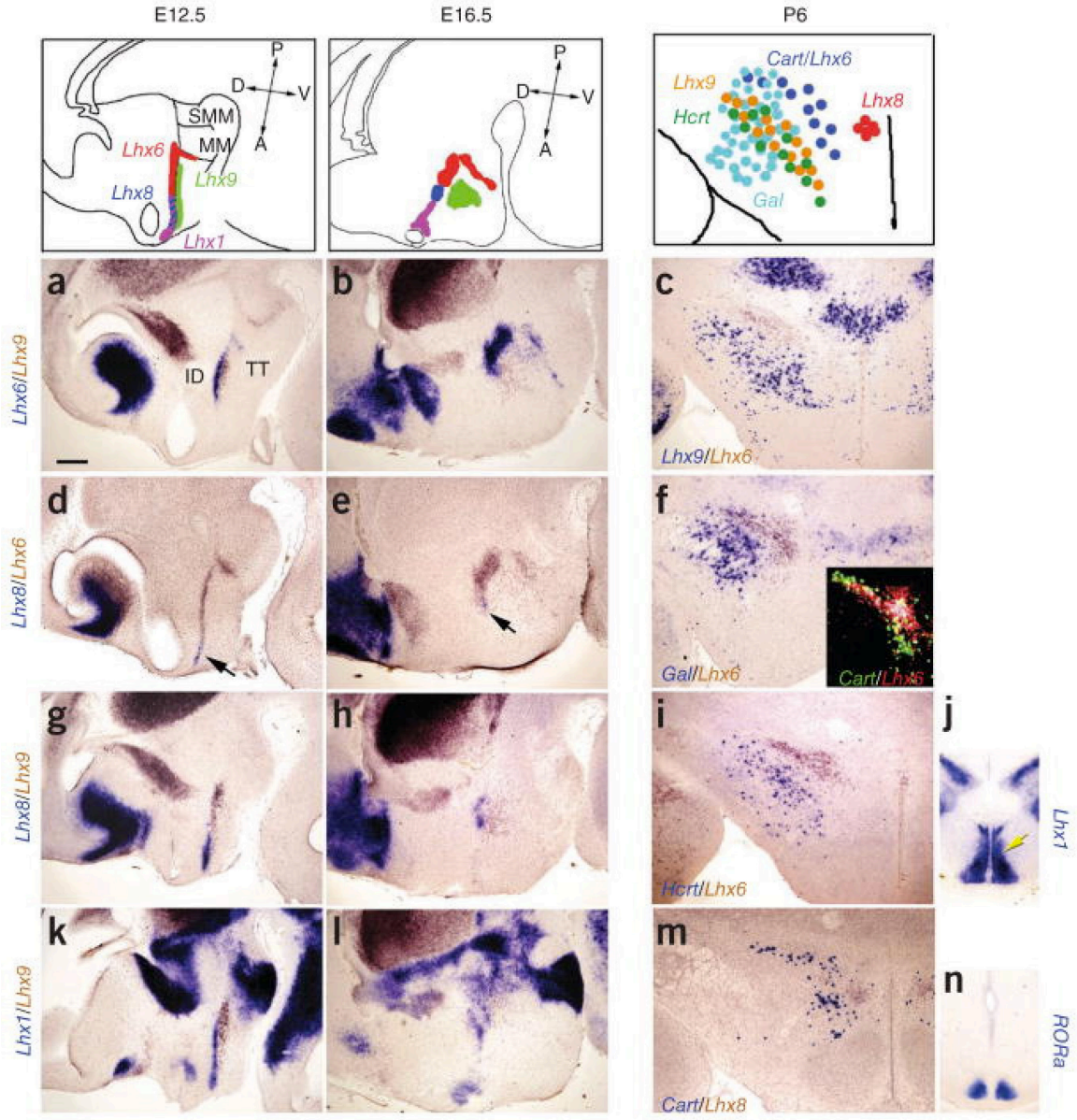

Figure B1.3.1 Lhx family members delineate various regions of the developing hypothalamus and some of the markers coexpressed with Lhx family genes. Lhx gene expression patterns weres showed schematically at E12.5 and E16.5. (a,b) Lhx6 (blue) and Lhx9 expression (brown) were expressed in the posterior portion of the intrahypothalamic diagonal (a), which pattern was preserved at E16.5 (b). (d,e) Lhx8 (blue) was found to be expressed anterior to the Lhx6-positive region (brown). (g,h) Lhx8 (blue) expression was anterior and dorsal to Lhx9 expression (brown). (k,l) relative Lhx1

(blue) expression region was anterior to Lhx9 and Lhx6 (brown), but overlapped with Lhx8. (c,f,i,m) Lhx6 overlapped with Cart. A conserved spatial relationship between Lhx9 (purple) and Lhx6 (brown) was shown in lateral hypothalamus at P6. Lhx6-positive cells (brown) were found medial and dorsal to galanin (Gal)-positive neurons (purple) partically coexpress with Lhx9 (f). Lhx6-positive cells (brown) were found medial and dorsal to hypocretin (Hcrt)-positive neurons (blue) partically coexpress with Lhx9 (i). In dorsomedial hypothalamic nucleus Lhx8 (brown) was expressed medial to Cart (blue) (m). Lhx1 expression corresponded to the Rorα-positive SCN at E16.5 is located at the anterior terminus of the zone. Scale bar represents 0.2 mm (a, b, d, e, g, h, k and l) and 0.3 mm (c, f, i, j, m and n). [40]

These studies show that expression of Lhx family genes delinate a series of hypothalamic nuclei which reside both between and lateral to the paraventricular nucleus and VMH.

In summary, Lhx6, a LIM homeodomain transcriptional factor family gene, is known to play a central role in various aspects of forebrain development, including tangential migration and differentiation of cortical GABAergic interneurons. During embryonic development, multiple Lhx family genes are expressed in continuous zone within the hypothalamus. In hypothalamus, however, the function of Lhx6 is uncharacterized. Identifying the function of Lhx6 in hypothalamus, and comparing this to its known function in cortical development, is a topic of considerable potential interest.

2. Sleep/Wake cycle regulators in the hypothalamus and other brain regions

A major focus of my thesis work it characterizing the behavioral functions of hypothalamic Lhx6-positive neurons. The hypothalamus is a key regulator of physiological homeostasis, including, but not limited to, regulating innate behaviors such as sleep, food intake, thermal regulation, and emotion. Discrete hypothalamic nuclei control different behaviors. An analysis of behavioral states that induce activity of

hypothalamic Lhx6 neurons was conducted as a part of my thesis research, and we found that hypothalamic Lhx6 neurons are differentially activated during the sleep/wake cycle. In order to to better detail the function of Lhx6-expressing neurons in the hypothalamus, I will introduce some background about neural circuitry that regulates the sleep/wake cycles.

2.1 sleep/wake states switching networks

Sleep is an innate behavior shared by virtually all animals, and is regulated by a complex and distributed network of sleep-promoting and wake-promoting neuronal subtypes [45]. Sleep/wake cycles can be roughly classified into three stages: wakefullness, rapid eye movement (REM) sleep and non-REM sleep, which can be clearly distinguished in rodents and human beings using electroencephalogram (EEG) and electromyogram (EMG) recordings. During non-REM sleep, the EEG exhibits a low-frequency (0.5~4Hz) and high amplitude activity, while EMG activity is low. On the other hand, REM sleep, which is the period during which vivid dreaming occurs, is characterized by high-frequency and low amplitude EEG activity, along with a complete paralysis of postural muscles without detectable EMG activity [46]. In contrast, the wakefulness stage is dominated by a high-frequency and low amplitude EEG activity as well as a high muscle tone as measured by EMG. Transition between sleep/wake states are associated with major changes in multiple physiological processes, including eye closure, breathing, arousability and muscle tone. The transition from wakefulness stage to non-REM sleep can take place over a few seconds or less in rodents, but may take anywhere from 10-60 seconds human beings [47,48]. Once non-REM sleep is initiated,

it is typically mantained from three to five minutes in rodents, while in human beings it might last between 40 mins and 1 hour. At the end of this bout, EEG activity begins to make another transition from non-REM sleep to REM sleep, a process which takes only a few seconds. During REM sleep, there is a complete loss of muscle tone, except muscle activity for breathing and rapid eye movements. An individual might switch back and forth between non-REM and REM sleep with occasional transitions to wakefullness during sleep time. As a result, sleep-wake transitions are rapid and bistable [49], regulated by mutual interactions between sleep-promoting and wake-promoting neurons (Figure 2.1.1). Cholinergic neurons located in the pedunculopontine and laterodorsal tegmental nuclei (PPT and LDT) at brainstem provide the main input from the mesopontine junction to the thalamus while monoaminergic and glutamatergic neurons within the same region send direct innervation to the hypothalamus, basal forebrain and cerebral cortex [50, 51] (Figure 2.1.1 a). Many neurons in the PPT and LDT are wake-promoting since they are usually active during wakefulness and REM sleep [52, 53], suggesting they can promote cortical activation. Orexin/hypocretin neurons in the lateral hypothalamus help boost this arousal pathway, and these neurons also send direct excitatory projections to the thalamus and cortex. A population of neurons in the ventrolateral and median peroptic nucleus (VLPO, MnPO) , containing

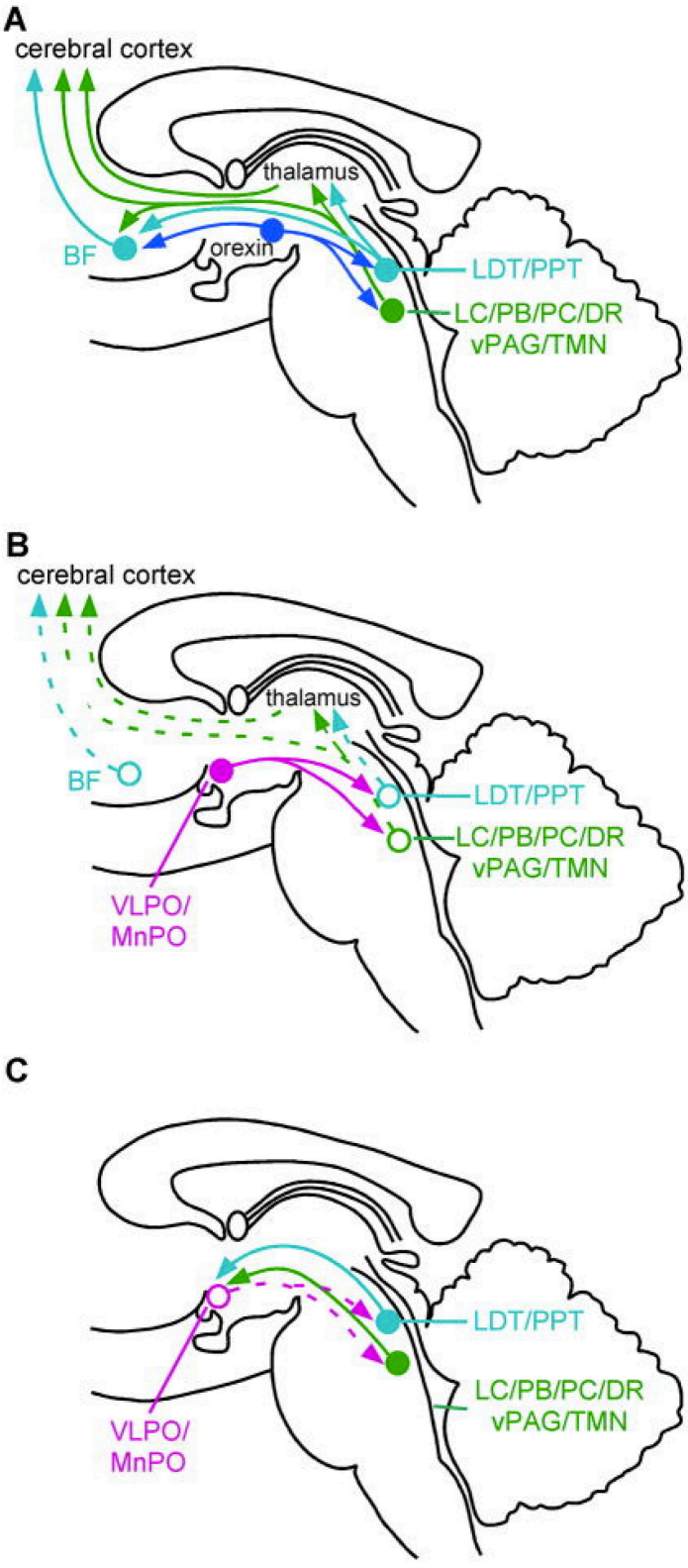
A
cerebral cortex
thalamus
BF
orexin
LDT/PPT
LC/PB/PC/DR
vPAG/TMN
B
cerebral cortex
thalamus
BF
LDT/PPT
LC/PB/PC/DR
vPAG/TMN
VLPO/
MnPO
C
LDT/PPT
LC/PB/PC/DR
vPAG/TMN
VLPO/
MnPO

Figure B2.1.1 sleep-wake transitions. (a) wake-promoting pathways from brainstem to hypothalamus, basal forebrain, thalamus and cerebral cortex. (b) sleep-promoting VLPO and MnPO inhibit components of arousal pathways from brainstem. (c) the ascending arousal systems can also inhibit VLPO. Abbreviations: DR, dorsal raphe nucleus (serotonin); LC, locus coeruleus (norepinephrine); LDT, laterodorsal tegmental nucleus (acetylcholine); PB, parabrachial nucleus (glutamate); PC, precoeruleus area (glutamate); PPT, pedunculopontine tegmental nucleus (acetylcholine); TMN, tuberomammillary nucleus (histamine); vPAG, ventral periaqueductal gray (dopamine).

the inhibitory neurotransmitters GABA and galanin, have been identified as sleep-promoting neurons that inhibit the components of the ascending arousal pathways in both hypothalamus and brainstem [54, 55] (Figure 2.1.1 b). Sleep-active neurons in VLPO also receives mutual inhibition from arousal-promoting neuronal subpopulations, including the histamine neurons in the tuberomammillary nucleus (TMN), dorsal raphe nucleus and ventral periaqueductal gray matter (vlPAG), parabrachial nuclues and LC [56, 57] (Figure 2.1.1 c). In short, this mutual inhibitory relationship between the arousal- and sleep-promoting systems can lead to rapid and complete transitions between waking and sleeping states by providing "flip-flop" switch conditions. This "flip-flop" term comes from electrical engineering which tried to explain the sharp transitions between two mutually opposed states [58]. However, this switch is stablized by hypocretin/orexin neurons in the lateral hypothalamus [59]. Activation of hypocretin/orexin neurons can trigger an animal to rapidly switch from sleep to wakefulness, and loss of orexins neurons or orexin neuropeptide leads to narcolepsy or cataplexy in both humans and other mammalian species [60, 61]. However, the activity of these hypocretin/orexin neurons are also under the control of local GABAergic transmission [59].

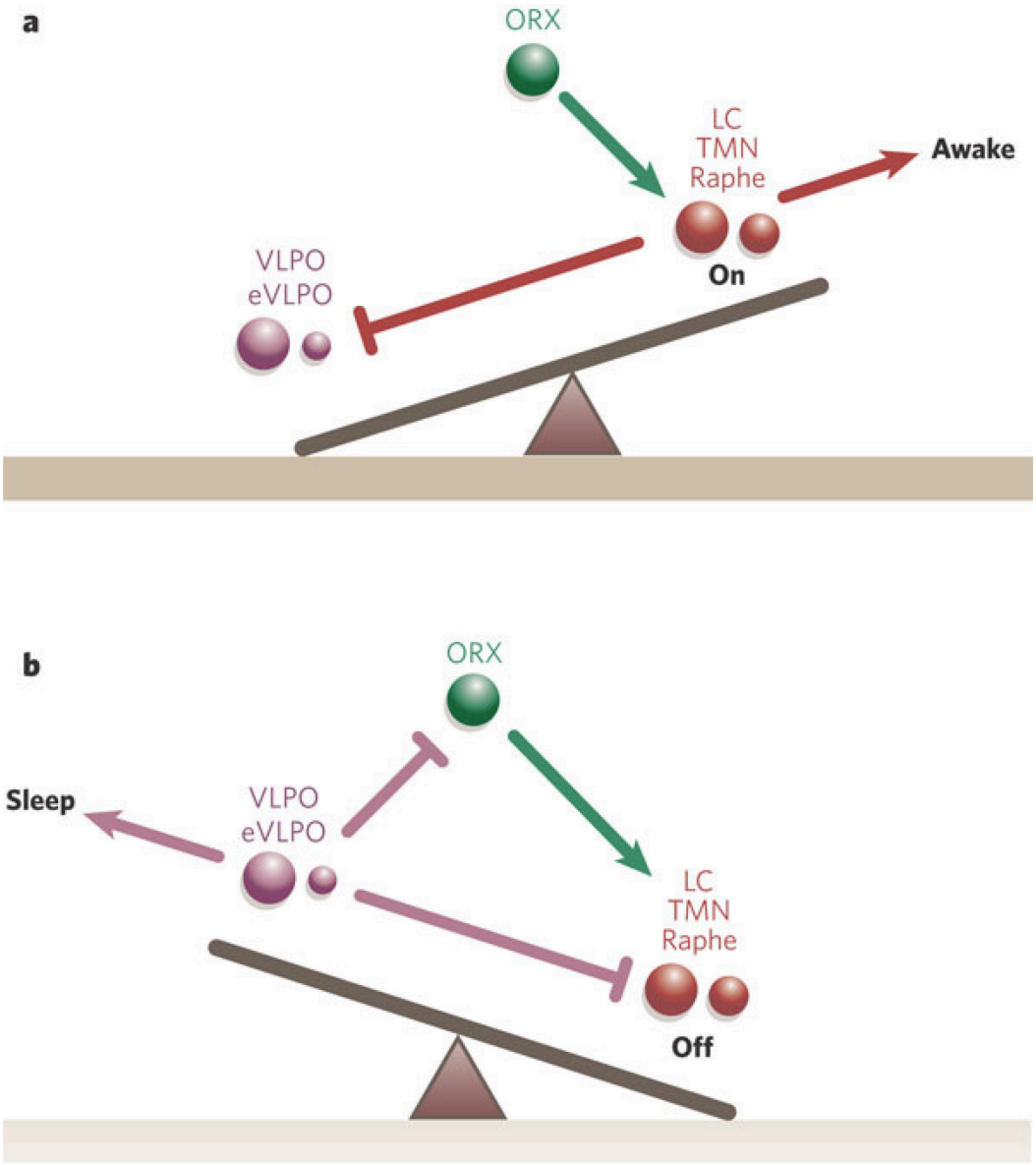

Figure B2.1.2 a flip-flop model for sleep-wake switching. (a) during wakefullness, the wake-promoting monoaminergic nuclei inhibits sleep-promoting ventrolateral peoptic nucleus (VLPO) with reinforcement from hypocretin/orexin neurons in lateral hypothalamus. (b) during sleep, VLPO is inhibiting hypocretin/orexin neurons for stablizing the inhibition to monoaminergic nuclei which results in a stable and sharp transitions between sleep and wake states [59].

2.2 Stabilization of sleep homeostasis in lateral hypothalamus.

As described in previous section, hypocretin peptides are produced exclusively by a group of large neurons in the lateral hypothalamus [62, 63, 64]. The lateral hypothalamus (LH) plays a central role in control of sleep-wake cycles and contains several subtypes of wake-promoting neurons, the best characterized of which are glutamatergic hypocretin (Hcrt)-expressing neurons [65, 66]. Although several inhibitory neuronal subtypes have been found to be presynaptic to Hcrt neurons [67, 68], their physiological role in modifying Hcrt–dependent regulation of sleep remain unclear (Figure 2.2.1) [69].

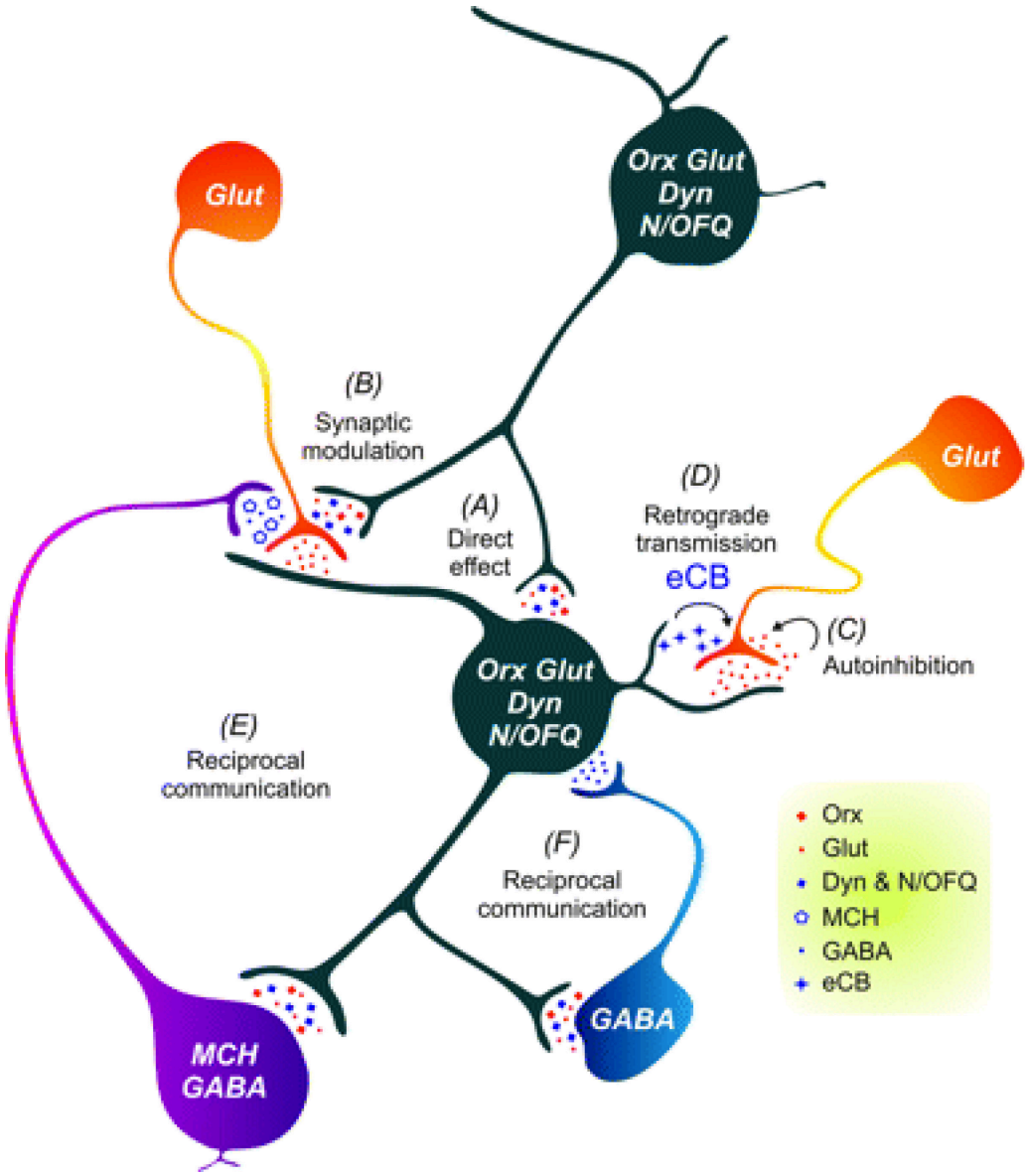

Figure B2.2.1 Local regulation on hypocretin/orexin neurons by other population of neurons.There are direct and indirect regulation by local transmitters on hcrt neurons, during which most of the inhibitory control comes from GABAergic neurons. [69]

Hypocretin released by Hcrt neurons activates Hcrt autoreceptors, and can increase presynaptic glutamate release [70, 71] (Figure 2.2.1 A, B). Reciprocal communications between hypocretin neurons and GABAergic neurons including melanin concentrating hormone (MCH) neurons are important for sleep/wake regulation, and promote both non-REM and REM sleep [72, 73, 74, 75] (Figure 2.2.1 E, F).

2.3 Functional characteristics of zona incerta

The Lhx6 neurons that are the focus of this study are located in both the LH and the zona incerta. The zona incerta (ZI), a highly heterogeneous structure located between the LH and the thalamic reticular nucleus, plays diverse roles in sensory-motor integration and sends efferent projections to multiple brain regions, including the cerebral cortex, central thalamus, LH and midbrain [76, 77]. Recent studies demonstrated that the ZI may regulate behavioral arousal through modulation of thalamocortical projections [78], and also modulate muscle paralysis seen during REM sleep [79]. Although the complete bilateral ablation of the ZI in rats does not affect sleep/wake cycles [80], the role of individual cell types within the ZI in controlling sleep is yet to be characterized. Lhx6 neurons express in the hypothalamus stretching from the ZI to posterior hypothalamus (PH) (see Chapter 1). This study will focus on the molecular and functional characterization of Lhx6-expressing neurons in ZI and, to a lesser extent, LH.

Methods

Animals.

All experimental animal procedures were approved by the Johns Hopkins University Institutional Animal Care and Use Committee. The BAC transgenic *Lhx6-eGFP* mouse line was generated as part of the GENSAT project [81], and obtained from MMRRC (Stock Number: 000246). *Hcrt-eGFP* transgenic mice were obtained from Luis de Lecea of Stanford University School of Medicine [82]. *Lhx6-Cre* mice were generously shared by Dr. Aryn Gittis of Carnegie Mellon University, and were originally generated by Dr. Nicoletta Kessaris of University College, London [83]. *Lhx6-CreER*^{T2} knock-in mice were generated by Z. Josh Huang of Cold Spring Harbor Laboratories were purchased from The Jackson Laboratory (Stock Number: 010776) [84]. *Foxd1-CreEGFP* knock-in mice [85] were obtained from Jackson Laboratories (Stock Number: 012463).

Lhx6$^{lox/lox}$ mice were obtained from Dr. Vassilis Pachnis from The Francis Crick Institute, London. The conditional *Lhx6* allele was generated via homologous recombination using a targeting construct in which loxP sites were placed in non-coding regions just 5' to coding exon 1b, and 3' to coding exon 3. The 5' homology is made up from a 3.1 kb *XbaI–Sac*I fragment containing the 5 upstream region and the first exon (1a) of *Lhx6*, whereas the 3' homology is made up from a 5.4 kb *ApaI–NheI* fragment. For the *Lhx6* targeting vector, the 2 kb genomic fragment between the homology regions is replaced by a 4 kb cassette, containing the following: (1) the 1b, 2 and 3 coding exons flanked by loxP sites (2) the neomycin resistance gene under the control of the

phosphoglycerate kinase (PGK) promoter (PGK-Neo) flanked by FRT sites. Targeting constructs were linearized and electroporated into E14Tg2A embryonic stem (ES) cells. Targeted clones were identified and analyzed in detail by Southern blotting using 5 and 3 external probes. Germline transmission of the mutant alleles was achieved using standard protocols. The phenotypic analysis presented was performed on animals from which the PGK-Neo cassette was removed by crossing founder conditional *Lhx6* animals with the *ACTB::FlPe* transgenic line [86]. For the maintenance of the *Lhx6* colony, we performed PCR using the following primers: Lhx6flR:GGAGGCCCAAAGTTAGAACC Lhx6flF:CTCGAGTGCTCCGTGTGTC.

Stereotaxic AAV injection and EEG/EMG implantation.

AAV vectors were obtained from vector cores of the University of Pennsylvania (AAV9.EF1a.flex.hChR2-eYFP) [87] and University of North Carolina (AAV9-EF1a.flex.hM3Dq-mCherry; AAV9-EF1a.flex.hM4Di-mCherry) [88]. For bilateral stereotaxic injection of AAV into the zona incerta, adult male mice (2~4 months old) were anaesthetized with ketamine/xylazine (100µl of 100mg/ml ketamine, 20mg/ml xylazine) and placed in a stereotaxic frame. The head skin was incised to expose the skull and gently scrape away connective tissue. After exposing the skull, bilateral craniotomies (~1 mm diameter each) were made to allow virus delivery (600-800nl at 40 nl/min). Stereotaxic coordinates: AP=-1.54mm, L=0.55mm, DV=-4.8mm, according to the reference atlas of Paxinos and Franklin [88]. Skin covering the boreholes was sutured closed following surgery.

For EEG/EMG recordings, four-channel tethered EEG/EMG biosensors (Pinnacle Technology Inc.) were anchored onto the mouse skull. The two front screws used for EEG1 signal recording were positioned at: AP: +2 mm, ML: ± 1.5 mm. The two back screws used for EEG2 signal recording were positioned at: AP: -4 mm, ML: ±] 1.5 mm). With the same implant, two EMG antenna electrodes were inserted into the left and right neck muscles. The EEG/EMG recording implant was secured to mount on the mouse skull with dental cement. In cases where EEG/EMG analysis of DREADD-injected mice was performed, this surgery was performed immediately following AAV injection.

Sleep recordings (EEG/EMG recording).

For all analysis of sleep behavior, after the mice were allowed a minimum of 10 days recovery in a 12-hour LD cycle following EEG/EMG biosensor implantation. We used the Pinnacle Technology EEG/EMG tethered recording system for sleep behavior evaluation. Implanted mice were tethered to a X100 preamplifier (Pinnacle Technology) and were housed in a 12-h dark/12-h light cycle (lights on between 7:00 (Zeitgeber time: ZT0) and 19:00 (ZT12) recording chamber. The mice were allowed 5~7 days to acclimatize to the recording chamber before recording. The EEG and EMG signals were preamplified ×5,000 and digitized at 14 bits, and then recorded. Signal acquisition was obtained using the Sirena acquisition suite (Pinnacle Technology Inc.) EEG/EMG traces were recorded for 48 hours for Lhx6 conditional knockout mice, and data from the second day extracted for analysis. For analysis of mice injected with AAV expressing flexed Gq and Gi-linked DREADDs, we used the virus-transfected animals with saline

injection as control compared to animals with Clozapine-N-oxide (CNO, Sigma-Aldrich; 0.5 mg/kg in saline) intraperitoneal (IP) injection. The following injection protocol was used for analysis of all animals injected with AAV expressing flexed DREADDs: on Day 1, we performed two consecutive saline injections at 12 hr intervals at ZT23 (6am) and ZT11 (6pm); on Day 2, we injected CNO at ZT23 and ZT11; alternatively, on Day 1, the saline was injected at ZT5 and ZT17, similar to the timing of the CNO injection on Day 2.

To validate the specificity and efficacy of AAV DREADD infection, following the termination of behavioral analysis, mice were given a single injection of CNO (0.5 mg/kg in saline) and sacrificed 1hr later by terminal anesthesia and transcardiac perfusion. Immunohistochemistry was then performed to detect both mCherry and c-fos expression.

EEG/EMG analysis.

Raw EEG/EMG signals were loaded into Neuroscore (DSI) for scoring. We set the high pass filter at 0.5 Hz and the low pass filter at 40Hz for both EEG channels. EMG signals were high pass filtered at 10 Hz and low pass filtered at 100Hz. EEG1 and EEG2 signals were further transformed to be temporal AR (autoregressive model) spectrums. Researchers were blinded as to genotype and/or treatment condition prior to data analysis. Sleep/wake state was visually scored by ~10 second epochs as either wake (low-voltage, high frequency EEG wave with high activity of EMG), rapid eye movement (REM, low-voltage, prominent θ frequency in EEG channel and low EMG) or non-REM

(NREM, high-voltage, low frequency EEG wave with low activity of EMG). The percentage of time spent in each behavioral state was then statistically evaluated.

For investigating the sleep/wake behavior of Lhx6 cKO mice, the EEG/EMG analysis was conducted for 24 hours for both control and Lhx6 cKO groups. In our analysis of sleep/wake behavior in mice expressing activating or silencing DREADDs, we analyzed data for 12 hours after either saline or CNO injection, as effects of CNO were not observed at longer than 10 hours post-injection. A 2-hour accumulation analysis was also conducted for evaluating temporal dynamics of sleep/wake states.

For spectral band analysis, we applied fast Fourier transform (FFT) to 5 second epochs of raw EEG waves of non-REM stage to calculate EEG power frequency within the frequency range of 0.1~125 Hz. Based on the sleep/wake stage labeling, we extracted a 2 hour period raw EEG wave of non-REM stage between 2 and 4 hours after injection of saline or CNO at ZT5 for EEG power spectrum analysis to evaluate the effect of activating or silencing Lhx6 ZI neurons. The EEG spectrum of the same time period (ZT7-ZT9) was also analyzed for the Lhx6 cKO mice. Artifacts were removed from analysis by visual inspection of raw EEG and EMG data, we manually removed the data epochs with noise associated with large movements (EMG muscle artifacts) that occurred during active wake and vigilance states, which cover ~10% of the recording interval. Movements were confirmed by analysis of videotape. In addition, a low-rank approximation was applied to remove the smaller Eigen factors from the raw data, and similar results were obtained to those seen using manual removal of artifacts. The frequency data was collapsed into 0.5 Hz bins. We standardized the frequency data by dividing a frequency baseline data of the same mouse recorded from the same Zeitgeber

time of a different day. The standardized frequency data were then averaged among each group of mice. To analyze the EEG frequency bands, relative power bins were summed as such: δ 0.5-4 Hz, low θ 4-6 Hz, high θ 6-10 α 10-20 Hz, β 20-40 Hz and [illegible]Hz. All the frequency bins and bands analyses were done using custom pipelines written using Matlab (MathWorks).

Behavioral analysis of Lhx6 cKO mice.

We conducted several behavioral tests to investigate the phenotype of Lhx6 cKO mice. These include:

Light-dark preference test. Each mouse was placed in an apparatus consists of a dark chamber and a light illuminated chamber. Mice can move freely between the two chambers. The duration of time each the mouse spent in dark chamber, light chamber or center were measured and normalized relative to the the whole experimental period.

Elevated plus maze (EPM) test. Each mouse was placed in the center of the EPM and videotaped for 5 min. Time spent in open and closed arms were determined from the video recording by blinded observers.

Open field test. Mice were placed in mice in the open field chamber and time spent in center and periphery was assessed for 30 min, using a Photobeam activity system to measure beam breaks.

Rotarod. Up to four mice were run at one time on a rotating rod that has the capacity to gradually accelerate up to 99.9 RPM. The Photobeam activity system was

used to record when the animal dropped off of the rod as rotation speed gradually increased. Average terminal rotation speed and time spent on the Rotarod was used for analysis.

Grip strength. Forelimb grip strength is measured as tension force using a computerized grip strength meter (GSM). Mice were lifted over the baseplate by their tails, and their forepaws allowed to grasp the steel grip. The tail of the each mouse was then placed in the center of the Single Axis Grip Strength Alignment Tool (SAGSAT), and the mouse is then gently pulled backward by the tail until its grip is released. The GSM is then used measure the maximal force before the mouse releases the bar. Three trials are performed for each mouse with a 1-minute resting period between trials.

Electrophysiological characterization of Lhx6 neurons and postsynaptic targeting on Hcrt neurons using optogenetics.

P25-P31 Lhx6-Cre;Hpcr-GFP or Lhx6-CreER^{T2};Lhx6-GFP mice were anesthetized with ketamine (50 mg/kg), dexmedetomidine (25 μm/kg) and the inhalation anesthetic, isoflurane (1-3%), and fixed in a custom-made stereotaxic frame. A small burr holes was made on skull, and 50-100 nl of AAV9-EF1α-hChR2(H134R)-mCherry viral vector (obtained from the University of Pennsylvania Vector Core) was pressure-injected into the zona incerta (AP=-1.35 mm, L=0.3 mm lateral, and DV=-4.7 mm) through a glass pipet (15-20 μm tip diameter, Drummond). The analgesic, buprenorphine (0.05 mg/kg), was administered to all mice post-operatively. Mice were sacrificed 11-18 days after virus injections and subjected to electrophysiological experiments.

Brain slice preparation and cell identification.

Mice were anesthetized with isoflurane, decapitated, and the brains were rapidly removed and chilled in ice-cold sucrose solution containing (in mM): 76 NaCl, 25 $NaHCO_3$, 25 glucose, 75 sucrose, 2.5 KCl, 1.25 NaH_2PO_4, 0.5 $CaCl_2$, and 7 $MgSO_4$; pH 7.3. Acute brain slices (300 μm) were prepared in a coronal orientation using a vibratome (VT-1200s, Leica). Slices were then incubated in warm (32-35°C) sucrose solution for 30 minutes and then transferred to warm (32-34°C) artificial cerebrospinal fluid (aCSF) composed of (in mM): 125 NaCl, 26 $NaHCO_3$, 2.5 KCl, 1.25 NaH_2PO4, 1 $MgSO_4$-$7H_2O$, 20 D-(+)-glucose, 2 $CaCl_2$-$2H_2O$, 0.4 ascorbic acid, 2 pyruvic acid, and 4 L-(+)-lactic acid; pH 7.3, 315 mOsm, and allowed to cool to room temperature. All solutions were continuously bubbled with 95% O2/5% CO2.

For whole-cell recordings, slices were transferred to a submersion chamber on an upright microscope (Zeiss AxioExaminer, Objectives: 5x, 0.16 NA and 40x, 1.0 NA) fitted for infrared differential interference contrast (DIC) and fluorescence microscopy. Slices were continuously superfused (2-4 ml/min) with warm oxygenated aCSF (32-34°C). Neurons were visualized with a digital camera (Sensicam QE; Cooke) using either transmitted light or epifluorescence. Hcrt neurons in *Lhx6-Cre;Hcrt-GFP* mice were identified based on their GFP expression. In *Lhx6-CreER^{T2};Lhx6-GFP* mice, Lhx6 neurons were categorized as either virus-infected, ChR2-expressing Lhx6 cells or uninfected cells based on the viral gene, mCherry expression and current response to 1s blue light stimulation.

Whole-cell recordings and analysis.

Glass recording electrodes (2-4 MΩ) were filled with an internal solution containing (in mM): 36.4 KCl, 96.4 $KMeSO_3$, 9.1 HEPES, 0.18 EGTA, 4 MgATP, 0.3 NaGTP, 20 phosphocreatine(Na), pH 7.3, 295 mOsm. Biocytin (0.25% weight/volume) was added to the internal solution. Whole-cell patch clamp recordings were obtained using Multiclamp 700B amplifiers (Molecular Devices) and digitized using an ITC-18 (Instrutech) controlled by custom software written in Igor Pro (Wavemetrics). The series resistance averaged 11.8 ± 4.4 MΩ SD (n = 39 neurons from 7 mice, all <30 MΩ) and was not compensated. For ChR2 photoactivation, a small circle (315 μm diameter) of blue light (6–600 mW/mm2) was delivered through the 40x objective lens using a fiber optic cable (920 μm diameter; Thorlabs) coupled to a blue LED (~470 nm; Luminous), and focused onto the recorded cell. To test GABAergic input onto the recorded neurons, cells were first washed in blockers of glutamate receptors, 5 μM 2,3-Dioxo-6-nitro-1,2,3,4-tetrahydrobenzo[f]quinoxaline-7-sulfonamide disodium salt (NBQX; AMPA receptor antagonist) and 5 μM (RS)-3-(2-Carboxypiperazin-4-yl)-propyl-1-phosphonic acid (CPP; NMDA receptor antagonist), and then washed in blockers of both glutamate receptors and GABA receptors, including 10 μM 6-Imino-3-(4-methoxyphenyl)-1(6H)-pyridazinebutanoic acid hydrobromide (SR95531; GABAA receptor antagonist, all from Tocris). The resting membrane potential was measured after whole-cell configuration was achieved. Neurons exhibiting a resting membrane potential greater than -60 mV were excluded from the analysis. The input resistance was determined by measuring the

voltage change in response to a 1 s hyperpolarizing current step (-10 to -25 pA). All signals were low-pass filtered at 10 kHz and sampled at 20-100 kHz.

Data analysis was performed in Igor Pro (Wavemetrics), Excel (Microsoft), and SigmaPlot (Systat Software). Data are presented as the mean ± SEM unless otherwise noted.

Immunohistochemistry (IHC).

Mice were anaesthetized with ketamine and transcardially perfused with 20mL 1X PBS followed by 50mL of 4% paraformaldehyde (m/v) in PBS. Brains were removed, fixed overnight in 4% paraformaldehyde, followed by 30% sucrose (m/v) in PBS overnight in 4°C for cryoprotection, and embedded and frozen in -80°C. Using a cryostat, the frozen brains were sectioned into 40 μm coronal slices for immunohistochemistry. Immunohistochemistry was performed as described previously with minor changes [89]. Brain sections were washed with 1x PBS and incubated with Superblock (Thermo Scientific, Cat: 37515) to block non-specific binding site. After brief washing, primary antibodies were diluted in a blocking solution of 5% horse serum in 0.25% Triton X-100 in PBS. The following primary antibodies were used: rabbit anti-GFP (1:500;A-6455, Invitrogen); mouse anti-Lhx6 (1:100; sc-271433(Clone A-9), Santa Cruz Biotechnology), goat anti-HRCT (1:400; sc-8070, Santa Cruz Biotechnology), rabbit anti-cFos (1:400; sc-52, Santa Cruz Biotechnology), rabbit anti-tyrosine hydroxylase(TH) (1:400; p4010-150, Pel-Freez), rabbit anti-parvalbumin(1:400; PV 27, Swant). Brain sections were incubated in primary antibodies and blocking solution

overnight at 4°C. Secondary antibody in blocking solution was then used to incubate the slides for 2 hr at room temperature. Secondary antibodies used were as following: Alexa Fluor 488 conjugated donkey anti Rabbit (1:500; A21206, Invitrogen); Alexa Fluor 488 conjugated donkey anti mouse (1:500; A212062 Invitrogen); Alexa Fluor 488 conjugated donkey anti Goat (1:500; A11055, Invitrogen); Alexa Fluor 594 conjugated donkey anti Rabbit (1:500; A21207, Invitrogen); Alexa Fluor 594 conjugated donkey anti mouse (1:500; A21203, Invitrogen); Alexa Fluor 594 conjugated donkey anti Goat (1:500; A11058, Invitrogen). After washing in 0.1% Triton X-100 in 1X PBS and staining for DAPI (1:5000; 10236276001, Roche), brain sections were mounted on positively charged slides with Vectashield Mounting medium (H-1500, Vector laboratories). Fluorescent images were taken using a Zeiss Axioskop 2 Mot Plus Microscope or Zeiss Meta 510 LSM confocal microscope.

Quantification of c-fos expressing cells.

To characterize ZI Lhx6 neurons activated under different lighting conditions, adult Lhx6-eGFP mice (2~4 months old) were deeply anaesthetized with ketamine at four time points across the light-dark cycle: 7AM (ZT0);1PM(ZT6);9PM (ZT14- lights off); 1AM (ZT18). For the 7am time point, mice were anesthetized a few minutes before lights on with minimal light exposure. All other mice were anaesthetized within 15 minutes of their time point group. Immediately after anesthesia, mice were transcardially perfused with 20mL 1X PBS followed by 4% paraformaldehyde (m/v) in 1X PBS. For analysis of cFOS expression during sleep deprivation, adult Lhx6-eGFP mice (2~4

months old) were sleep-deprived starting at 7AM (ZT0), until 1PM for a total of 6 hours. To facilitate sleep deprivation, mice were monitored in new cages with new beddings, given water and food ad libitum, and occasionally touched gently with a soft brush when they seemed drowsy, as described [89]. Control mice were not disturbed and allowed to sleep freely. Mice in the Sleep Deprivation group and control group were anesthetized at 1pm and transcardially perfused and stained according to the protocol for Immunohistochemistry. Mice in the Sleep Deprivation with Recovery Sleep group were permitted to sleep at 1pm for 1h and then perfused at 2pm. All cell counting was conducted blind on 3x2 tiled images of the ZI using ImageJ. The area used for counting was demarcated by the Lhx6 cells in the ZI labeled by Lhx6-eGFP. For each animal, 4 brain sections were analyzed bilaterally, and the percentage of cFOS-positive neurons in Lhx6-eGFP positive neurons was compared by nonparametric statistical methods (see **Statistics**).

Fluorescent *In Situ* Hybridization (FISH) with Immunohistochemistry (IHC).

We performed FISH staining on Lhx6-EGFP mouse with *in situ* markers including *Gad1*, somatostatin (*Sst*) and *Npy*. The RNA probes were generated using the following EST sequences as templates: *Gad1* (GenBank accession #AI845043), *Sst* (GenBank accession #AI848192), *Npy* (GenBank accession #AI848386). Brains were removed from transgenic Lhx6-eGFP mice within 5 minutes after euthanasia and fixed overnight in 4% paraformaldehyde (m/v) in PBS at 4°C followed by incubation in 30% sucrose (m/v) in PBS overnight in 4°C for cryoprotection. The embedded and frozen

brains were sectioned into 40 μm using a cryostat and then mounted onto positively charged slides. For in situ hybridization, all equipment was cleaned with 0.3M Sodium hydroxide and RNAaseZap and all solutions were DEPC-treated and autoclaved.

I*n situ* hybridization follows as previously described [90] with some alterations. Briefly, slides are fixed in 4% paraformaldehyde (m/v) in 1X PBS for 15 minutes and then cell membranes are digested by incubation in 1μg/mL Proteinase K with 50 mM Tris pH 7.5 and 5mM EDTA in 1X PBS for 15 minutes. After re-fixation in 4% paraformaldehyde, the brain sections undergo acetylation with 0.27% acetic anhydride and 10% 1M TEA (pH 8) in 1X PBS. The slides are then washed in 1X PBS, incubated in 0.1% Triton X-100 in PBS for 1h and then quenched in 1% hydrogen peroxide in PBS for 30 minutes to eliminate endogenous peroxidase activity. Next, the slides are incubated in hybridization buffer (50% formamide, 5X SSC) for two hours and then incubated overnight under siliconized coverslips in Heat activated DIG-conjugated RNA probes diluted in hybridization buffer at 68°C. The next day, a 5X SSC (saline sodium citrate) wash was followed by two 0.2X SSC washes to remove the coverslips and to eliminate nonspecific probe binding. The slides were then washed with 0.3% Triton X-100 in PBS and incubated in blocking buffer (0.1 Triton X-100, 1% HISS in 1x PBS) for 1h. For detection of the Lhx6, IHC for anti-eGFP was combined with the subsequent *in situ* hybridization steps. The slides are incubated overnight at 4°C in a blocking solution containing rabbit anti-GFP antibody (1:500; A-6455, Invitrogen) and Anti-Digoxigenin-POD antibody (1:1000; 1207733, Roche). After washing the slides in 0.3% Triton-X 100 multiple times on the third day, probe signal was recovered by Cy3-tyramide amplification reagent (1:125; NEL752001KT, TSA^{TM} Plus Cyanine 3/Cyanine 5 system,

PerkinElmer) in 1X amplification diluent and monitored frequently by fluorescent microscopy for the timing of signal appearance. Slides were washed, quenched in 1% hydrogen peroxide and 0.3% Triton-X 100 in PBS, and blocked in blocking solution (0.2% Triton X-100, 1% Horse Serum, 0.1% BSA powder) for 1h. Primary antibody signal is then detected by species specific Alexa fluorophores in Alexa Fluor 488 conjugated donkey anti Rabbit (1:500; A21206, Invitrogen); incubated with blocking solution for 2h. Slides were then washed and coverslipped in Vectashield. Fluorescent images were taken using a Zeiss Axioskop 2 Mot Plus Microscope or Zeiss Meta 510 LSM confocal microscope.

Statistics.

For c-fos immunohistochemistry analysis, each group contained data 3~4 mice, with a total of bilateral sides of 4 brain slices analyzed for each mouse, which resulted in inter-dependence in each group. As a result, to analyze this data, we applied linear mixed-effect model fit by REML, a nonparametric method. Two-tailed, one-way ANOVA was applied to evaluate the difference among multiple groups. Shapiro-Wilk Normality Test was used to test normal distribution of data in electrophysiological whole-cell recordings, and paired t-test was used to test statistical significance before and after $GABA_A$ receptor antagonist treatment in ChR2 photostimulation experiment. All the sleep/wake data analysis was primarily performed by two-tailed paired t-test, and later confirmed by nonparametric method, Wilcoxon-Mann- Whitney test. The statistics were run in statistical program language R (R Foundation for Statistical Computing) and Excel (Microsoft).

Results

Chapter 1. Expression pattern of Lhx6 in hypothalamus morphology of hypothalamic Lhx6-positive neurons

1.1 Expression of Lhx6 in Zona incerta (ZI) and its neuronal morphology

To fully characterize the expression pattern of Lhx6 in the adult hypothalamus, we used a GENSAT BAC eGFP transgenic line [81] that faithfully recapitulated the endogenous expression pattern of Lhx6 in both telencephalon and diencephalon (97.8% of eGFP+ cells are Lhx6+). In the diencephalon, Lhx6 was selectively expressed in a subset of cells in a contiguous zone that stretched from the ventral ZI, through the dorsomedial hypothalamic nucleus (DMH) and the lateral hypothalamus (LH), the posterior hypothalamus (PH) and ultimately to the premammillary bodies as previously described in the embryonic and early postnatal brain [40]. Figure 1.1.1 shows the expression pattern of Lhx6 in ZI. The morphology of ZI Lhx6-expressing neurons are mostly bipolar (Figure 1.1.1) with two long-range processes stretching along the ZI region. These large neurons are likely the source of the long-range projections we observe to amygdala, midbrain and brainstem (see Chapter 3.3). These ZI Lhx6-expressing neurons also co-express the GABAergic marker GAD1/2, which will be

described further in Chapter 2.

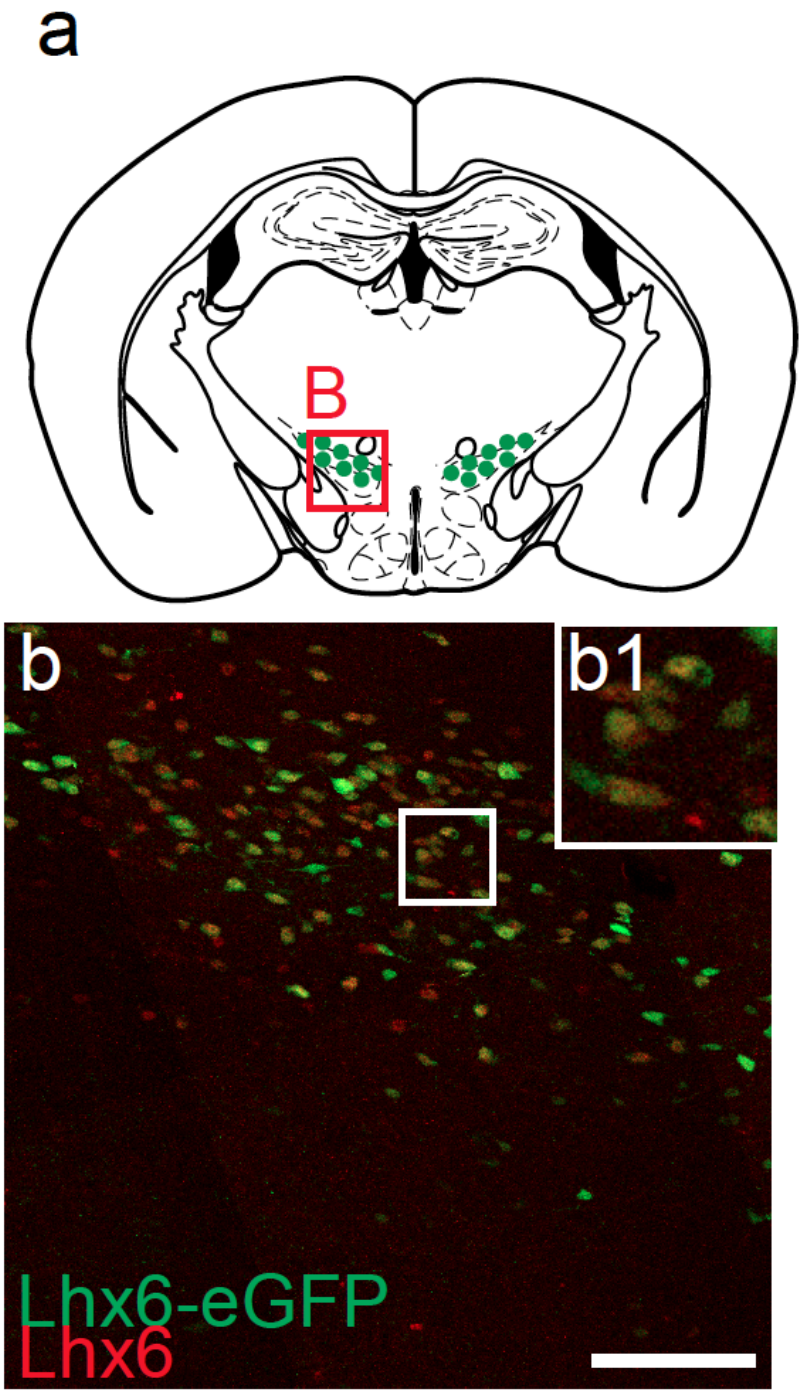

Figure 1.1.1 (a) Schematics showing the distribution of Lhx6+ neurons across the rostrocaudal axis of the diencephalon. Red boxes indicate schematic distribution of Lhx6+ neurons (green) in the zona incerta (ZI). Co-expression of eGFP (green) in Lhx6-eGFP line with Lhx6 immunostaining (red) in the ZI (b). GFP signal fills the cell

cytoplasm, while Lhx6 immunostaining is nuclear. Magnified images of b are shown in b1.

1.2 Expression of Lhx6 in the dorsomedial hypothalamus (DMH) and its neuronal morphology

The domain of Lhx6 expression in the hypothalamus forms a continuous zone along the anterior-posterior axis from ZI to PH. When Lhx6 merges from lateral ZI to DMH, the pattern and morphology of the DMH Lhx6-expressing neurons chages, as shown in Figure 1.2.1 The other markers that are co-expressed with the DMH Lhx6-expressing neurons will be discussed in more detail in Chapter 2. 1

1.3 Expression of Lhx6 in the posterior hypothalamus (PH) and its neuronal morphology

Similar to the DMH, Lhx6-expressing neurons in the PH resemble small stellate cells, and also co-express GABAergic markers (Figure 1.3.1).

1.4 Summary

In summary, unlike Lhx6-expressing neurons in the cortex, Lhx6-expressing neurons in the hypothalamus form a continuous and previously uncharacterized domain, which extends from the ZI to the PH and the premammillary nucleus, with a scattered subset found in the DMH. Furthermore, the morphology of Lhx6-expressing neurons across different regions of the developing diencephalon are heterogenous, and multiple

subclasses of Lhx6-expressing neurons exist in the hypothalamus, a finding which will be described in more detail in Chapter 2. So far, no studies have characterized either the development or function of hypothalamic Lhx6-expressing neurons. In the next chapter, I will discuss the developmental characteristics of hypothalamic Lhx6-expressing neurons, and describe how hypothalamic Lhx6-expressing neurons differ from cortical Lhx6-expressing neurons in this and other respects.

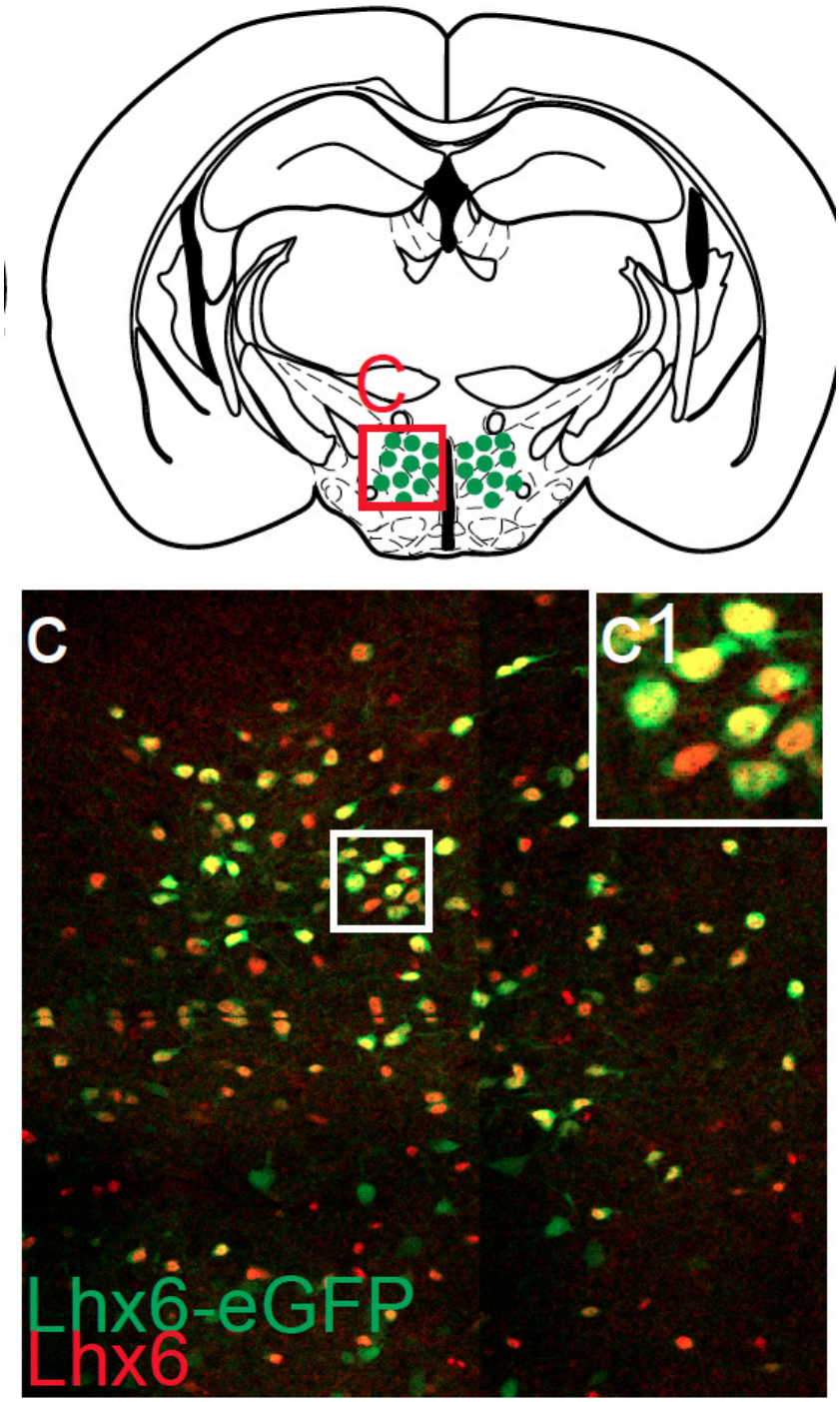

Figure 1.2.1 (upper) Schematics showing the distribution of Lhx6+ neurons across the rostrocaudal axis of the diencephalon. Red boxes indicate schematic distribution of Lhx6+ neurons (green) in the dorsal medial hypothalamus(DMH). Co-expression of eGFP (green) in Lhx6-eGFP line with Lhx6 immunostaining (red) in the DMH (c). GFP signal fills the cell cytoplasm, while Lhx6 immunostaining is nuclear. Magnified images of b are shown in b1.

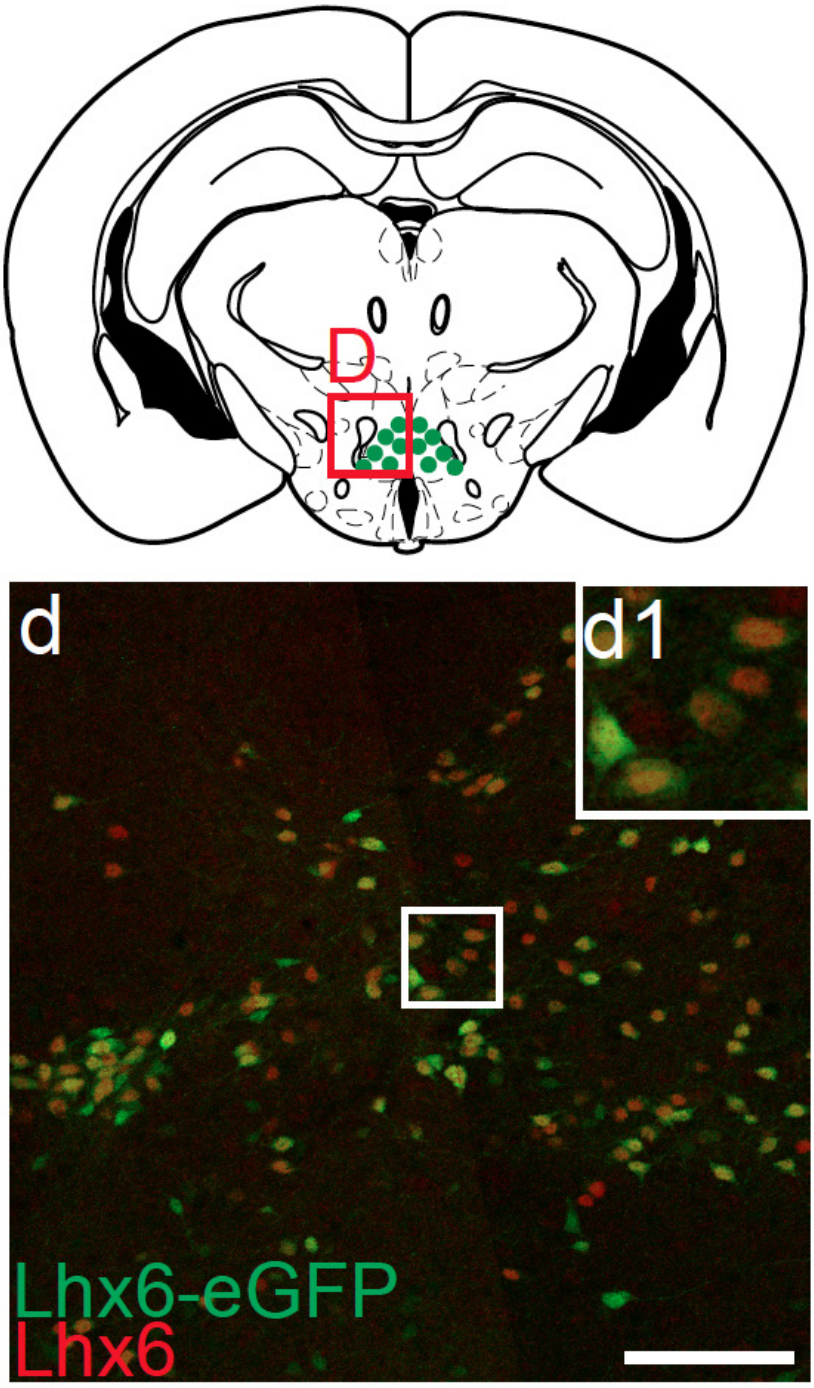

Figure 1.3.1 (upper) Schematics showing the distribution of Lhx6+ neurons across the rostrocaudal axis of the diencephalon. Red boxes indicate schematic distribution of Lhx6+ neurons (green) in the posterior hypothalamus(PH). Co-expression of eGFP (green) in Lhx6-eGFP line with Lhx6 immunostaining (red) in the PH (c). GFP signal fills the cell cytoplasm, while Lhx6 immunostaining is nuclear. Magnified images of b are shown in b1. Scale bar: 100um.

Chapter 2. Heterogeneity of hypothalamic Lhx6-expressing neurons

One critical way to study a uncharacterised population of neurons in the brain region is to screen out multiple gene expression in this population, which can tell you about potential framework of its neuronal development and physiological functions. This is especially true in the hypothalamus, where most if not all neuronal populations are associated with innate behavior regulation. Furthermore, different cell types can be classified based on the expression pattern of specific transcription factors, neurotransmitters and neuropeptides. We identified the LIM homeodomain transcription factor as a marker of a previously uncharacterized neuronal subpopulation that is distributed broadly across the posterior and lateral hypothalamus. In addition, we were looking for other molecular markers which define hypothalamic Lhx6-expressing neurons more clearly, and can provide us with the potential developmental characteristics and behavioral functions of hypothalamic Lhx6-expressing neurons. In this chapter, we applied RNA-Seq analysis to analyze hypothalamic Lhx6-expressing neurons, and used histological methods to co-localize other markers with Lhx6 in the hypothalamus.

2.1 RNA-Sequence analysis of hypothalamic Lhx6-expressing neurons

For RNA-Seq analysis, we used the GENSAT BAC eGFP transgenic line (Lhx6-EGFP mouse), which faithfully recapitulated the endogenous expression pattern of Lhx6 in both the telencephalon and the diencephalon. We collected P1 and P8 Lhx6-EGFP

offspring and dissected out the hypothalamus and the cortical region separately. We then dissociated tissues using the protocol of Worthington papain dissociation kit [91]. The dissociated cells were then transferred to the Fluorescence-activated cell sorting (FACS) facility at the Johns Hopkins School of Public Health to collect Lhx6-EGFP neurons from the hypothalamus and the cortex. FACS allowed us to separate hypothalamic Lhx6-expressing neurons into two groups, one with higher and one with lower GFP expression. This reflects the fact that hypothalamic Lhx6-expressing neurons are heterogenous. Lhx6-expressing neurons located at the ZI and the PH represent at least two subsets of neurons. The analysis of dissociated cells are shown in Figure 2.1.1, and reveals two different sizes of Lhx6-EGFP neurons.

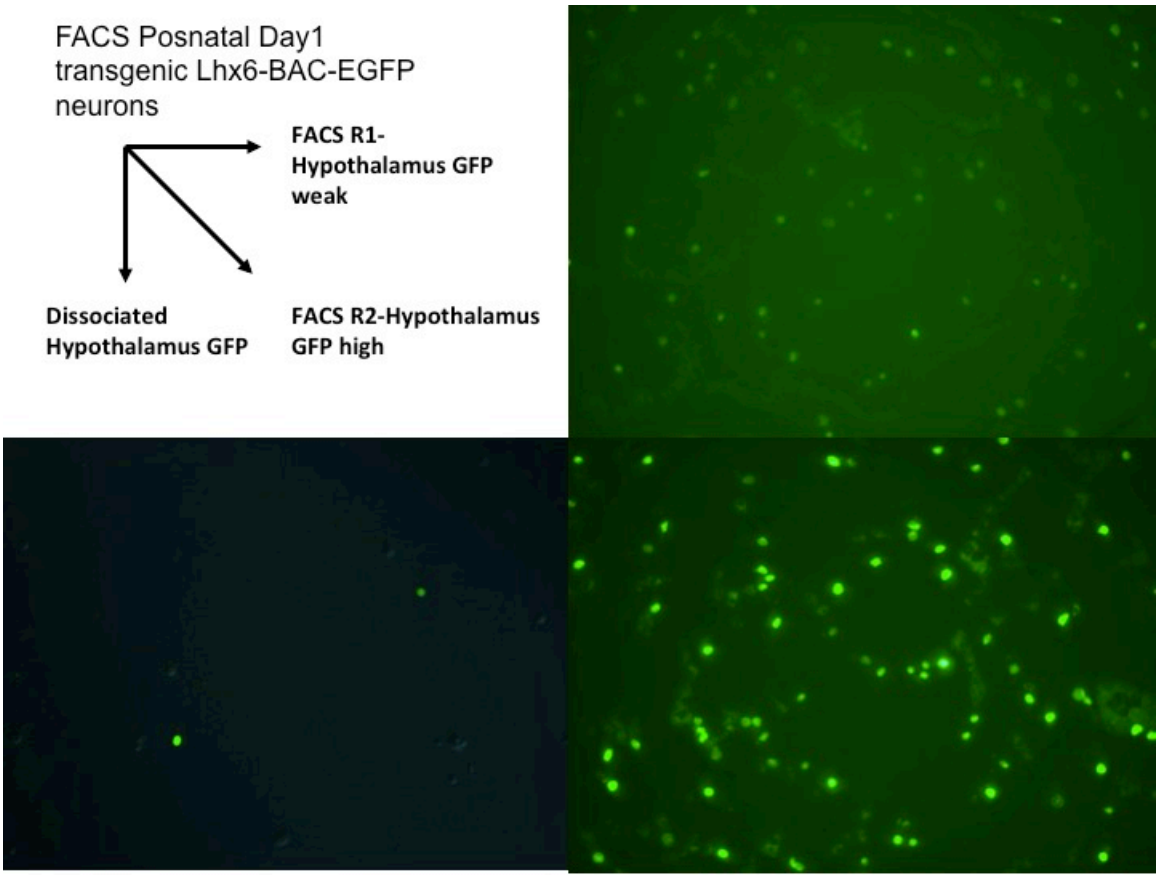

Figure 2.1.1. (lower left) the dissociated cells from hypothalamus tissues. (upper right)FACSorted Lhx6-EGFP cells with lower GFP expression. (lower right) FACSorted Lhx6-EGFP cells with higher GFP expression.

After FACS, we extracted RNA from both dissociated Lhx6-positive cells and Lhx6-negative cells (as control) in the hypothalamus and the cortex using the QIAGEN RNA extraction kit. Extracted samples were submitted for RNA-Seq analysis of Lhx6-positive or Lhx6-negative neurons. Here in Figure 2.1.2, I show an example of RNA-Seq analysis from hypothalamic Lhx6-exressing neurons with high GFP expression. The first column lists individual genes. The second column shows the expression level of GFP-positive cells, while the 3rd column shows the expression level of GFP-negative cells. As we expected, Lhx6 is highly enriched in the hypothalamic GFP-positive cells, demonstrating the specificity of the transgene and the efficiency of the sorting. All the other genes listed here are markers that are expressed in specific hypothalamic nuclei, but not enriched in hypothalamic Lhx6-expressing neurons. These include Ghrh (expressed in the arcuate nucleus), Oxt (expressed in PvN/SON), and Olig1 (expressed in oligodendrocytes). This indicates the hypothalamic Lhx6-expressing cells are distinct from other major subclasses of hypothalamic cells.

Gene symbol	GFP+ FPKM	GFP- FPKM	log2(fold_change)	Where expressed?
Lhx6	263.38	4.21	-5.97	Lhx6-GFP+
Foxd1	0.09	1.26	3.77	Anterior hypothalamus
Six3	0.32	3.32	3.39	Anterioventral hypothalamus
Fezf2	0.02	2.22	6.99	Anterior+premamillary nucleus
Ghrh	0.83	8.09	3.28	Arcuate nucleus
Nfia	2.86	51.05	4.16	Astrocytes
Foxj1	0.20	4.27	4.43	Ependymal cells
Lhx9	0.57	7.35	3.69	Hcrt neurons
Otx2	0.25	8.96	5.14	Mamillary nucleus
Foxb1	0.05	2.13	5.42	Mamillary nucleus
Olig1	0.46	15.00	5.03	Oligodendrocytes
Olig2	0.05	2.94	5.76	Oligodendrocytes
Lef1	0.13	1.52	3.55	Premamillary nucleus
Oxt	1.10	12.78	3.54	PvN/SON
Avp	2.07	98.35	5.57	PvN/SON
Nr1d1	1.72	9.27	2.43	SCN
Dio2	0.24	2.97	3.64	Tanycytes
Lhx2	0.31	8.89	4.85	Tuberoventral hypothalamus

Figure 2.1.2. Example of Deep RNA-sequencing analysis for hypothalamic Lhx6-EGFP neurons. The GFP+ FPKM column indicates the expression level of hypothalamic Lhx6 GFP positive cells, against the GFP- FPGM column which shows the hypothalamic GFP negative cell gene expression level. q-value in log2(fold change) column indicates from statistic if there is a significant difference .

Somatostatin (Sst), NPY , the markers of interneurons [92], are also enriched in the hypothalamic Lhx6-expressing neurons. However, our later histological identification demonstrated that both Sst and NPY were just intermingled with hypothalamic Lhx6-expressing neurons but not colocalized.

Figure 2.1.2 shows the analysis of hypothalamus Lhx6-expressing neurons with high GFP expression versus GFP-negative cells. Each dot represents one gene. In this figure, the X-axis shows gene expression level of hypothalamus Lhx6-expressing neurons with high GFP expression, and Y-axis shows same gene expression level in GFP-negative cells in the hypothalamus. There were two apparent clusters here: the right

one shows the higher level of gene expression in GFP-positive cells than GFP-negative cells, while the left cluster shows the opposite distribution. Arx, Lmo3, ErbB4 enrichment in Lhx6-positive cells indicates a possible role of Lhx6 in maturation and/or development of hypothalamic neurons. Other genes enriched in Lhx6-positive cells include glutamate receptors and calcium channels. Corticotrophin-releasing hormone (CRH) is enriched in a subset of Lhx6-expressing neurons. Aromatase, also known as estrogen synthetase or estrogen synthase, is an enzyme responsible for biosynthesis of estrogens. Specifically, aromatase is responsible for the aromatization of androgens into estrogens [93].

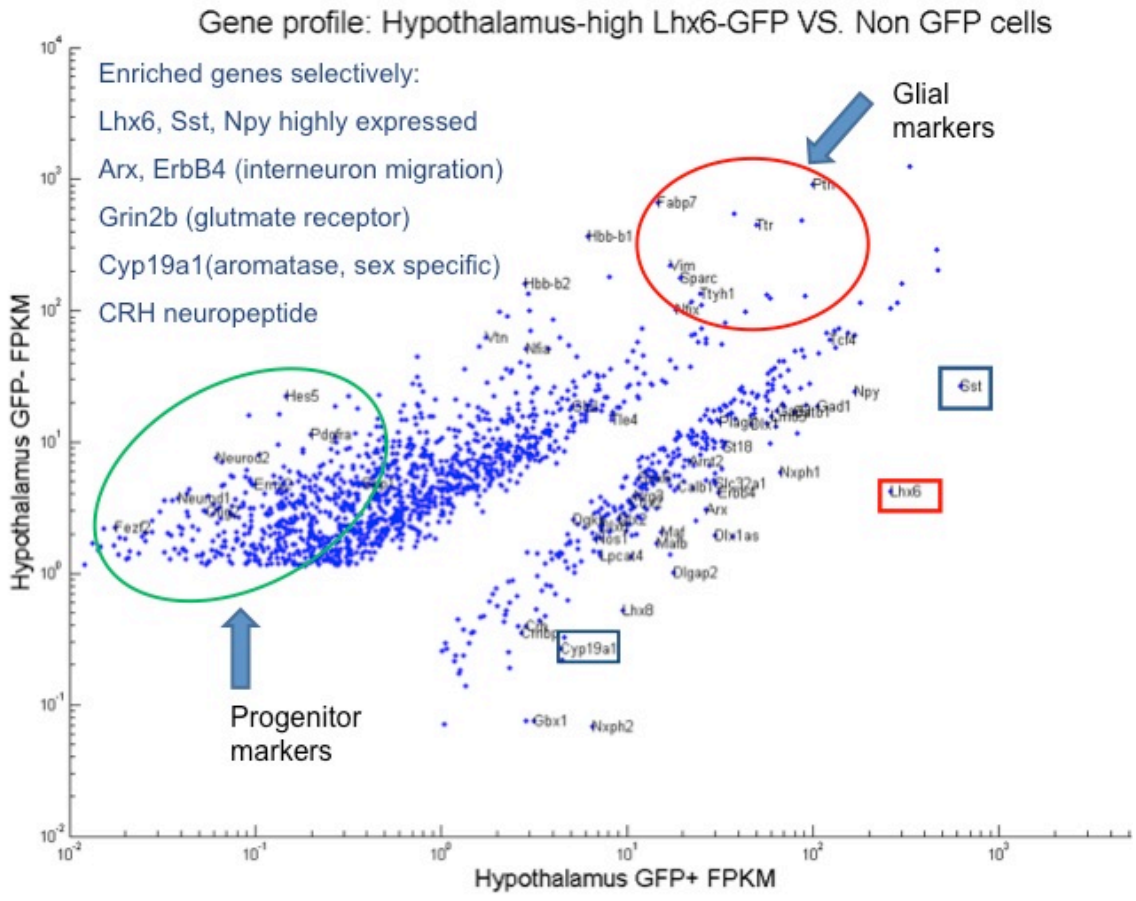

Figure 2.1.3. Gene expression level comparison between P1 hypothalamic Lhx6-positive cells(x axis) and hypothalamic Lhx6-negative cells(y axis). The right cluster of blue dots showed are the genes enriched in Lhx6+ cells, while the left cluster are the genes not enriched in Lhx6+ cells.

2.2 RNA-Seq of hypothalamic Lhx6-expressing neurons compared to telencephalic Lhx6-expressing neurons.

We have also run RNA-Seq on cortical Lhx6-expressing neurons. Hypothalamic and cortical Lhx6-expressing neurons share some of the same gene patterns, but there are also substantial differencse between them, implying that Lhx6 may have different developmental and functional roles in these two brain regions. Figure 2.2.1 shows the similarity in gene profile between hypothalamic Lhx6-expressing neuron and cortical Lhx6-expressing neurons.

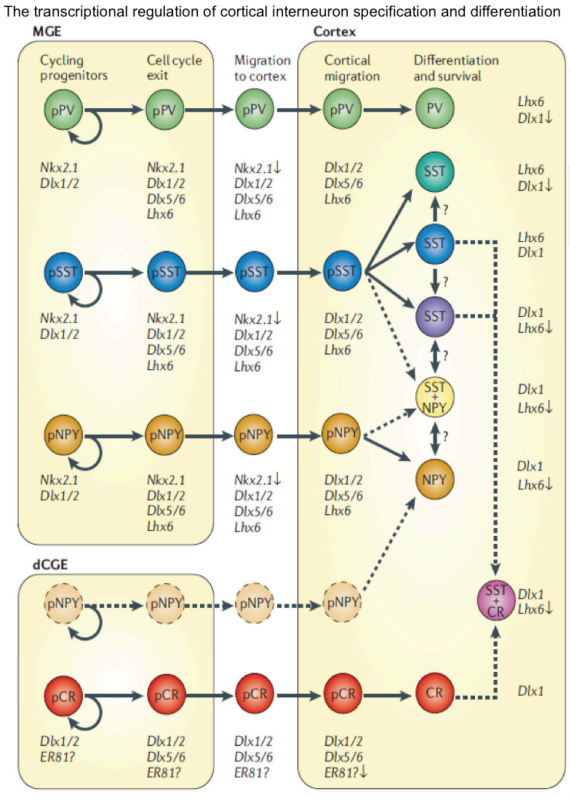

Similarity of gene expression between hypothalamus and cortex

Gene	Hypo-GF	Hypo-GFP-	Fold-chai	q-value	Function
Gad1	106.1	18.7	-2.51	0.0000	GABA synthesis
Gad2	63.9	17.3	-1.88	0.0031	GABA synthesis
Slc6a1	69.5	18.7	-1.89	0.0018	GABA transporter
Slc32a1	29.7	4.9	-2.61	0.0000	GABA transporter
Sst	623.8	26.5	-4.55	0.0000	GABA co-transmitter
Npy	168.8	24.1	-2.81	0.0000	GABA co-transmitter
Nos1	6.8	1.9	-1.87	0.0110	GABA co-transmitter
Lhx6	263.4	4.2	-5.97	0.0000	Transcription factor
Lhx8	9.5	0.5	-4.17	0.0010	Transcription factor
Arx	26.7	3.1	-3.12	0.0000	Transcription factor
Satb1	79.3	17.0	-2.23	0.0000	Transcription factor
Maf	15.2	2.1	-2.88	0.0000	Transcription factor
Dlx5	17.0	4.6	-1.88	0.0061	Transcription factor
Dlx2	9.0	2.6	-1.81	0.0085	Transcription factor
Dlx1	46.4	13.6	-1.77	0.0000	Transcription factor
Dlx6	7.2	2.3	-1.66	0.0346	Transcription factor
Cux2	10.4	3.4	-1.60	0.0020	Transcription factor
Sox6	11.6	5.3	-1.13	0.0000	Transcription factor
Grin2d	9.7	2.9	-1.76	0.0267	Glutamate receptor
Grik3	10.2	3.6	-1.51	0.0213	Glutamate receptor
Grm5	25.7	10.9	-1.24	0.0010	Glutamate receptor
Grip1	16.6	5.2	-1.67	0.0001	Glutamate receptor clustering
Gria1	82.6	11.7	-2.82	0.0000	Glutamate receptor
Grik1	14.5	3.1	-2.22	0.0000	Glutamate receptor
Nxph1	66.6	5.8	-3.51	0.0000	Synaptogenesis
Nrxn3	92.0	19.1	-2.27	0.0000	Synaptogenesis
Nxph2	6.6	0.1	-6.60	0.0000	Synaptogenesis
Erbb4	31.1	4.1	-2.93	0.0000	Tangential migration
Sema3a	9.9	2.1	-2.25	0.0000	Tangential migration
Nrg3	10.9	3.9	-1.50	0.0067	Tangential migration

Figure 2.2.1. Comparison of gene expression pattern between hypothalamic Lhx6 and cortical Lhx6 neurons. The left panel showed in cortex the transcription factor expression profiles throughout specification, migration and differentiation of cortical interneurons deriving from the medial ganglionic eminence (MGE). The right panel showed part of the gene list which were enriched in both hypothalamic Lhx6 and cortical lhx6 neurons.

Both hypothalamic and cortical Lhx6-expressing neurons express similar transcription factors such as Dlx family members and Arx. They also express similar genes involved in, GABA syntheisis, synaptic GABA transport, and a number of neuropepties such as Npy. However, hypothalamic Lhx6 neurons selectively expressed a number of other genes, including the neuropeptides Nts and Penk, along with the calcitonin receptor Calcr. The expresion profile in Lhx6-expressing neurons between two brain regions as shown in Figure 2.2.2. There are 206 genes that are enriched in Lhx6-positive neurons (>2-fold elevated relative to Lhx6-negative neurons) and shared by both Lhx6 -expressing neurons in the hypothalamus and the cortex, while 102 genes are uniquely expressed in hypothalamic Lhx6-expressing neurons and 104 genes in the cortex.

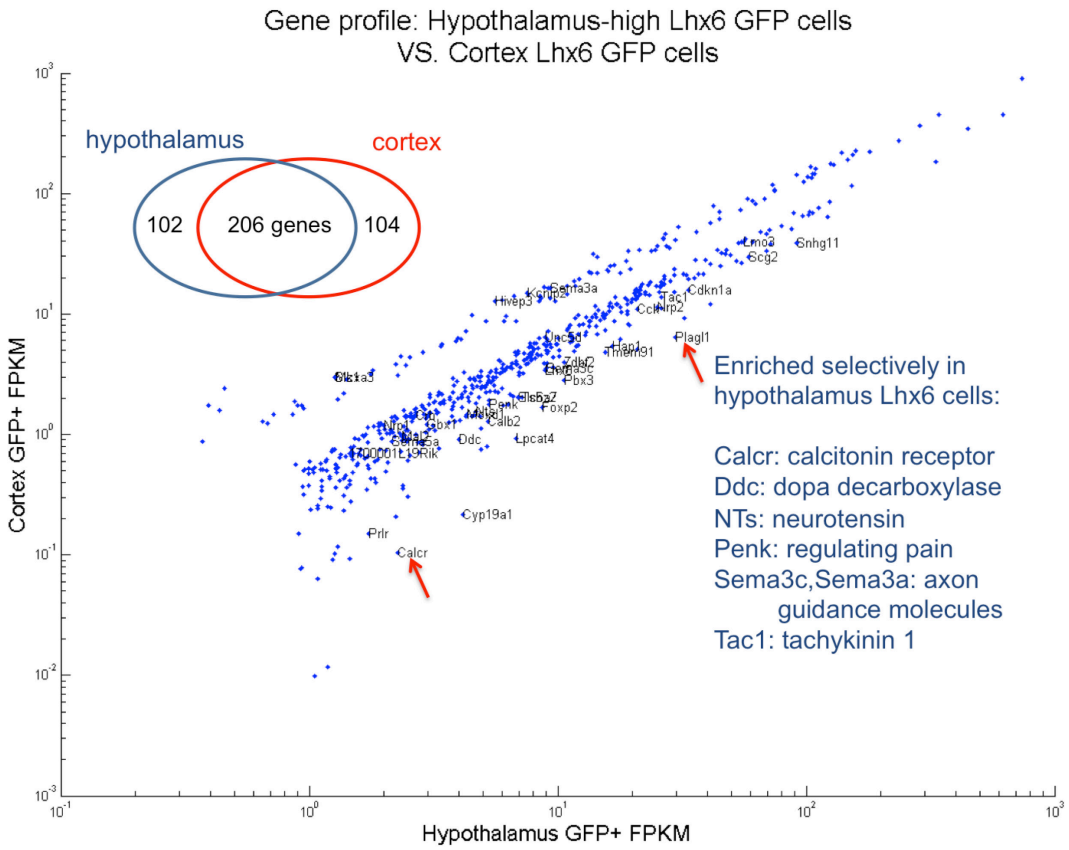

Figure 2.2.2. Gene expression level comparison between P1 hypothalamic Lhx6-positive cells(x axis) and cortical Lhx6-positive cells(y axis). The right cluster of blue dots showed are the genes enriched in hypothalamic Lhx6+ cells, while the left cluster are the genes enriched in cortical Lhx6+ cells.

2.3 Zona incerta Lhx6-expressing neurons co-express GABAergic marker

This RNA-Seq data revealted that hypothalamic Lhx6-expressing cells co-express markers of GABAergic neurons, including Gad1 and the vesicular GABA transporter Slc32a1 (Figure 2.3.1 and Figure 2.3.2 i-l). Lhx6 is expressed in ~70% of cortical interneurons, and is essential for specification of parvalbumin (Pvalb) and somatostatin (Sst)-expressing neurons in the cortex [25]. In sharp contrast to telencephalic Lhx6-expressing neurons, we have failed to observe substantial colocalization of diencephalic Lhx6-expressing neurons with either Pvalb or Sst in the zona Incerta or the lateral

hypothalamus (Figure 2.3.2 a-h).

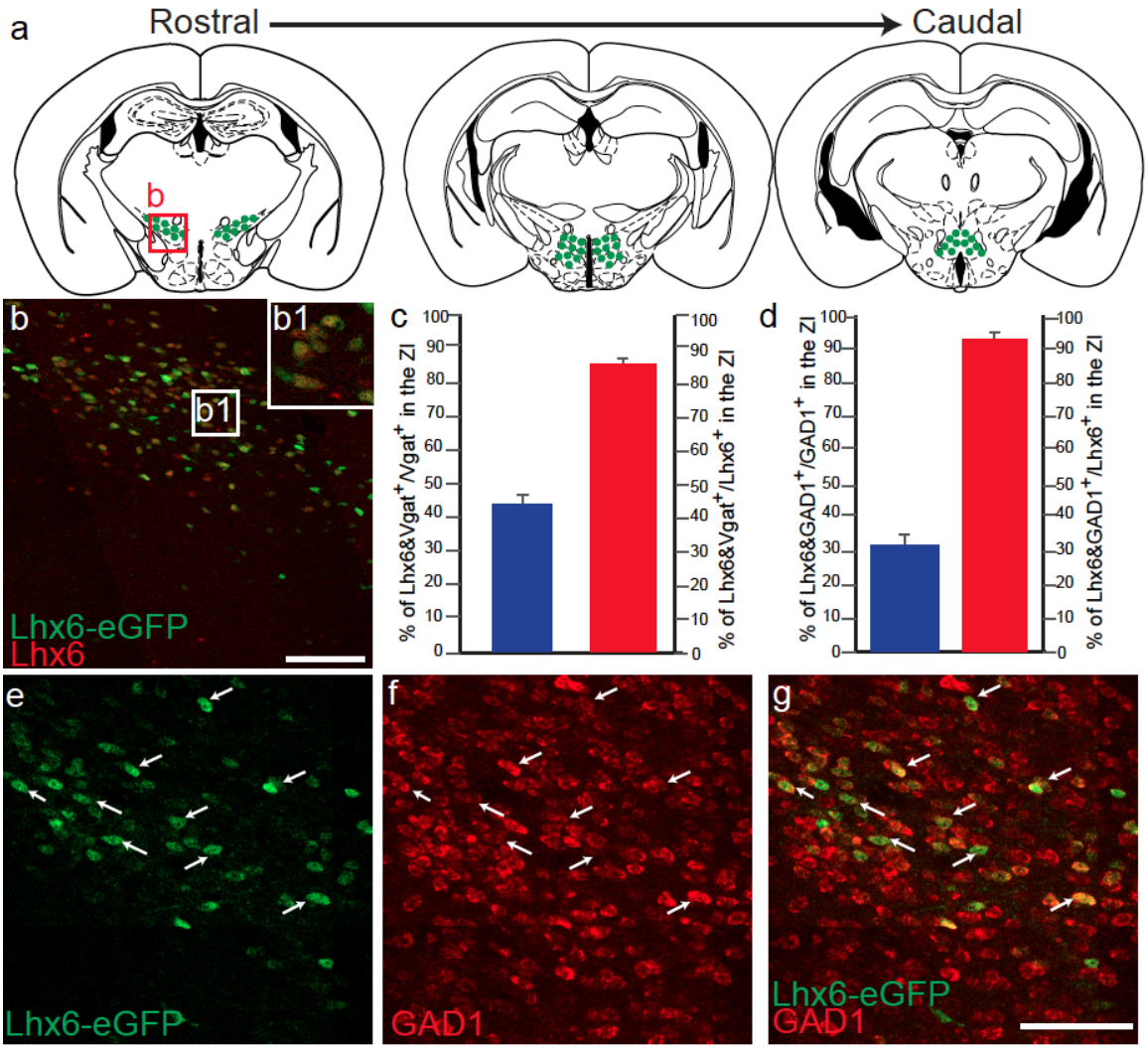

Figure 2.3.1. Lhx6-expressing neurons in the zona incerta are GABAergic (a) Schematics showing the distribution of Lhx6+ neurons across the rostrocaudal axis of the diencephalon. Red boxes indicate schematic distribution of Lhx6+ neurons (green) in the zona incerta (ZI), with representative images of the ZI shown in (b). (b) Co-expression of eGFP (green) in Lhx6-eGFP line with Lhx6 immunostaining (red) in the ZI. GFP signal fills the cell cytoplasm, while Lhx6 immunostaining is nuclear. Magnified image of b is shown in b1. Scale bar = 100 µm. (c) A bar graph on the left (blue) showing the percentage Lhx6-immunostained neurons and TdTom expression in the Slc32a1-Cre;Ai9 line relative to the number of Vgat-Cre;Ai9+ neurons in the ZI. A bar graph on the right (red) showing the percentage Lhx6-immunostained neurons and TdTom expression from the Slc32a1-Cre;Ai9 line over the number of Lhx6-immunostained neurons in the ZI. N=3

mice in each group.(d) A bar graph on the left (blue) shows the percentage Lhx6-immunostained neurons and GAD1 expression from fISH relative to the fraction of GAD1+ neurons in the ZI. A bar graph on the right (red) shows the percentage Lhx6-immunostained neurons and GAD1 expression from fISH over the number of Lhx6-immunostained neurons in the ZI. N=3 mice in each group.(e-g) Co-localization of GFP in Lhx6-eGFP mice (green, e) with GAD1 mRNA expression from fISH (red, f) in the ZI. Merged image of e and f are shown in g. Arrows indicate a few examples of Lhx6 and Gad1 co-localization. Scale bar = 100 µm.

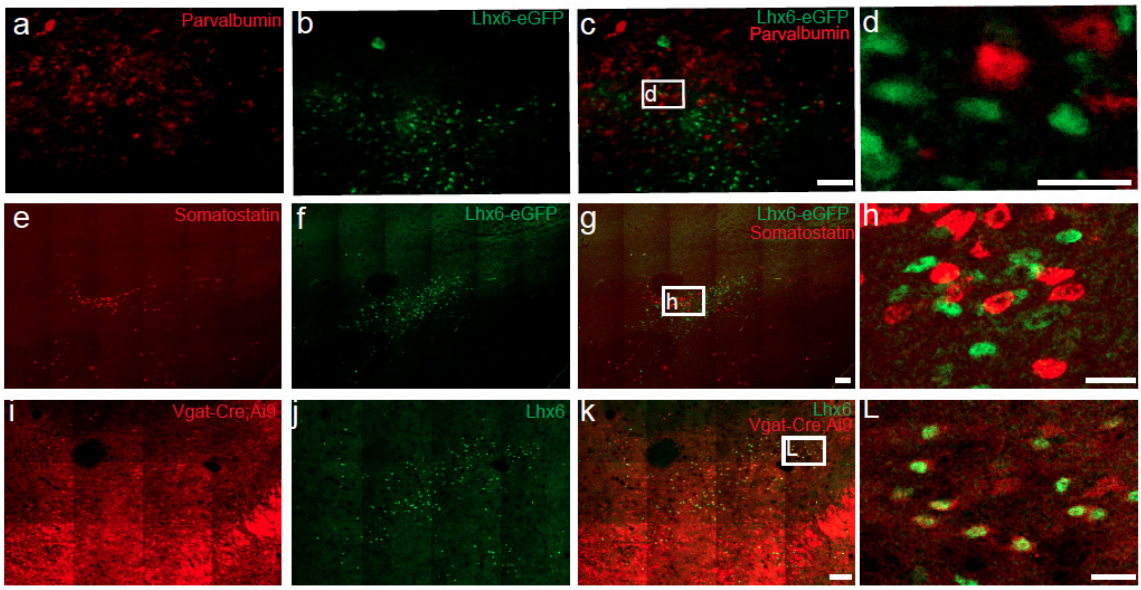

Figure 2.3.2. Immunohistochemical analysis of Lhx6-expressing neurons with common cortical interneuron markers. (a-d) Representative images showing parvalbumin-immunostained neurons (a, red) in the ZI and Lhx6-eGFP neurons (b, green) in the ZI. Merged image of a and b are shown in c. Magnified image of c is shown in d. a-c, Scale bar = 100 µm. d, scale bar = 25 µm. (e-h) Representative images showing somatostatin neurons from fISH (e, red) in the ZI and Lhx6-eGFP neurons (f, green) in the ZI. Merged image of e and f are shown in g. Magnified image of g is shown in m. e-g, Scale bar = 100 µm. h, scale bar = 25 µm. (i-l) Representative images showing Vgat-Cre;Ai9 (i, red) and Lhx6-immunostained neurons (j, green) in the ZI. Merged image of i and j are shown in l. Magnified image of l is shown in l. i-k, Scale bar = 100 µm. l, scale bar = 25 µm

Hypothalamic Lhx6-expressing neurons are GABAergic and can release GABA, thus function as interneurons. The highest density of Lhx6-expressing cells are observed

in the ventral zona incerta, with Lhx6 represents 31% and 44% of all Gad1 and Slc32a1-positive cells in this region, respectively (Figure 2.3.1 c,d).

2.4 Hypothalamic Lhx6-expressing neurons are heterogeneous at the molecular level

Using both RNA-seq data and fluorescence in situ hybridization (fISH), we have identified more molecular markers that are co-expressed with sub-populations of hypothalamic Lhx6-expressing neurons. These include Dopamine Receptor D2 (Drd2), Proenkephalin (Penk), Calbindin, Neurexophilin1(Nxph1) (Figure 2.4.1) Tac1, and Vstm2a (not shown).

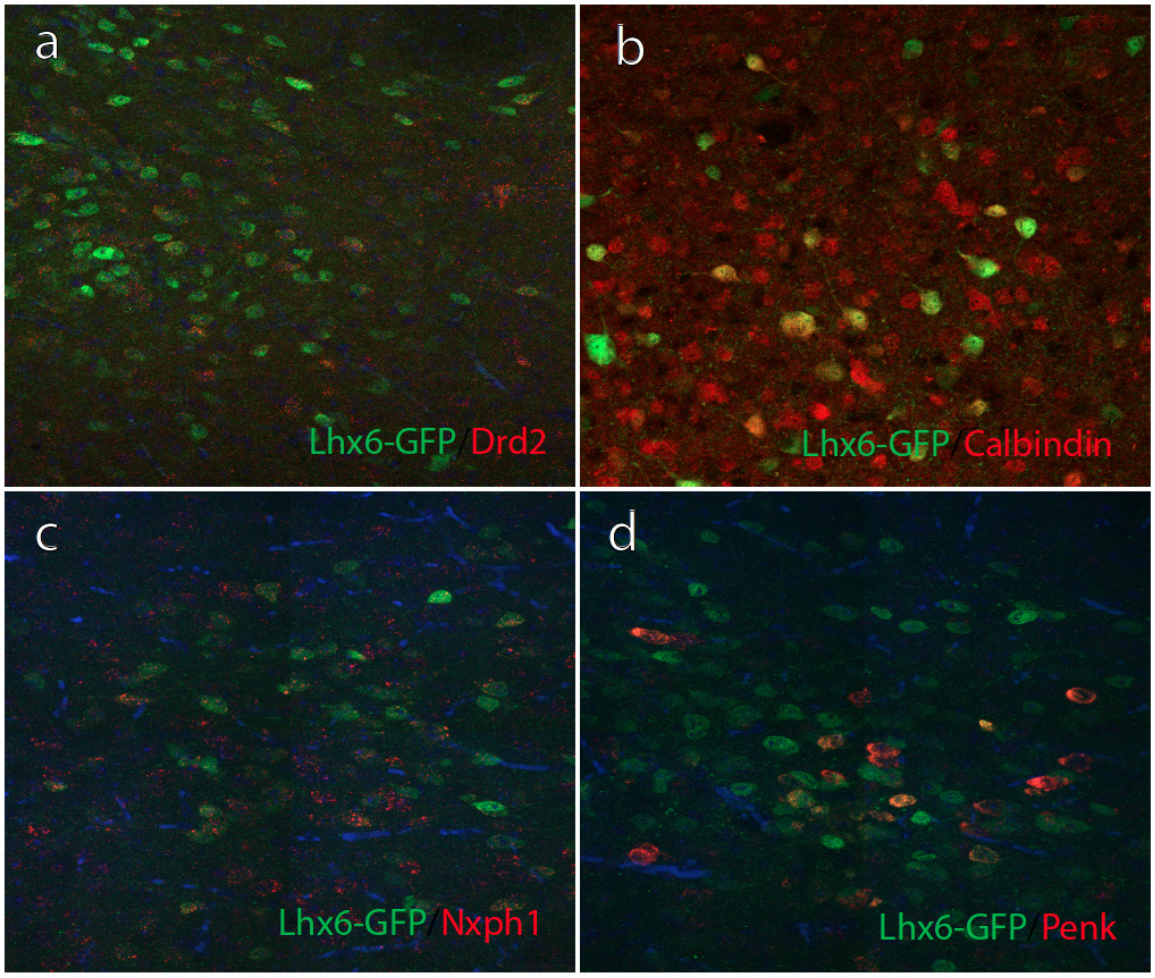

Figure 2.4.1. Immunohistochemical analysis of Lhx6-expressing neurons with some other molecular markers. (a) Dopamine Receptor D2 (Drd2), (b)Calbindin, (c) Neurexophilin1(Nxph1), (d)Proenkephalin(Penk),

Thus, hypothalamic Lhx6-expressing neurons are highly heterogeneous, and may be multifunctional. For the functional studies which will be shown in the next chapter, we have focused on Lhx6-expressing neurons in the zona incerta (ZI). The ZI is adjacent to the lateral hypothalamus where two sleep/wake cycle population of neurons, hypocretin and melanin-concentrating hormone (MCH)-expressing cells are located. As a result, ZI Lhx6-expressing neurons might also be involved with sleep/wake regulation. Here we

show that ZI Lhx6-expressing neurons are not either hypocretin or MCH-expressing neurons (Figure 2.4.2).

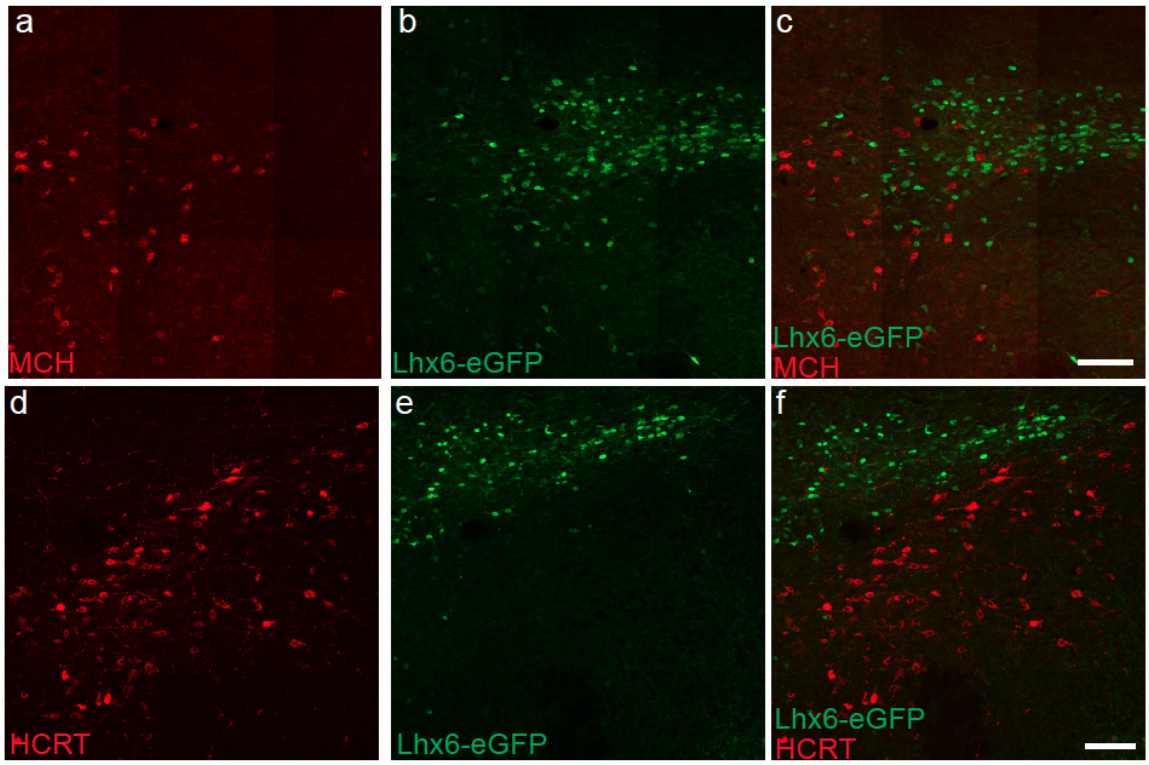

Figure 2.4.2. Immunohistochemical analysis of Lhx6-expressing neurons.(a-c) Representative images showing MCH-immunostained neurons (a, red) in the LH and Lhx6-eGFP (b, green) neurons in the ZI. Merged image of a and b are shown in c. Scale bar = 100 µm. (d-f) Representative images showing HCRT-immunostained neurons (d, red) in the LH and Lhx6-eGFP neurons (e, green) in the ZI. Merged image of d and e are shown in f. Scale bar = 100 µm.

2.5 Receptors of wake-promoting neurotransmitters expressed in hypothalamic Lhx6-expressing neurons

We have also used RNA-Seq on P8 Lhx6-EGFP offspring to determine that hypothalamic Lhx6-expressing neurons are highly enriched for both nicotinic and muscarinic acetylcholine receptors, along with the Gi-coupled 5HT1a and 5HT1b

serotonin receptor subtypes (Figure 2.5.1, Figure 2.5.2), which indicates hypothalamic Lhx6-expressing neurons in the hypothalamus might receive input from wake-promoting neurons. Since Gi-coupled inhibitory receptors for wake-associated neurotransmitters are particularly prominent in Lhx6-positive neurons, it also suggests that hypothalamic Lhx6-expressing neurons might be sleep-promoting. Finally, since acetylcholine is known to act as both a wake-promoting and REM-promoting neurotransmitter[52], it is also possible that these neurons may be activated during REM sleep.

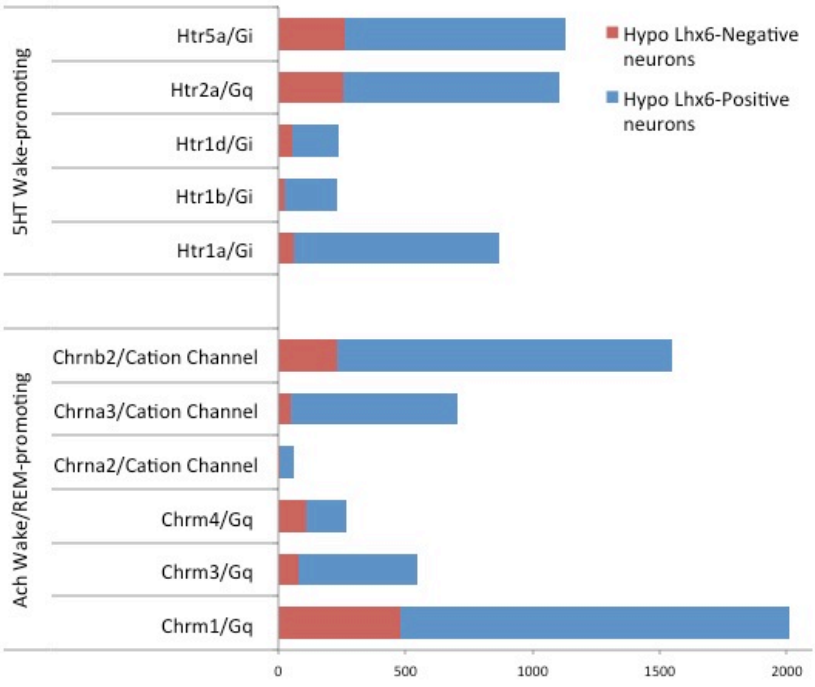

Figure 2.5.1. Receptors for wake-promoting and REM-promoting neurotransmitters enriched in P8 hypothalamic Lhx6 neurons. The blue bar shows the gene expression levels in hypothalamic Lhx6-positive neurons. The red bar shows the gene expression levels in hypothalamic Lhx6-negative neurons.

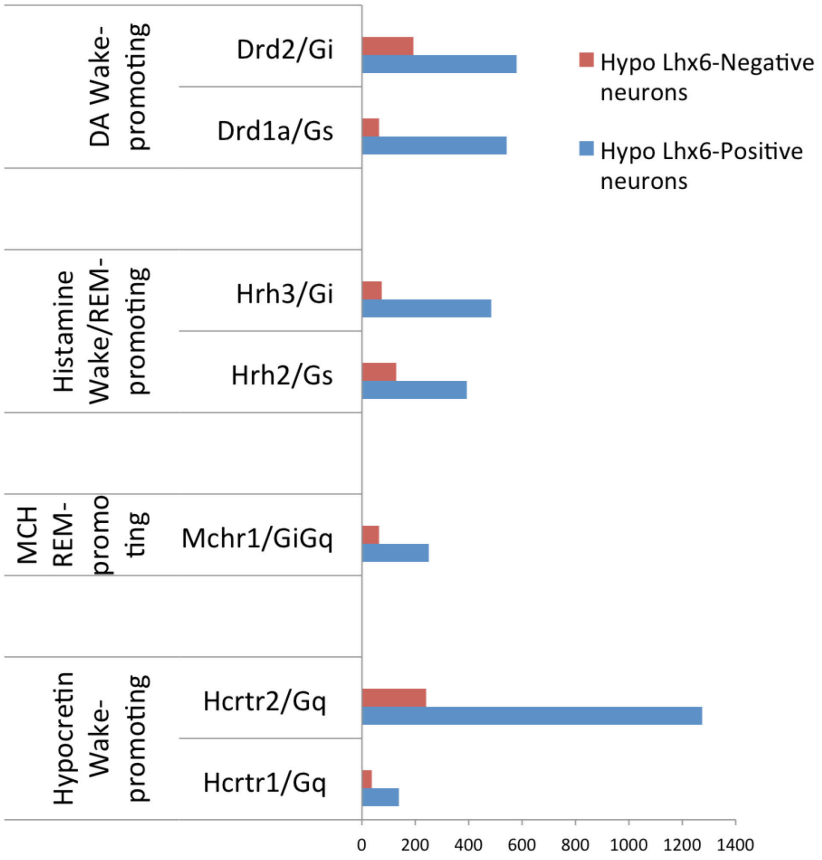

Figure 2.5.2. (continue to Figure 2.5.1)Wake-promoting and REM-promoting Receptors enriched in P8 hypothalamic Lhx6 neurons. Blue bar showed the gene expression levels in hypothalamic Lhx6-positive neurons. Red bar showed the gene expression levels in hypothalamic Lhx6-negative neurons.

In summary, hypothalamic Lhx6-expressing neurons are GABAergic interneurons, and co-express a considerable number of genes with cortical Lhx6-expressing neurons. We also show that hypothalamic Lhx6-expressing neurons show unique gene expression patterns which may confer different developmental characteristics and behavior function upon these cells.

Chapter 3. Developmental characteristics of hypothalamic Lhx6 neurons

I showed previously in Chapter 1 how Lhx6, a transcription factor, is necessary for cortical interneuron precursors to migrate and differentiate. In this chapter, I aim to investigate whether the developmental role of Lhx6 in the hypothalamus would be similar or different to the cortex.

3.1 Hypothalamic Lhx6-expressing neurons do not undergo tangential migration

Lhx6-expressing interneuron precursors undergo long-distance tangential migration in the developing telencephalon to populate dorsal structures such as the cortex and hippocampus [31,32]. This raises the question as to whether a similar process would occur in the hypothalamus. Previous studies have reported that hypothalamic neuronal precursors undergo tangential migration during development [107, 108]. Understanding the extent to which this occurs will improve our understanding of hypothalamic cell lineage, and defects in cell migration during development may underlie a wide range of genetic disorders of metabolism, mood and social interaction. We first fate mapped Lhx6-expressing cells by crossing Lhx6-CreER^{T2} knock-in mouse with a Cre-dependent R26IAP reporter line (generously shared from the Nathans lab) in the hypothalamus and treated with tamoxifen at the gestational time points of E10, E12.5 and E14. The pups were taken down at P1 and P8 and Cre-dependent AP expression was observed. By carefully observing the distribution of tamoxifen-induced Lhx6 expression, we did not see a difference in the distribution of Lhx6 when treated with tamoxifen at different

embryonic time points. We concluded that hypothalamic Lhx6-expressing neurons do not undergo a long distance dispersal, but rather migrated radially and differentiated close to their point of origin (Figure 3.1.1).

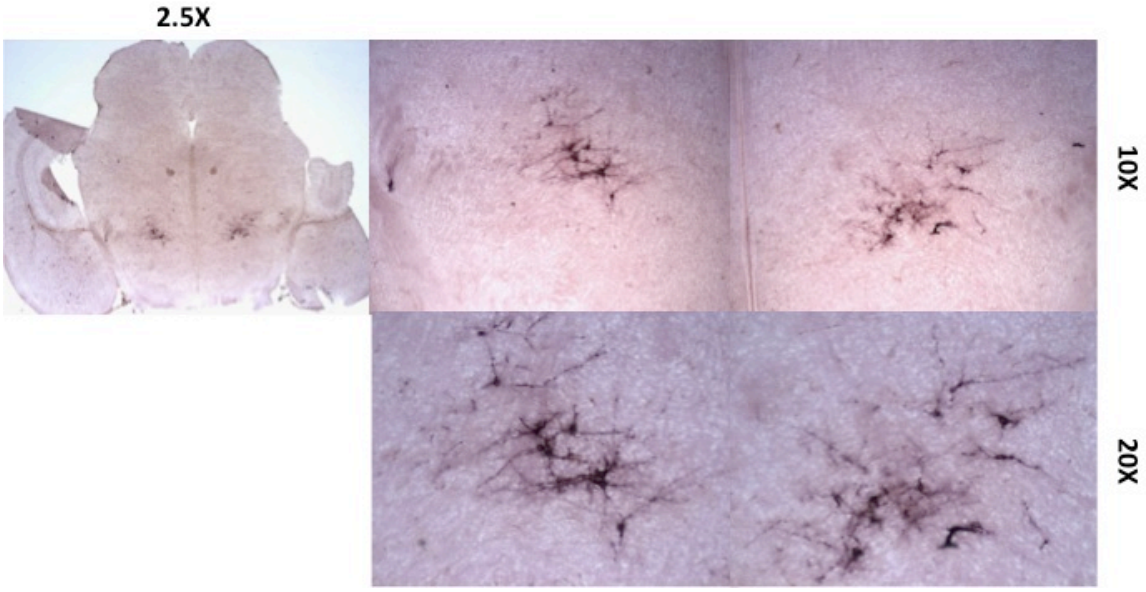

Figure 3.1.1 Hypothalamic Lhx6 neurons of P1 pup brains do not migrate demonstrated by fate mapping of Lhx6 neurons by giving tamoxifen at E12.5.coronal sections showed different magnification pictures. The leftmost was under 2.5X, while the right four panels were under 10X and 20X showing the left and right side of the lateral hypothalamus.

3.2 Lhx6 is required for the survival of hypothalamic Lhx6-expressing neurons

As previously mentioned, Lhx6 labeled a specific group of neurons in the developing and adult zona incerta(ZI), dorsomedial hypothalamus (DMH) and posterior hypothalamus (PH). To first characterize the role of Lhx6 hypothalamic development, we used homozygote Lhx6-CreER^{T2} knock-in mice as functional nulls, which would not survive pass the third postnatal week. We observed that Lhx6 null mice lacked

expression of Lhx6 mRNA in the hypothalamus. However, Lhx6 mRNA expression (but not protein expression) in telencephalic structures such as the cortex, hippocampus and amygdala was still observed (Figure 3.2.1).

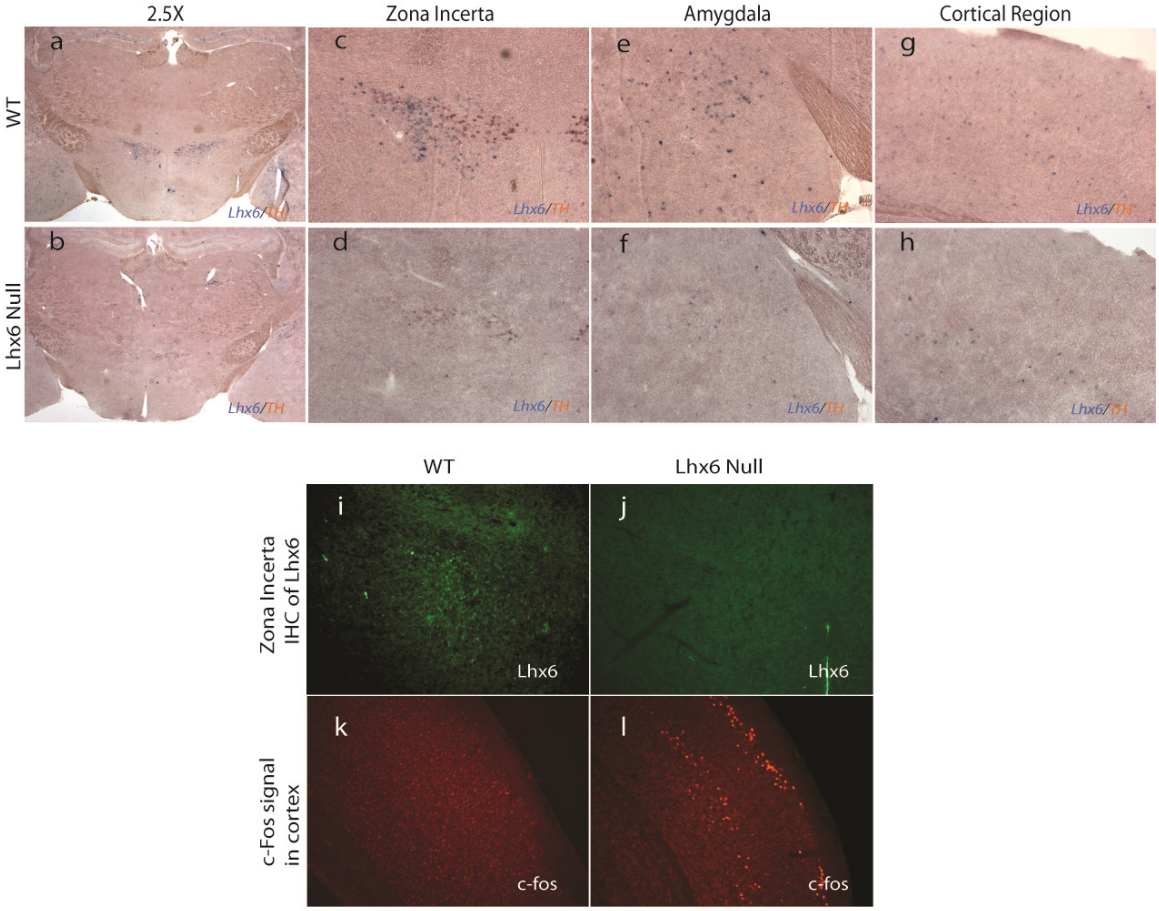

Figure 3.2.1. Lhx6 expression in P18 homozygous Lhx6CreER mice. Lhx6 was not expressed in hypothalamus (Zona incerta) of homozygous Lhx6CreER mouse (a, b, c,d) by a two-color ISH analysis of Lhx6(blue) and TH(brown), but was retained in amygdale and cortical region (e, f, g, h) . TH, tyrosine hydroxylase. Lhx6 protein was completely absent in hypothalamus(i,j) and other brain regions(not shown) and abnormally high levels of c-fos staining were observed in Lhx6 mutant cortex (k, l).

This led us to hypothesize that the Lhx6-expressing neurons in the hypothalamus either fail to survive or fail to maintain Lhx6 expression in the hypothalamus of mutant

animals. In either case, this shows that Lhx6 plays a fundamentally different roles in the development of hypothalamic neurons compared to telencephalic interneurons. To test whether Lhx6 is required for the survival of hypothalamic neurons, we crossed Lhx6-CreER, $Lhx6^{lox/lox}$ mice and Ai9-Tdtomato to generate Lhx6-CreER/$Lhx6^{lox}$;Ai9 mice. Loss of Lhx6 expression in this line by a tamoxifen-induced recombination should also activate Tdtomato expression. If Lhx6-expressing neurons in the hypothalamus require the Lhx6 gene for their survival, Lhx6-expressing neurons would die after the Cre activation, and Lhx6-negative, TdTomato-positive cells should not be observed. In contrast, if Lhx6-expressing neurons survive but just lose Lhx6 expressin, those neurons would express Tdtomato but not Lhx6. We used this Lhx6-CreER/$Lhx6^{lox}$;Ai9 line to delete Lhx6 expression by gavage delivery of tamoxifen at E16 (chase to P0) and P10 (chase to P16) (Figure 3.2.2) and compared these results to Lhx6-CreER, $Lhx6^{+}$;Ai9 mice as the control group. By immunostaining using antibody against Lhx6 and Tdtomato, we generated green cells (only Lhx6+), red cells (only Tdtomato+) and yellow cells (both Lhx6+ and Tdtomato+). We found that there are fewer number of red cells in mutant hypothalamus (Red cells/Red cells+Yellow cells ratio E16: 0.08, P10:0.14) than mutant telencephalic structures (cortex or amygdala) (Red cells/Red cells+Yellow cells ratio E16:0.58, P10:0.36), which is in contrast to the control animals hypothalamus (Red cells/Red cells+Yellow cells ratio E16: 0.00, P10:0.001) and telencephalic structures (cortex or amygdala) (Red cells/Red cells+Yellow cells ratio E16:0.36, P10:0.038). These findings indicate that Lhx6 is required for the maintenance of Lhx6 neurons in the hypothalamus but not in telencephalic structures (Figure 3.2.3).

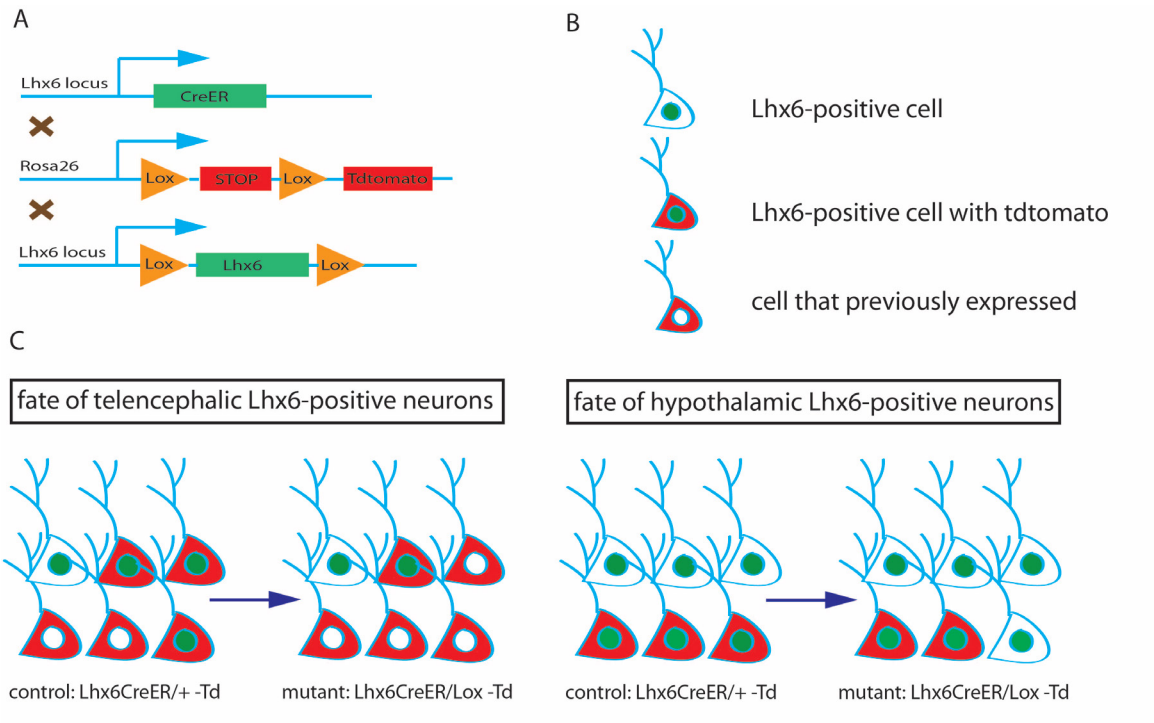

Figure 3.2.2 . Schematic procedure explain Lhx6 is required for the survival of Lhx6-expressing neurons in hypothalamus, but not in telencephalic structures. (A) Schematic indicate the generation of mouse Lhx6CreER/lox:Ai9. (B) Lhx6CreER/lox:Ai9 mutant animal showed less red cells in zona incerta compared to Lhx6CreER/+:Ai9 control animal. (C) a reduction in the number of red hypothalamic neurons relative to yellow neurons when compared to Lhx6-expressing cells of the telencephalon(R/R+Y: ratio of red cells in relative to the total number of red and yellow cells).

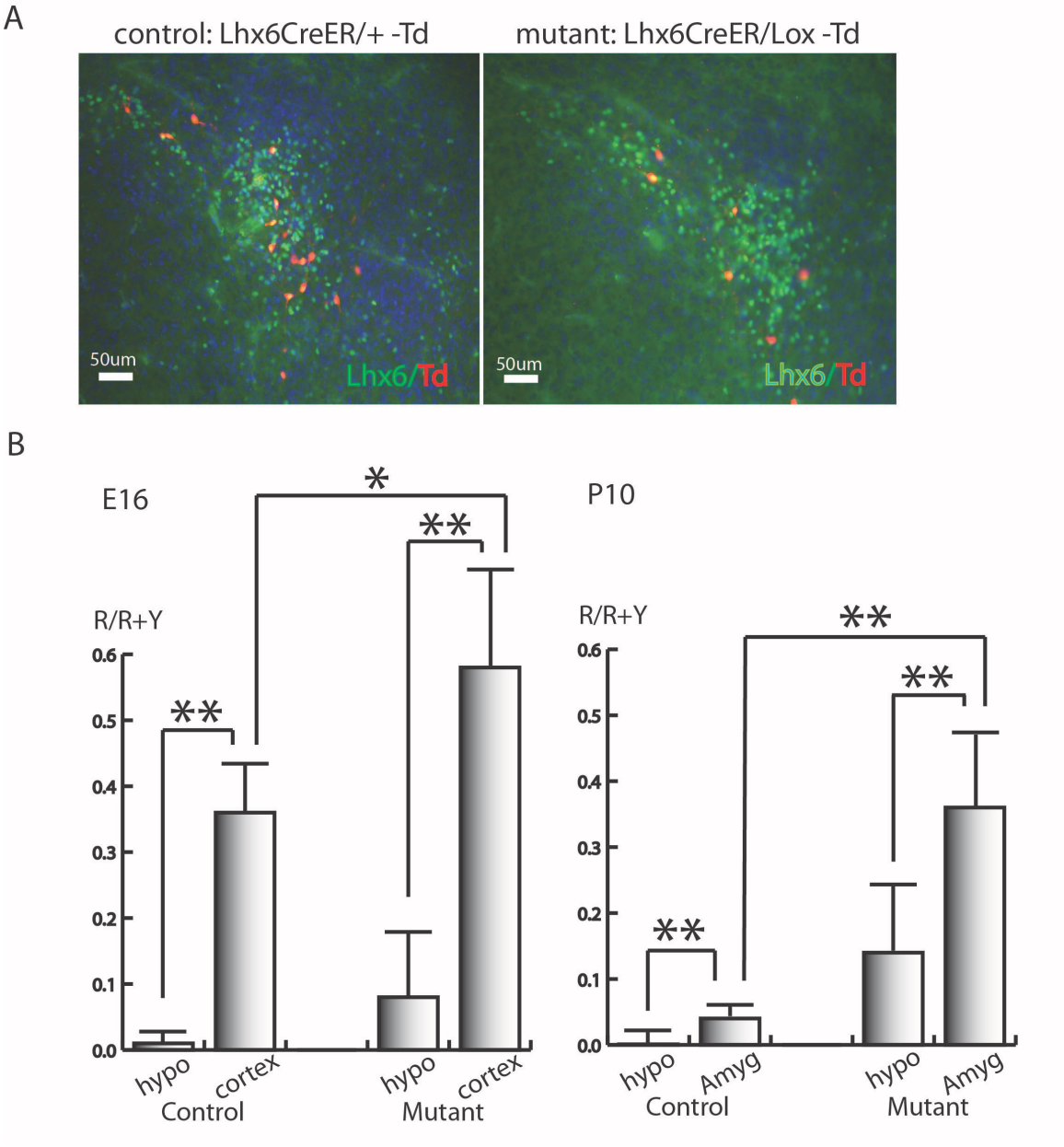

Figure 3.2.3. Experimental demonstration that Lhx6 is required for hypothalamic Lhx6-positive cells survival. (A) control staining (Lhx6CreER/+ -Td) compared to mutant staining (Lhx6CreER/Lox -Td); (B)controls and mutants statistics on R/R+Y (number of red cells divided by total of red and yellow cells) compared between hypothalamic and cortical Lhx6 cells tamoxifen injected at E16 or P10.

In conclusion, in the absence of Lhx6, Lhx6-expressing neuronal precusors in telencephalon fail to migrate and/or fail to differentiate but will not lead to cell death.

However, Lhx6 is necessary for the survival of Lhx6-expressing neurons in the hypothalamus.

3.3 Zona incerta Lhx6-expressing neurons send long-range projections to areas containing wake-active neurons.

Although hypothalamic Lhx6-expressing neurons do not undergo tangential migrate, their axonal processes reach out to send long-range projections to the amygdala, midbrain and brainstem. Here I show the local and long-range projections of hypothalamic Lhx6-expressing neurons. To first characterize postsynaptic projections of the Lhx6+ ZIv neurons, we injected AAV9-FLEX-ChR2-eYFP virus into the ZI of P60 Lhx6-CreERT2 knock-in mice [84] (Fig. 3.3.1 a). Following injection of 4-OHTx, we observed local projections both within the ZI and adjacent LH (Fig. 3.3.1 b-e). The neuropil of YFP-positive transduced cells overlapped with the distribution of A13 dopaminergic cells (Fig. 3.3.1 b,d). Furthermore, projections were also associated with cell bodies of LH Hcrt+ neurons (Fig. 3.3.1 d,e).

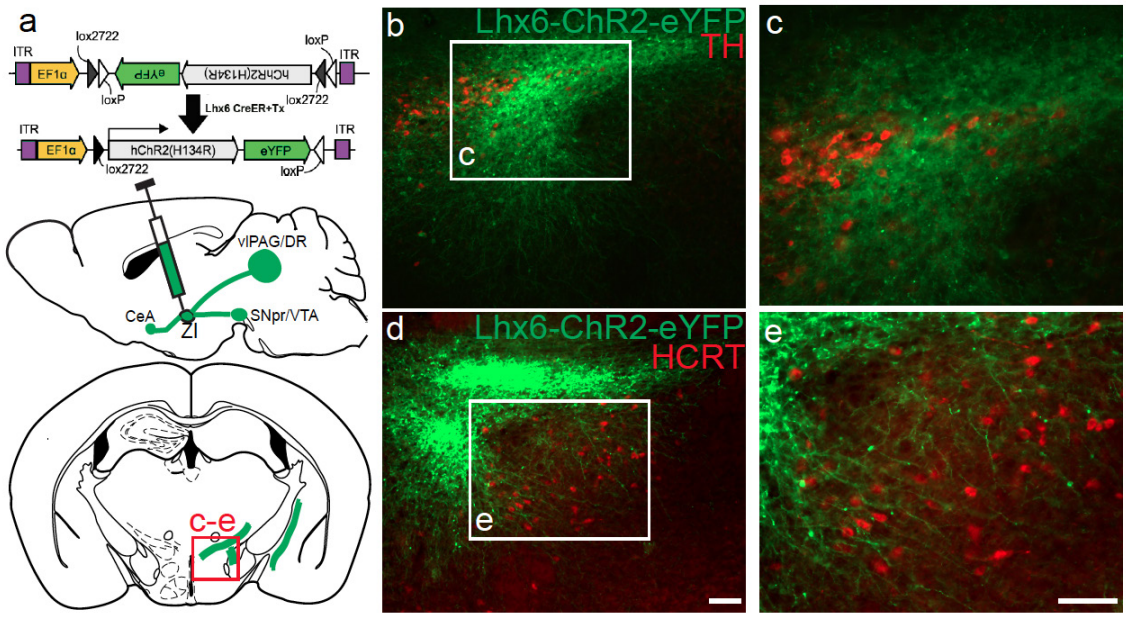

Figure 3.3.1 Lhx6-expressing neurons locally project to HCRT-expressing neurons in the lateral hypothalamus (a) Schematics of ChR2-eYFP virus construct and virus injection site in the ZI of Lhx6-Cre line. (b-e) Distribution of ChR2-eYFP injected Lhx6+ neurons (green) in the ZI (b, d) and neural projections of Lhx6+ neurons in the lateral hypothalamus (LH, k). TH immunostaining (red) was used to demarcate A13 dopaminergic neurons in the ZI (b), and hypocretin (HCRT, red) was used to demarcate the LH (d). Magnified images of the ZI and LH are shown in c, e respectively. Note that Lhx6+ neurons in the ZI project around HCRT-expressing neurons in the LH (d). Scale bar = 100 μm.

A limited number of selective long-distance projections were also observed. A small ascending projection to the central nucleus of amygdala was seen (Fig. 3.3.2), along with much more extensive descending projections to monoaminergic midbrain and hindbrain populations. These include pars compacta of the substantia nigra, the ventral tegmental area and the dorsal raphe nucleus (DR). Substantial descending projections were also observed to the ventrolateral periaqueductal gray (vlPAG) (Figure 3.3.2). Essentially identical results were observed following transduction of Lhx6-Cre mice (Fig. 3.3.2; data not shown). These targets overlap substantially with previously reported projections of GABAergic ZI neurons16 (Fig. 3.3.3 a-h), but differ in that no projections

to thalamus are observed . Pvalb-expressing GABAergic ZI neurons, in contrast, project extensively to the thalamus, but not to LH or midbrain targets of Lhx6+ cells (Fig. 3.3.3 i-p). It seems clear that hypothalamic Lhx6-expressing neurons postsynaptically target wake-promoting cells in different brain regions, which provides us the direction for functional studies for hypothalamic Lhx6-expressing neurons, which have primarily focused on sleep/wake cycle regulation.

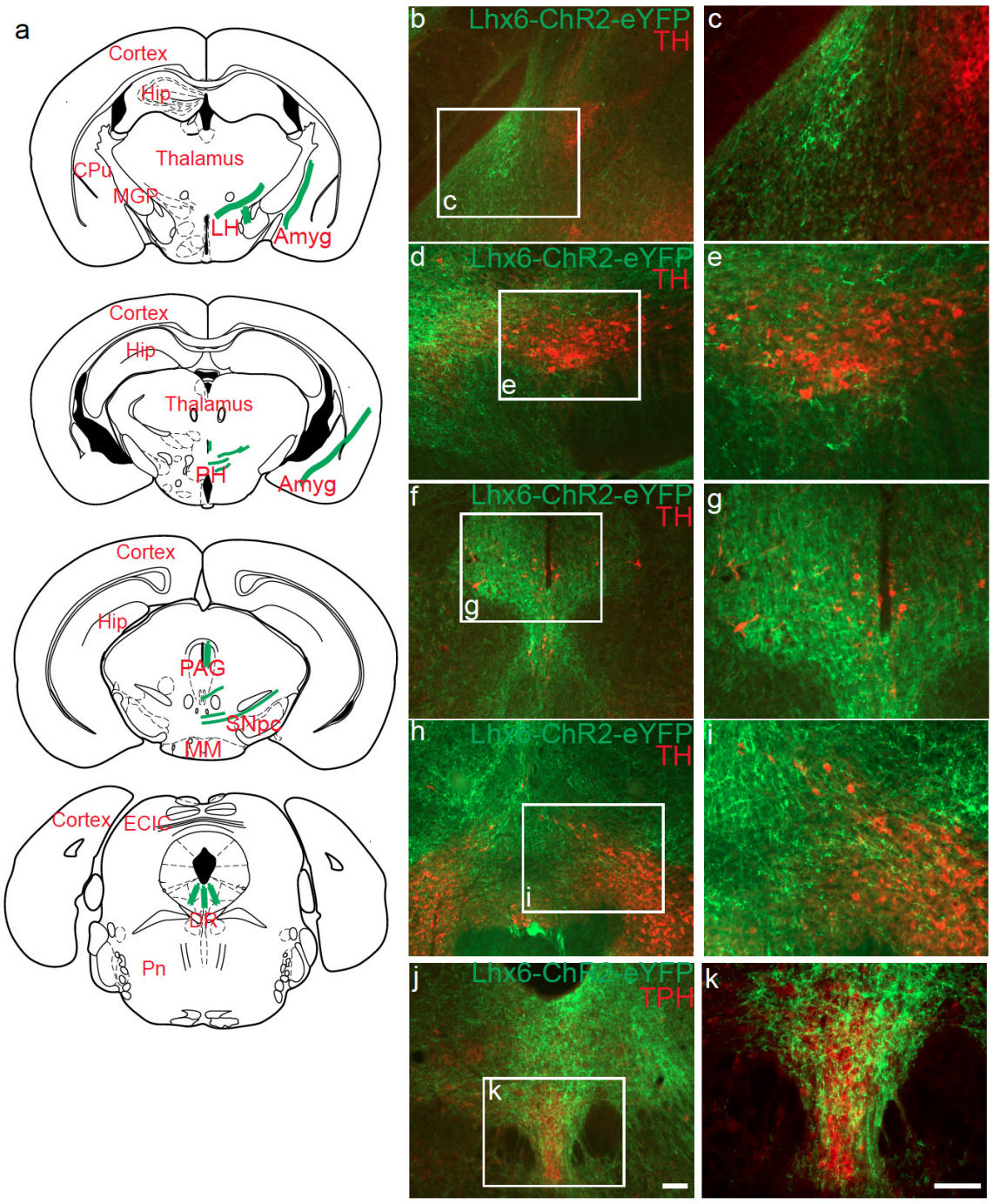

Figure 3.3.2 Additional data showing mapping of neural projection sites of Lhx6-expressing neurons in the ventral of Zona incerta.(a) Schematics showing neural projection sites of Lhx6+ neurons in the ZI across multiple brain regions after ChR2-eYFP virus injection into the ZI of Lhx6-Cre line. Amyg = amygdala, CPu = caudate putamen, DR = dorsal raphe nucleus, ECIC = external cortex of the inferior colliculus, Hip = hippocampus, LH = lateral hypothalamus, MGP = medial globus pallidus, MM = mammillary nucleus, PAG = periaqueductal gray, PH = posterior hypothalamus, Pn =

paranigral nucleus, SNpc = substantia nigra. (b-k) Representative images of eYFP-positive axonal processes of Lhx6-+ neurons of the ZIv (green) in amygdala (b), substantia nigra (d), periaqueductal gray (PAG) (f), ventral tegmental area (VTA) (h), and dorsal raphe nucleus (DR)(j). TH (red) immunostaining was used to demarcate amygdala, substantia nigra, PAG, and VTA in b, c, d, e, f, g, h, and i, and TPH (red) immunostaining was used to demarcate DR in j and k. Magnified images of b, d, f, h, and j are shown in c, e, g, i, and k respectively. Scale bar = 100 µm.

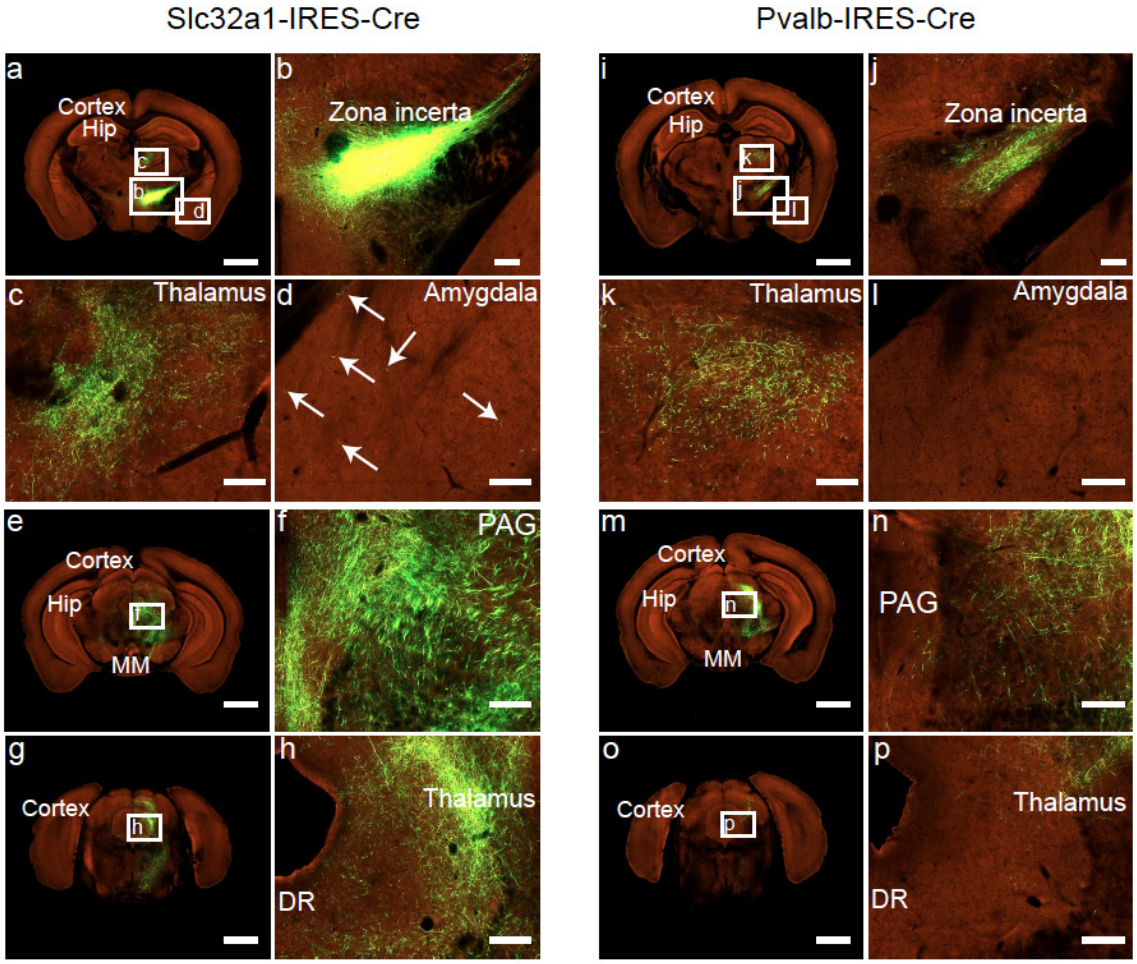

Figure 3.3.3 Projection sites of Slc32a1 and Pvalb-expressing cells in the ZI.

(a, e, g) Low-powered images of Slc32a1-Cre mouse injected with flexed rAAV-eGFP in ZI. High-powered images demonstrate infection in ZI and LH (b), central thalamus (c, f), amygdala (d), and PAG (h). White arrows indicate sparse GFP+ processes in (d). (i, m, o) Low-powered images of Pvalb-Cre mouse injected with flexed

rAAV-eGFP in ZI. GFP+ processes are detected in ZI (j) and central thalamus (k, n). No signal is detected in amygdala (l), while very little signal is seen in PAG (p). Amyg = amygdala, DR = dorsal raphe nucleus, Hip = hippocampus, MM = mammillary nucleus, PAG = periaqueductal gray. All data was obtained from Allen Brain Atlas Mouse Connectome Project. Experiment number 17106613 for Scl32a1-IRES-Cre and 301539438 for Pvalb-IRES-Cre. Scl32a1-IRES-Cre (section 73 (a-d), section 58 (e-f), section 44 (g-h)). Pvalb-IRES-Cre (section 68 (i-l), section 60 (m-n), section 45 (o-p)).

In this chapter, we characterized the developmental functions of Lhx6 in thehypothalamus. Unlike Lhx6-expressing neurons in the cortex, hypothalamic Lhx6-expressing neurons do not undergo long-range tangential and Lhx6 is essential for the survival. In addition, hypothalamic Lhx6-expressing neurons send both local and long-range projections. These postsynaptic targets of Lhx6-expressing neurons in the hypothalamus provided us to hypothesize that hypothalamic Lhx6-expressing neurons might be involved with sleep/wake cycle regulation. The next chapter will test the behavioral functions of hypothalamic Lhx6-expressing neurons.

Chapter 4. c-Fos functional screening for hypothalamic Lhx6-expressing neurons

As described in Chapter 1, most studies of hypothalamic neurons focus on their role in regulating innate behaviors. In the previous chapter, we looked at the markers, locations and postsynaptic targets of hypothalamic Lhx6-expressing neurons, and we found some clues which directed us to hypothesize hypothalamic Lhx6-expressing neurons might be involved with sleep/wake regulation. To characterize this further, we first applied immunohistochemical staining for c-Fos, an immediate early gene that is a faithful marker of neuronal activation, to determine what behavioral states activated hypothalamic Lhx6 neurons. In addition to sleep/wake behavior testing, we ran many other behavior paradigms. We observed robust and selective differences in Lhx6 neuronal activity in during periods of elevated sleep pressure in the zona incerta, and not in other hypothalamic Lhx6-expressing neurons.

4.1 Many different behavior paradigms do not selectively activate Lhx6-expressing neurons in hypothalamus

To screen out the potential behavior functions for hypothalamic Lhx6-expressing neurons, we conducted various behavior paradigms and c-fos staining. Since Lhx6-expressing neurons are located in the zona incerta, which plays an important role in somatosensory processing, we tested whether whisker stimulation might activate ZI Lhx6-expressing neurons. Further, since the posterior hypothalamus has been reported to

play a role in thermoregulation, we placed mice into cold room for 30 mins and checked c-fos staining. We also also fasted mice for 24 hours as to check their hunger behavior. We placed bobcat urine into animal cages to induce innate fear response, which is also modulated by neurons in the posterior hypothalamus, which resulted in immediate cessation of movement upon sensing the bobcat urine smell. However, none of the behavior paradigms resulted in selective activation of c-Fos expression in hypothalamic Lhx6-expressing neurons.

4.2 Zona incerta (ZI) Lhx6-expressing neurons are highly activated with high sleep pressure at Zeitgeiber Time 0 (ZT0)

Both sleep probability and sleep pressure are highest at the start of the light phase in nocturnal animals such as mice [94]. If hypothalamic Lhx6-expressing neurons are sleep-promoting, we would predict they will be most active at the time of highest sleep (lights on). We tested this by assessing immunohistochemical colocalization of c-fos and eGFP staining in the ZI of Lhx6-eGFP mice that were maintained on 14:10 hr light:dark cycle, we identified that c-fos expression was elevated in Lhx6+ ZI neurons at ZT0 (lights on) relative to ZT14 (lights off) (Figure.4.2.1a-e). Based on these results, it appears that ZI Lhx6-expressing neurons are most active at times of high sleep pressure. We can hypothesize that ZI Lhx6-expressing neurons are sleep-promoting.

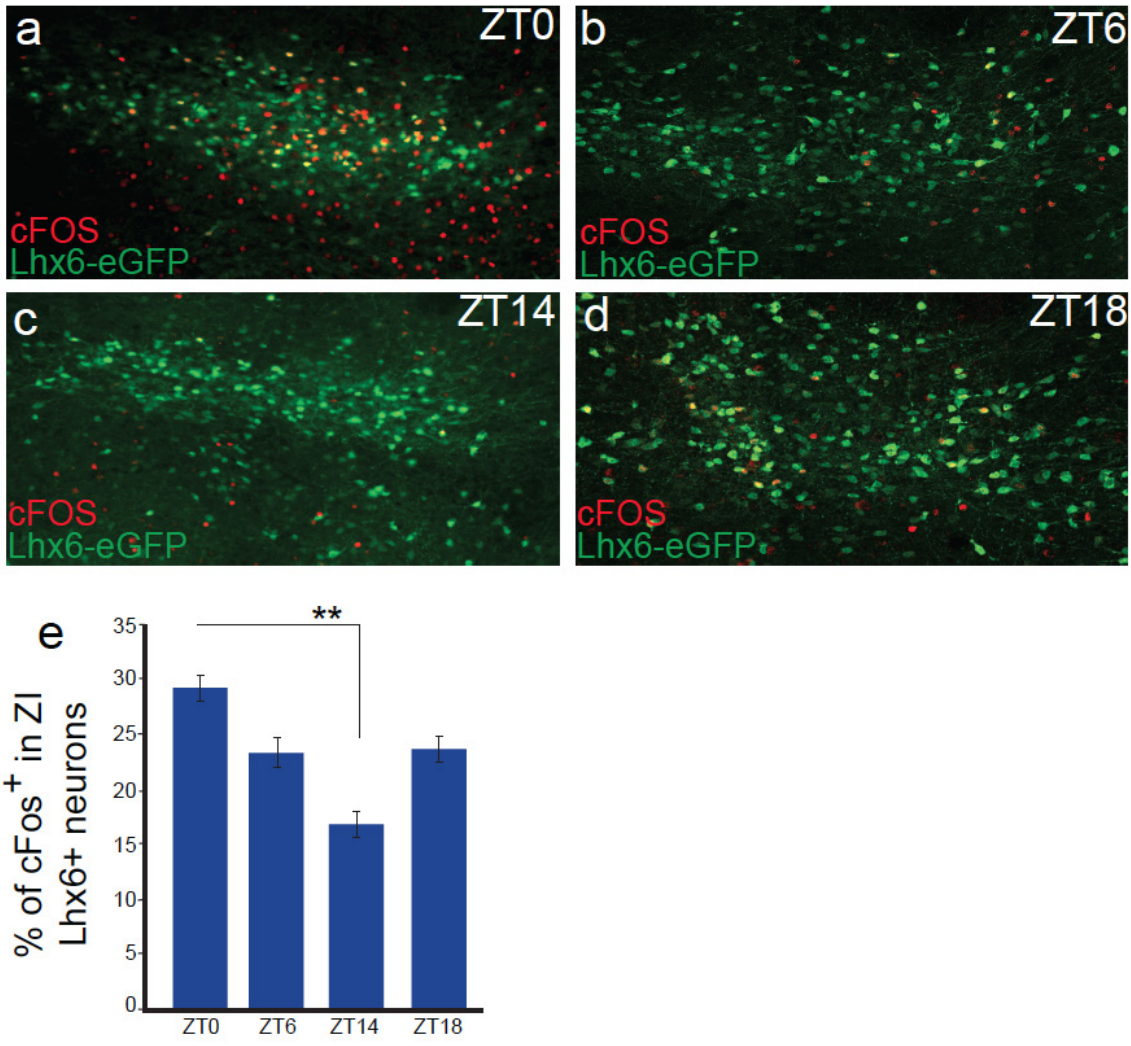

*Figure 4.2.1 The activity of Lhx6-expressing neurons in the ZI is activated by sleep pressure. Representative images of cFOS immunostaining (red) and Lhx6-eGFP expression (green) in the ZI across Zeitgeber time (ZT) – ZT0 (a), ZT6 (b), ZT14 (c), ZT18 (d), Scale bar = 100 µm. Bar graphs show the percentage of cFOS+ Lhx6+ neurons in the ZI across ZT (e) *= P < 0.05, ** = P < 0.01, linear mixed-effect model fit by REML; P=0.0367 (e), Two tailed one-way ANOVA. N=4 mice in each group, 4 brain sections were analyzed bilaterally for each mouse.*

4.3 Zona incerta Lhx6-expressing neurons are sensitive to sleep pressure when sleep deprived or sleep recovered

Since ZI Lhx6-expressing neurons are most activate during the time of day with highest sleep pressure, we tested whether induction of artificial sleep pressure through sleep deprivation could also activate ZI Lhx6-expressing neurons. To sleep deprive the mice, we kept the mice awake by touching the animals gently with a small brush and stimultted them with novel toys. This procedure lasted for 6 hours from ZT0 (7am) to ZT6(1pm). We also performed an analysis of sleep deprivation combined with recovery, in which the mice were allowed to sleep for one hour after the same 6 hours sleep deprivation. We observed that both sleep deprivation and sleep deprivation combined with recovery sleep significantly increased c-fos expression in Lhx6+ ZIv neurons (Fig. 2k-m), demonstrating that these neurons were activated by both sleep itself and high sleep pressure. These data further highlight that Lhx6-expressing neurons in the ZI could potentially function as sleep-promoting neurons.

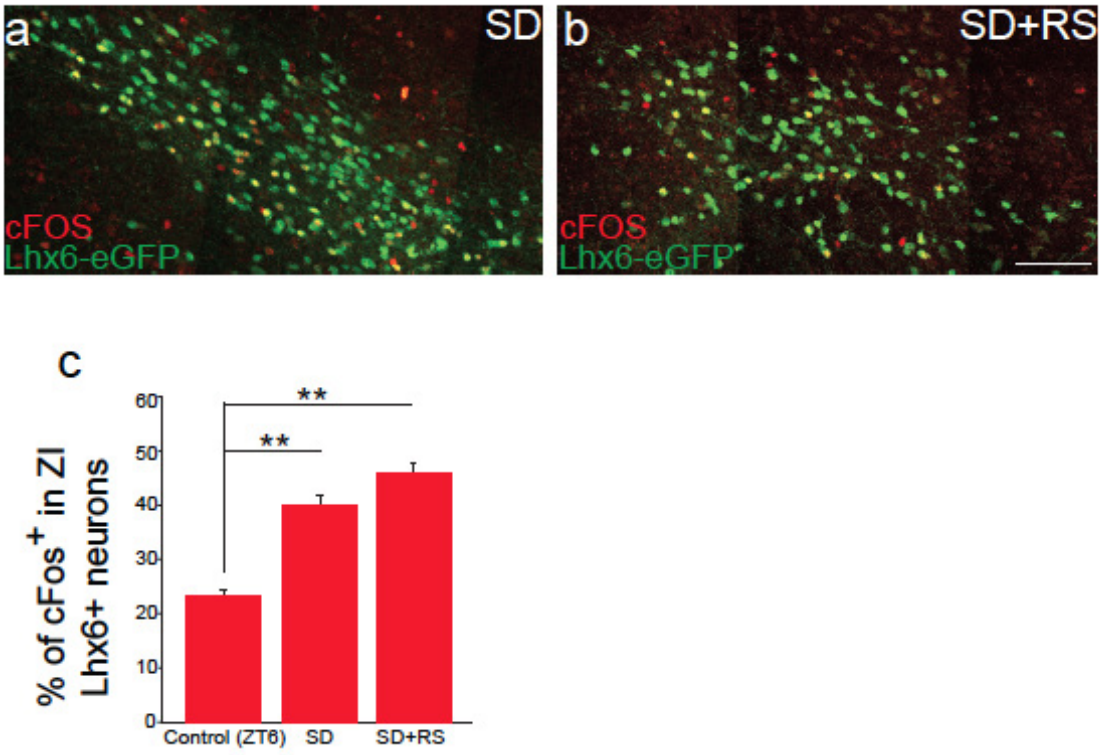

*Figure 4.3.1 The activity of Lhx6-expressing neurons in the ZI is activated by sleep deprivation and recovery. Representative images of cFOS immunostaining (red) and Lhx6-eGFP expression (green) in the sleep-deprived (a) and sleep-deprived with recovery sleep (b), Scale bar = 100 μm. Bar graphs show the percentage of cFOS+ Lhx6+ neurons in the ZI across ZT (c) *= P < 0.05, ** = P < 0.01, linear mixed-effect model fit by REML; P=0.0383 (c), Two tailed one-way ANOVA. N=4 mice in each group, 4 brain sections were analyzed bilaterally for each mouse.*

In summary, to study the potential function of hypothalamic Lhx6-expressing neurons, we first applied c-fos staining to identify which specific behavior paradigm can activate the cells. We found out ZI Lhx6-expressing neurons were highly activated by sleep pressure, and that ZI Lhx6-expressing neurons are potentially sleep-promoting. To direct demonstrate this, I will describe genetic and chemogenetic experiments in the next chapter which demonstrate that ZI Lhx6 neurons are both necessary and sufficient to promote sleep sleep in the next chapter.

Chapter 5. Sufficiency and necessity of zona incerta Lhx6-positive neurons' role in sleep/wake regulation

These studies have begun to shed light on the physiological functions of hypothalamic Lhx6-expressing neurons, in particular neurons located in the zona incerta (ZI). From our c-fos staining experiments, we knew that sleep pressure can activate ZI Lhx6-expressing neurons. To prove that ZI Lhx6-expressing neurons are involved in sleep/wake regulation, we have conducted both intersectional genetic and chemogentic experiments to demonstrate that ZI Lhx6 neurons are both necessary and sufficient to promote sleep.

5.1 Conditional knockout of Lhx6 in hypothalamus results in sleep reduction

We observed that straight Lhx6 knock-out mice die at 3 weeks postnatal due to failure to wean properly, as previously described, and are not suitable for studying sleep physiology. However, intersectional Cre/lox studies can induce selective deletion of Lhx6 in the developing hypothalamus, which may be suitable for these studies. Since deletion of hypothalamic Lhx6 appears to lead to death of these cells, this allows a powerful and effective methods of determining whether hypothalamic Lhx6-expressing neuronal death can affect sleep behavior. To fulfill this, we have used Foxd1-Cre knock-in mice, as Foxd1 shows selective and widespread activity in prethalamic and hypothalamic and neuronal progenitors within the CNS (Figure 5.1.2 a)[95]. We used this line to generate Foxd1-Cre;$Lhx6^{lox/lox}$ mice. This resulted in a showed selective loss

of Lhx6 throughout the hypothalamus and ZI, relative to Foxd1-Cre;Lhx6$^{lox/+}$ controls as determined by immunostaining, while Lhx6 expression in telencephalic structures such as cortex and amygdala was preserved (Figure 5.1.1).

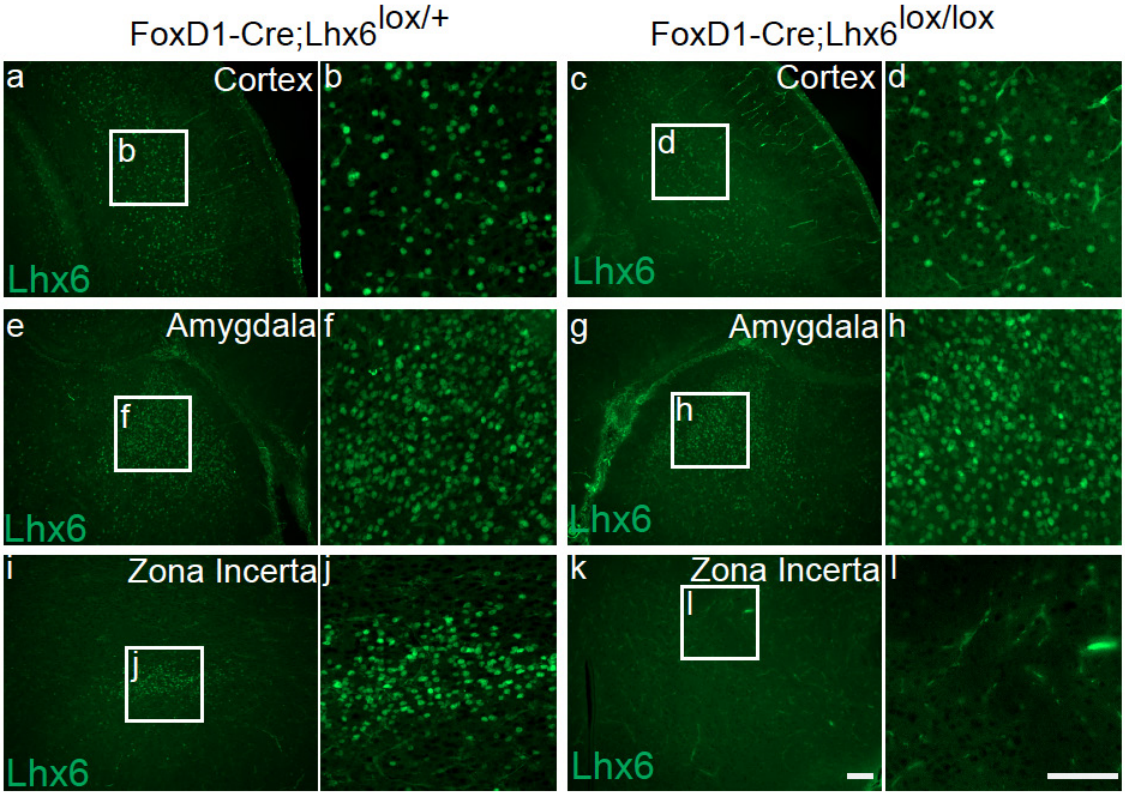

Figure 5.1.1. Lhx6 expression was selectively deleted in the diencephalon but kept in the telencephalon of Lhx6 conditional knockout Foxd1-Cre;Lhx6$^{lox/lox}$ (CKO) line.

Representative images of Lhx6-immunostaining (green) in the cortex (a-d), amygdala (e-h), and ZI (i-l) of control (a, b, e, f, i, j) and CKO (c, d, g, h, k, l) groups. Magnified images of a, c, e, g, i, and k are shown in b, d, f, h, j, and l respectively. Note that an absence of Lhx6 expression in the ZI of CKO group. Scale bar = 100 µm.

Foxd1-Cre;Lhx6$^{lox/lox}$ mice were viable, and no obvious developmental, anatomical, or behavioral defects were observed (Figure 5.1.2). These mice were then tested using a series of behavioral studies, including open field, light-dark preference,

elevated plus-maze, grip strength and rotarod, and no differences were observed relative to Foxd1-Cre;Lhx6$^{lox/+}$ controls. Analysis of wheel running behavior also revealed that circadian activity rhythms were normal (example showed in Figure 5.1.3).

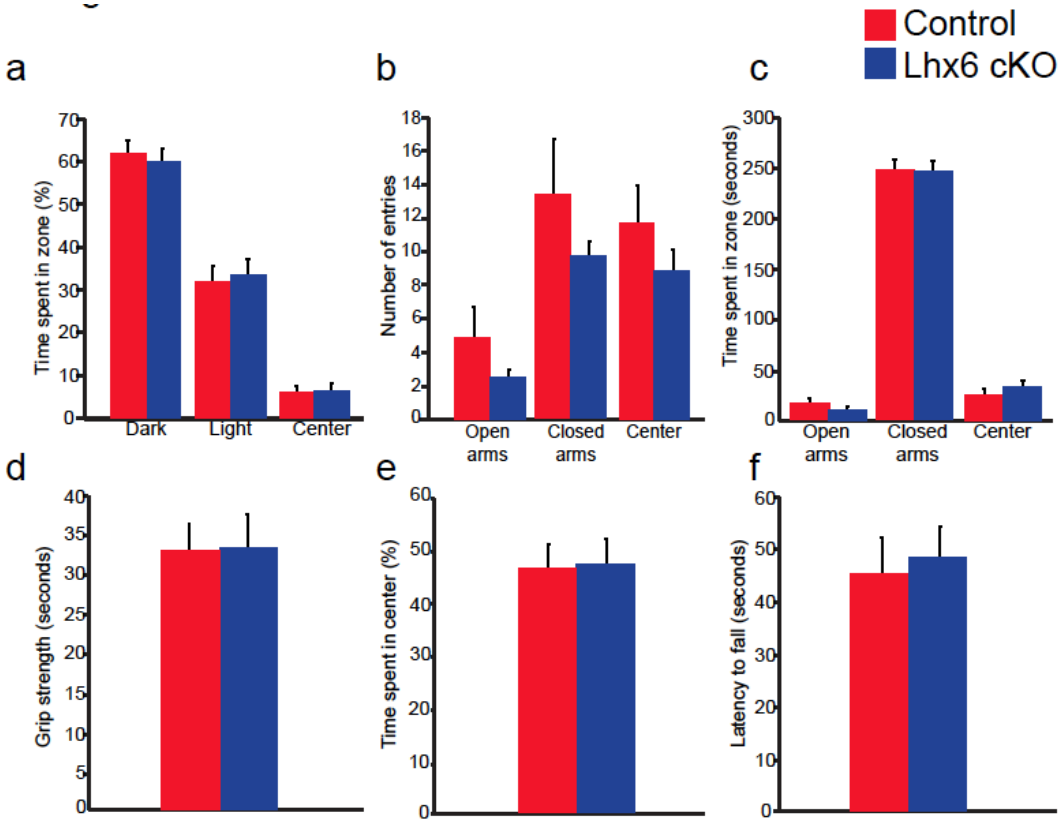

Figure 5.1.2 Lhx6 CKO mice do not display obvious behavioral abnormalities other than changes in sleep patterns.Light-dark preference test (a), elevated plus maze (b & c), grip strength (d), open field test (e), and rotarod (f) were conducted in control (red) and CKO (blue) groups, including analyzing dark. No significant difference, P>0.1 for all behavior readouts, two-tailed paired t-test, Wilcoxon-Mann-Whitney test. N = 8 control and 8 CKO mice.

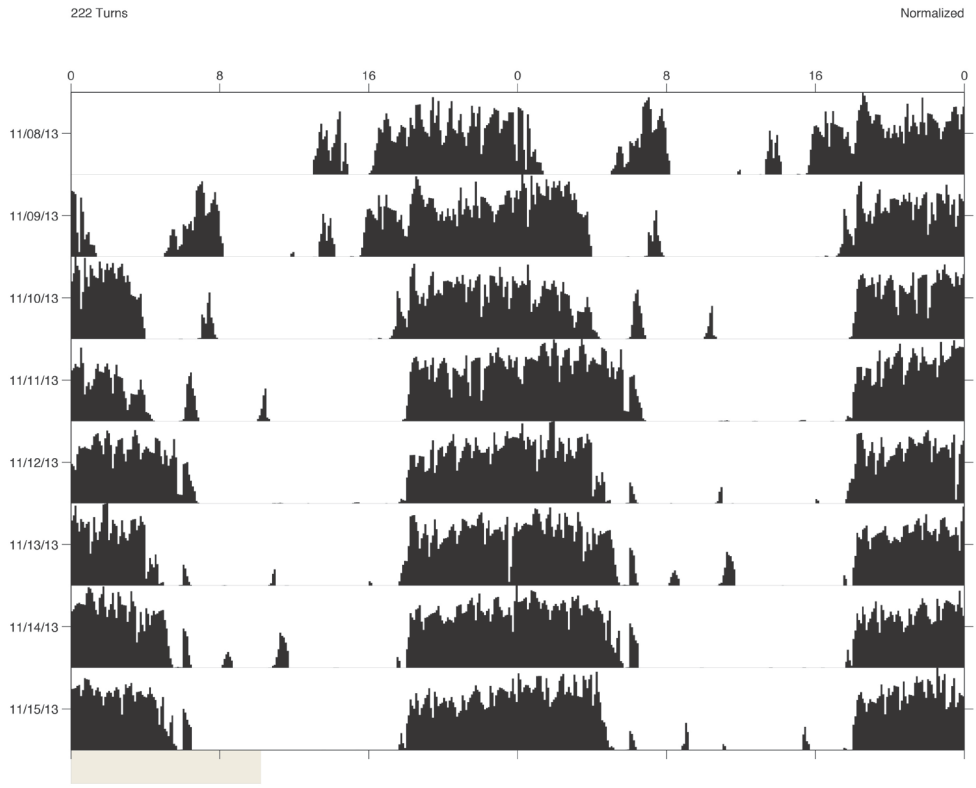

Figure 5.1.3 An example of wheel running behavior on Lhx6 conditional knockout mice with normal circadian rhythm.

To test sleep behavior, we implanted a EEG/EMG chip on the mouse skull for recordings (Figure 5.1.4). A tethered wire was connected to the chip for transferring the EEG/EMG signal to a preamplifier, which upload the data into a computer (Figure 5.1.5). The EEG/EMG traces and hands-on data sleep stages analysis was shown in Figure 5.1.6. All the sleep behavior experiment was conducted this manner.

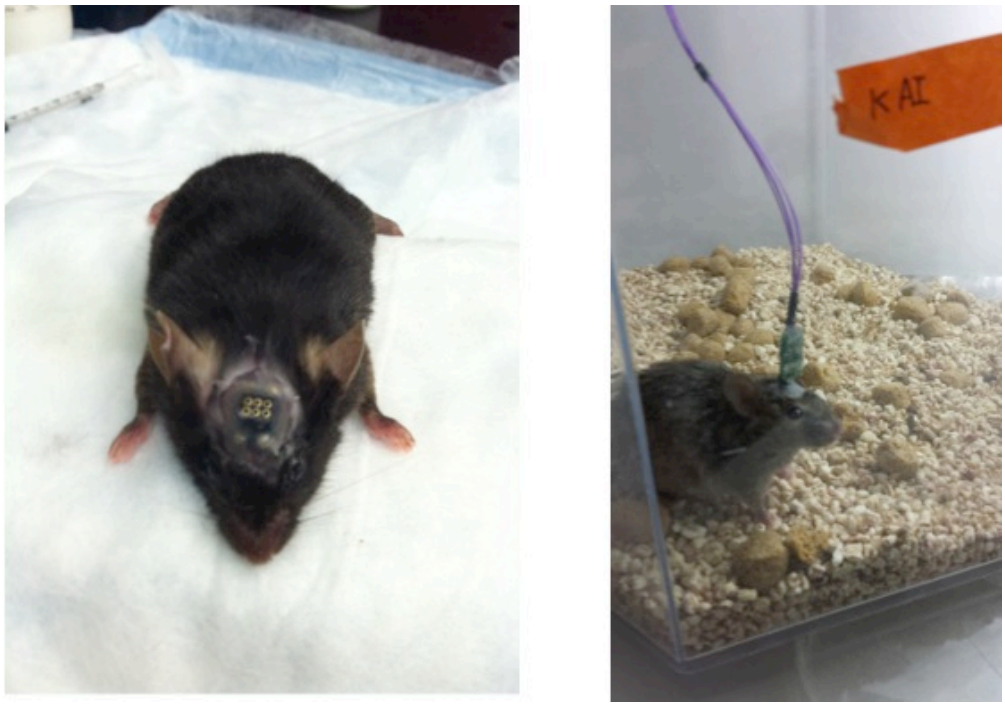

Figure 5.1.4 EEG/EMG implantation surgery on mouse (left) and wire tethered connected to a preamplifier (right).

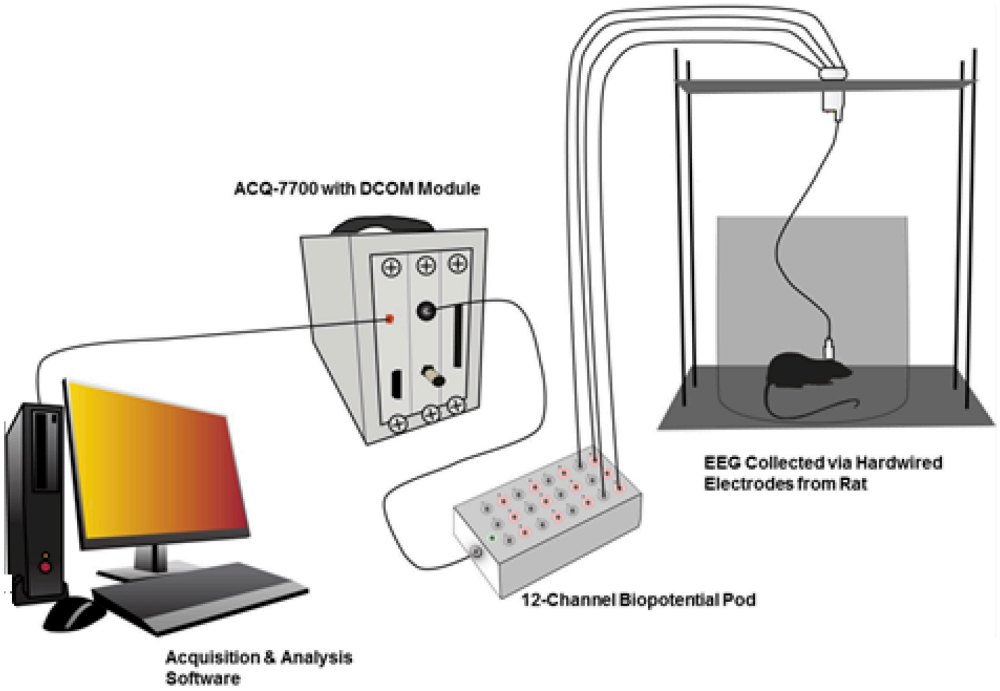

Figure 5.1.5 schematic map showing how to record EEG/EMG signals from DSI website https://www.datasci.com/solutions/neuroscience/sleep-research

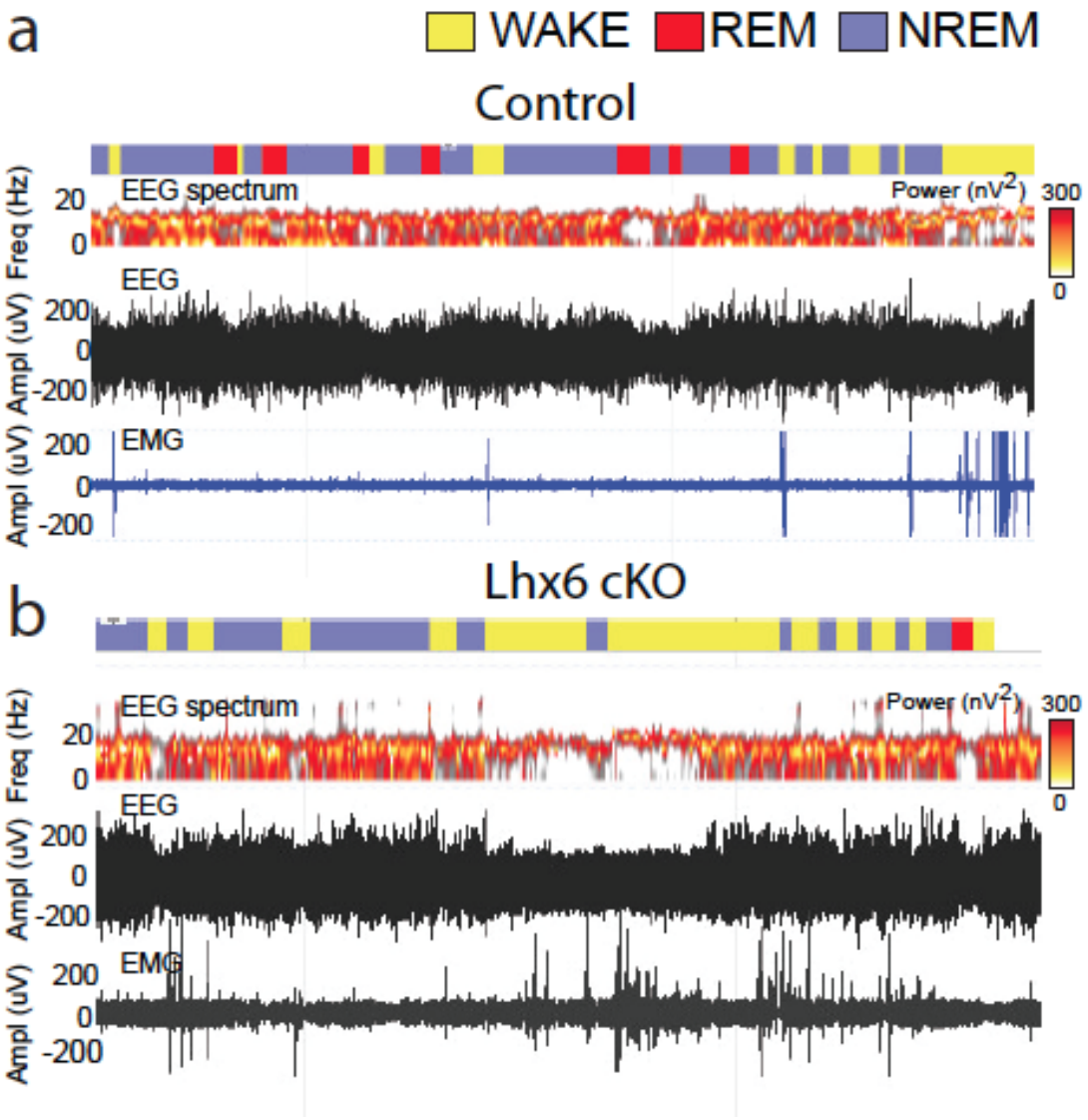

Figure 5.1.6 EEG/EMG example traces and data analysis. (a) control example, the upper colorful line was hands-on labeling for sleep stages, WAKE(yellow), REM(red) and non-REM(purple); 2nd line, spectrum of EEG signal; 3rd line, raw EEG signal; bottom line, raw EMG signal (b) Lhx6 conditional knockout example.

A blinded analysis of EEG and EMG data obtained from adult male *Foxd1-Cre;Lhx6*$^{lox/lox}$ mice revealed a highly significant increase in the fraction of time spent awake, and a corresponding reduction in both NREM and REM sleep (Figure 5.1.7 b-e).

Spectral analysis of *Foxd1-Cre;Lhx6*$^{lox/lox}$ mice revealed a strong reduction in the delta wave band, confirming the disruption of NREM sleep in these animals. However, the relative decrease in the fraction of REM sleep in mutant mice was even more dramatic than that of NREM. These data demonstrate that disrupting the differentiation of hypothalamic Lhx6-expressing neurons results in strong and selective decreases in sleep time.

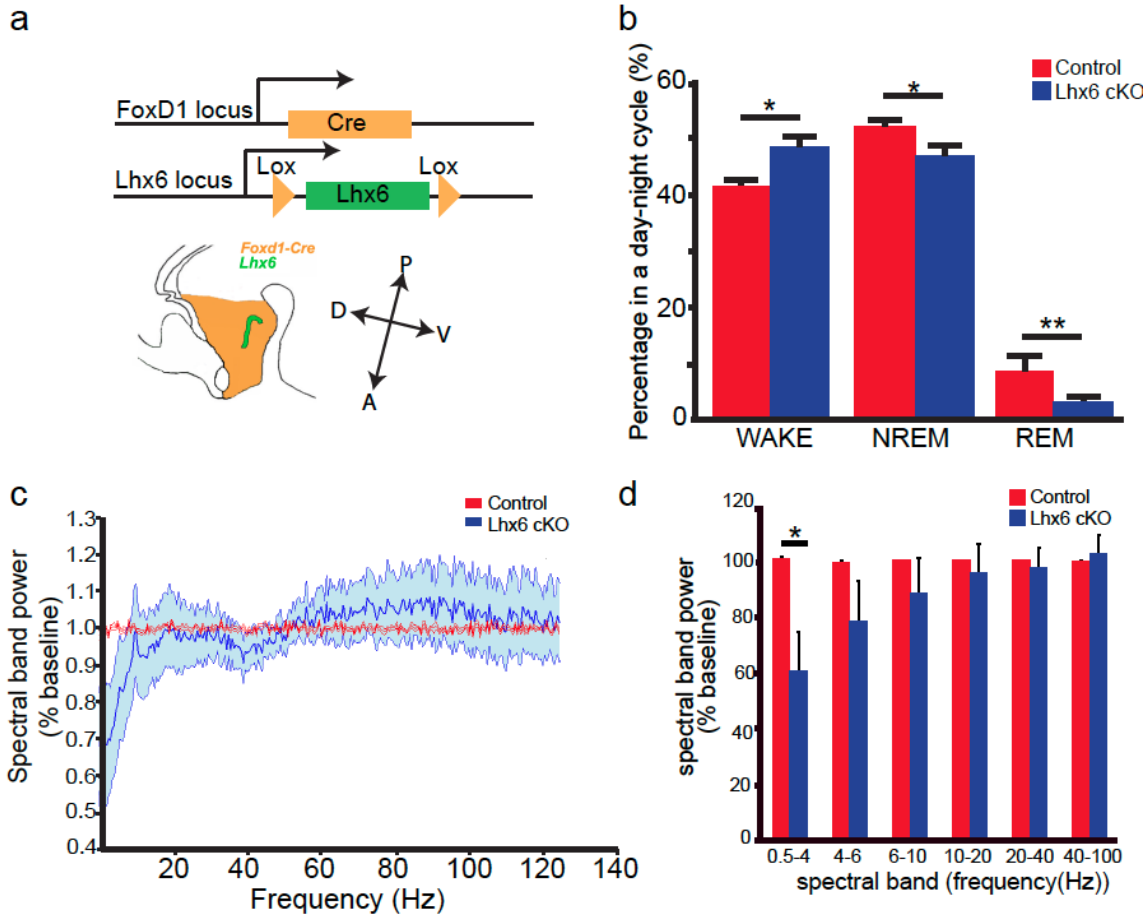

Figure 5.1.7 Selective loss of Lhx6 expression in the diencephalon reduces both NREM and REM sleep(a) Schematics showing generation of the diencephalic-specific Lhx6 conditional knockout (CKO) line by crossing Foxd1-Cre and Lhx6$^{lox/lox}$ *lines.(b) EEG analysis showing the percentage of day-night cycle - wake, NREM sleep, and REM sleep - in control (Foxd1-Cre;Lhx6*$^{lox/+}$*) and CKO groups. * = P < 0.05, ** = P < 0.01, two-tailed paired t-test, Wilcoxon-Mann- Whitney test. N = 8 control and 8 CKO mice. (c-d) A*

*graph showing fast Fourier transform (FFT) analysis of EEG power spectrum frequency of NREM stage of CKO line (blue) compared to the baseline (control, red)(c), with a bar graph showing collapsed EEG frequency data of spectrum band between control (red) and CKO group (blue)(d). * P < 0.05, two-tailed paired t-test, Wilcoxon-Mann-Whitney test. N = 8 control and 8 CKO mice.*

The conditional knockout of Lhx6 in the hypothalamus led to disruption in both REM and non-REM sleep, which demonstrated that hypothalamic Lhx6-expressing neurons are necessary to promote sleep. However, to sufficiently provide evidences to support that ZI Lhx6-expressing neurons can directly regulate sleep, we needed to directly manipulate the activity of ZI Lhx6-expressing neurons and observe sleep/wake activity.

5.2 Chemogenetic activation of zona incerta (ZI) Lhx6-expressing neurons promotes both REM and non-REM sleep

We applied DREADD-based chemogenetic analysis [96] to selectively activate and silence Lhx6+ ZI neurons to directly test whether Lhx6+ ZIv neurons were necessary and sufficient for induction of sleep. We first had to rule out any non-DREADD-based effect on sleep of clozapine N-oxide (CNO), the ligand used to activate DREADD constructs. When CNO was delivered to mice previously by bilateral stereotaxic injections of AAV9-FLEX-mCherry to the ZI, we observed no differences in EEG/EMG activity compared to mice injected with saline (Figure 5.2.1).

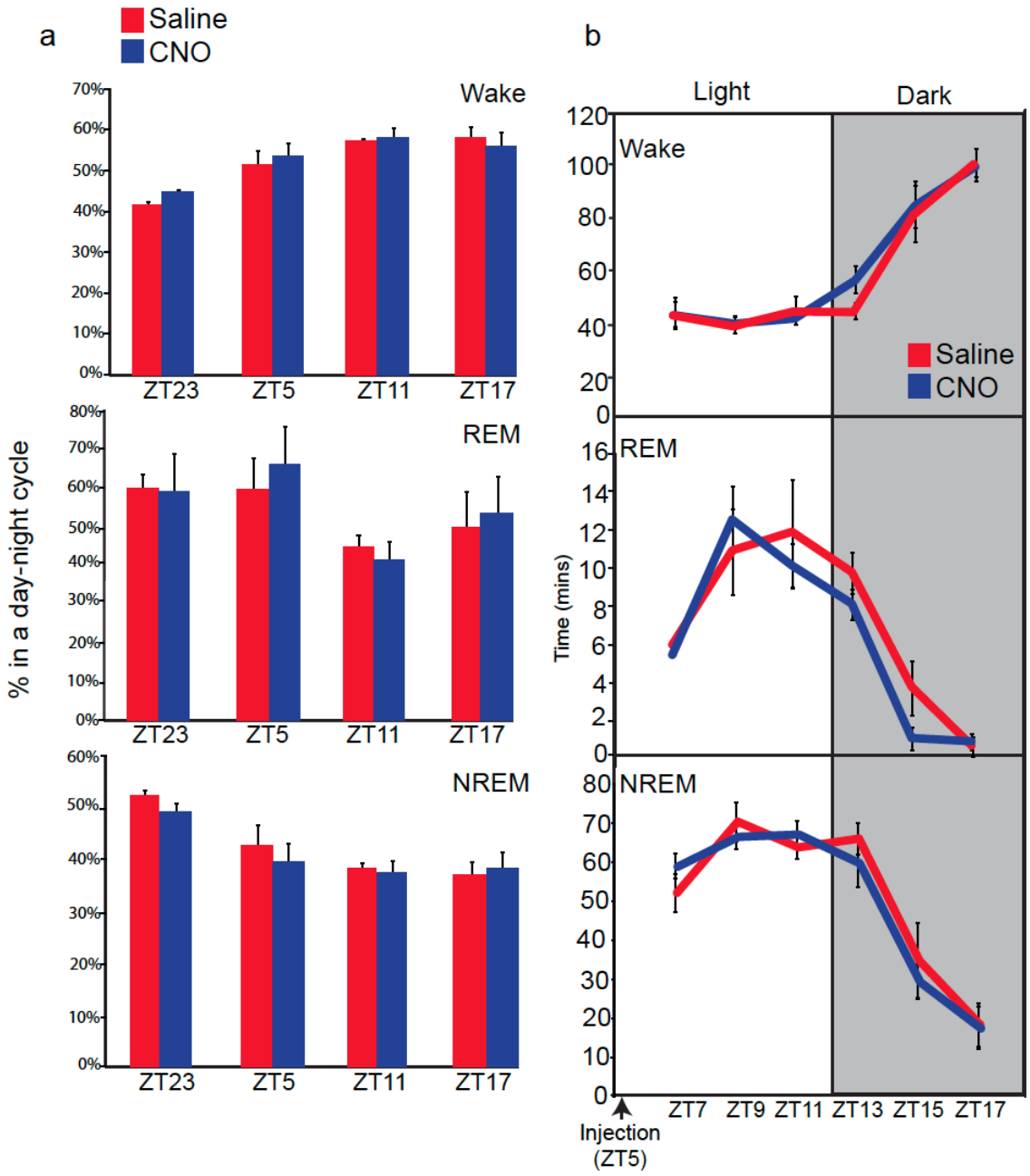

Figure 5.2.1 CNO does not affect sleep in Lhx6-Cre mice injected with AAV-mCherry in the ZI. (a) EEG analysis showing the percentage of day-night cycle with wake (top), NREM sleep (middle), and REM sleep (bottom) across ZT with saline- or CNO-injection in AAV9-mCherry group. (b) Graphs of EEG analysis showing amount of time spent across ZT in wake (top), NREM sleep (middle), and REM sleep (bottom) after injection of saline- or CNO-injection at ZT5 in AAV9-mCherry group.

This finding is in line with previous studies that have used DREADD-based approaches to study sleep [97, 98, 99]. We next conducted bilateral stereotaxic injections of AAV9 encoding the Cre-dependent hMD3q Gq-coupled activating DREADD to the ZI of Lhx6-Cre mice (Figure 5.2.2 a,b; Figure 5.2.3). After intraperitoneal injection of CNO, by c-Fos staining we observed robust induction of c-fos activity in transduced cells relative to vehicle after 1hr of injection, which can confirm successful DREADD activation of Lhx6+ neurons (Figure 5.2.4) by the Gq DREADDs. As a result, this DREADDs chemogenetic tools could allow us to test whether Lhx6+ ZIv neuron activation was sufficient to induce sleep by activation of ZI Lhx6 neurons. At all times tested except ZT23, when sleep pressure is highest, we observed a significant increase in time spent in REM during the 12 hrs after CNO injection. Meanwhile, significant decreases in wake time and increases in NREM sleep were observed following CNO administration at ZT5 and ZT11, with a strong increase in the delta band during NREM sleep (Figure 5.2.2 c,d; Figure 5.2.3). These effects were strongest between 2 and 8 hrs following CNO administration, and returned to baseline by 12hrs post-injection. A substantial increase in the delta band was observed during NREM sleep after CNO delivered at ZT5, between 2 to 4 hrs post-injection. Selective transduction of Lhx6+ ZI neurons was confirmed by postmortem examination of all tested animals in DREADDs experiments (Figure 5.2.5).

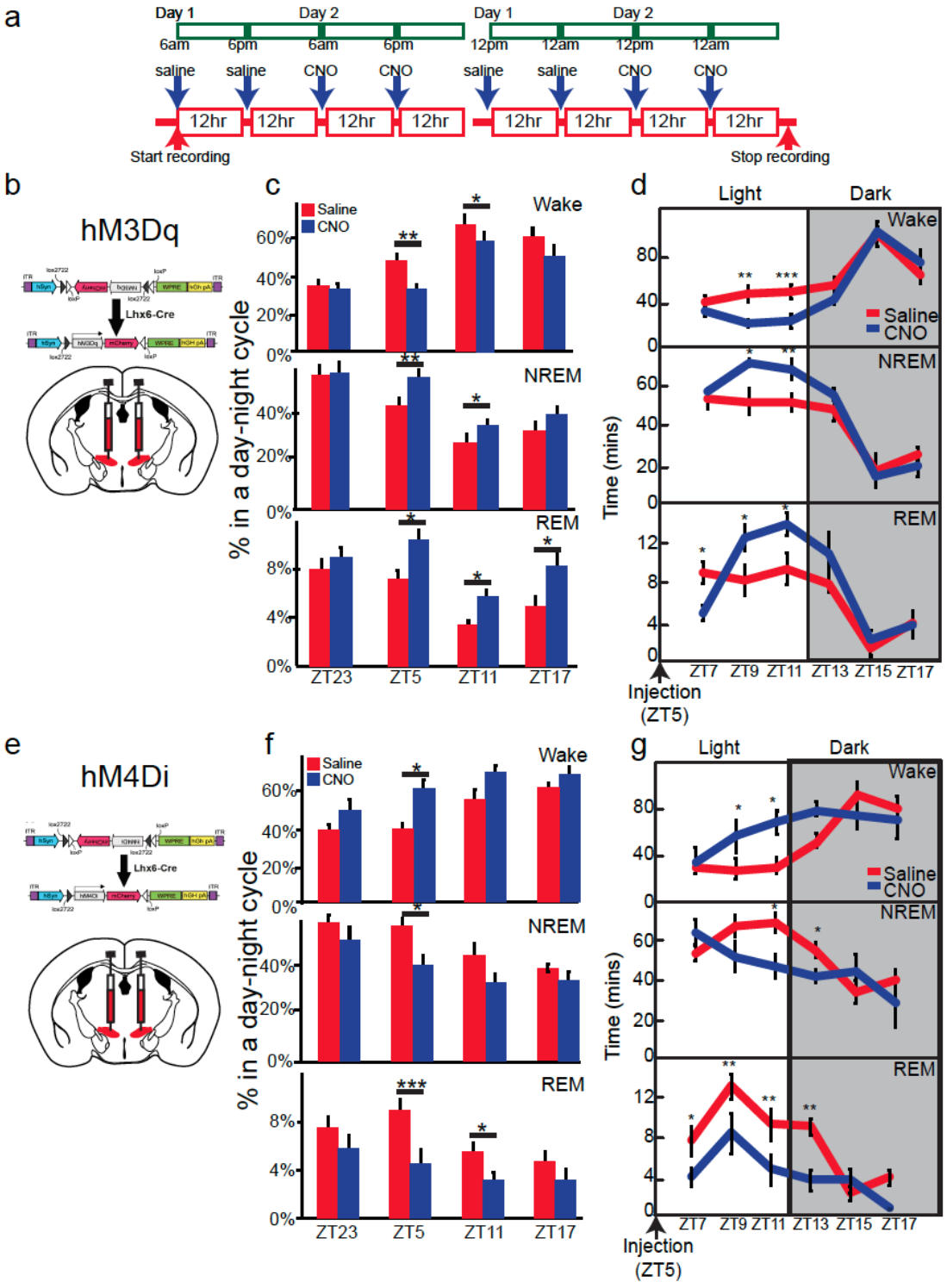

Figure 5.2.2 DREADD-dependent activation or inhibition of Lhx6-expressing neurons in the ZI can induce or inhibit NREM and REM sleep(a) Schematics showing sleeping recording paradigm (EEG and EMG recording) with saline- or CNO-injection in hM3Dq (B-D) or hM4Di (E-G) groups. Each individual mouse is assayed under the conditions indicated.(b) Schematics showing hM3Dq-mCherry virus construct and injection of virus

*into the ZI of Lhx6-Cre line.(c) EEG analysis showing the percentage of time spent during the 12 hour post-injection interval in wake (top), NREM sleep (middle), and REM sleep (bottom) - across ZT with saline- or CNO-injection in hM3Dq groups. * =P < 0.05, ** = P < 0.01, two-tailed paired t-test, Wilcoxon-Mann-Whitney test. N = 8 mice. (d) Graphs of EEG analysis showing amount of time in wake (top), NREM sleep (middle), and REM sleep (bottom) after injection of saline- or CNO-injection at ZT5 in hM3Dq groups. * = P < 0.05, ** = P < 0.01, two-tailed paired t-test, Wilcoxon-Mann-Whitney test. N = 8 mice. (e) Schematics showing hM4Di-mCherry virus construct and injection of virus into the ZI of Lhx6-Cre line.(f) EEG analysis showing the percentage of 12-hour interval cycle with wake (top), NREM sleep (middle), and REM sleep (bottom) with saline- or CNO-injection in hM4Di groups. * < 0.05, ** = P < 0.01, *** = P <0.001, two-tailed paired t-test, Wilcoxon-Mann-Whitney test. N = 8 mice.(g) Graphs of EEG analysis showing amount of time spent during the 12 hour post-injection interval in wake (top), NREM sleep (middle), and REM sleep (bottom) after injection of saline- or CNO-injection at ZT5 in hM4Di groups. * = P < 0.05, ** = P < 0.01, two-tailed paired t-test, Wilcoxon-Mann-Whitney test. N = 8 mice.*

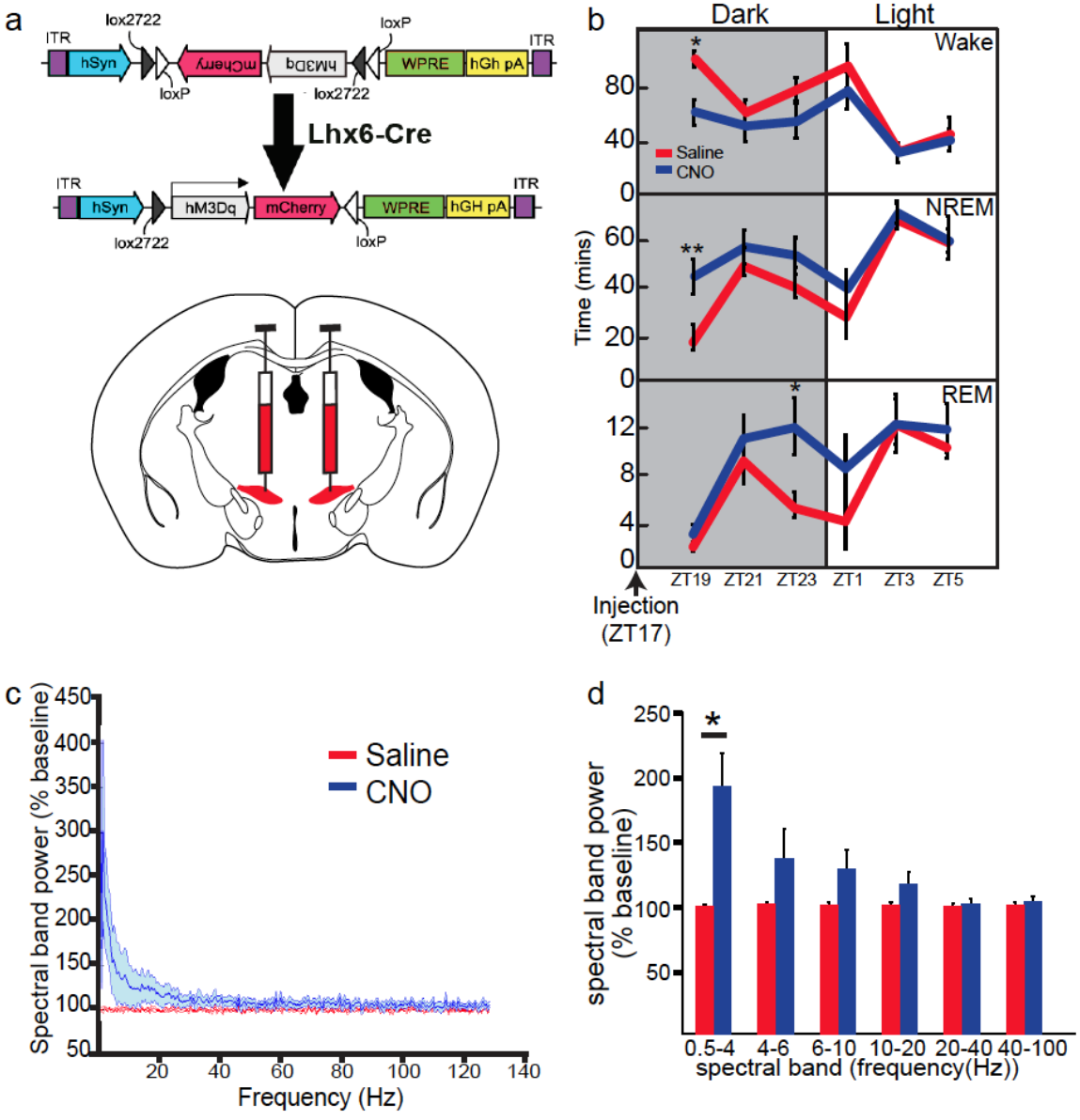

*Figure 5.2.3 Additional data from Gq DREADD-injected Lhx6-Cre mice (continuation from Figure 5.2.2).(a) Schematics showing the construct of AAV-hM3Dq virus and the injection site of virus into the ZI of Lhx6-Cre line. (b) Graphs of EEG analysis showing amount of time spent across ZT in wake (top), NREM sleep (middle), and REM sleep (bottom) after injection of saline- or CNO-injection at ZT17 in hM3Dq groups. * = P < 0.05, ** = P < 0.01, two-tailed paired t-test, Wilcoxon-Mann- Whitney test. N = 8 mice.*

(c-d) A graph showing fast Fourier transform (FFT) analysis of EEG power spectrum frequency of NREM stage of CNO-injected AAV-hM3Dq-infected mice (blue) compared to the baseline (saline-injection, red)(c), with a bar graph showing grouped EEG frequency data obtained from spectrum band analysis of saline- (red) and CNO-

*injected (blue) hM3Dq groups (d). * = P < 0.05, two-tailed paired t-test, Wilcoxon-Mann-Whitney test. N = 8 mice.*

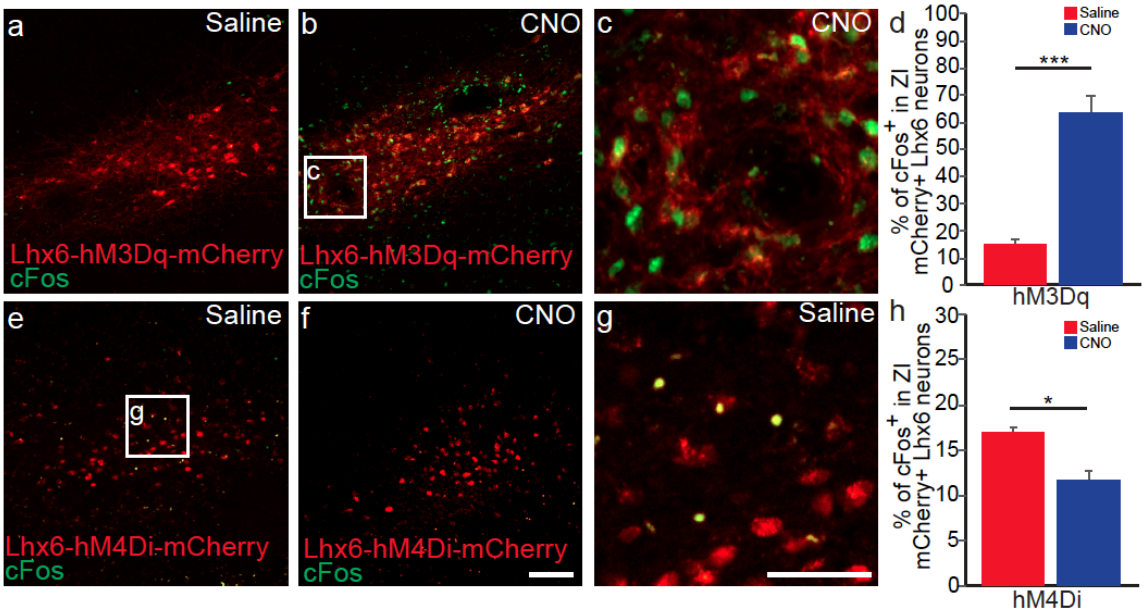

Figure 5.2.4 CNO activates c-fos expression in AAV-hM3Dq-injected Lhx6-Cre mice.

*(a-c) Representative images showing hM3Dq-mCherry expression (red) and cFOS immunostaining in the ZI of Lhx6-Cre line after saline (a) or CNO (b) injection. Magnified image of b is shown in c. Scale bar = 100 µm. (d) A bar graph showing the percentage cFos-immunostained neurons in hM3Dq-mCherry+ Lhx6-expressing neurons in the ZI. N = 4 mice/saline, N = 5/mice/CNO. *** = P < 0.001 (e-g) Representative images showing hM4Di-mCherry expression (red) and cFOS immunostaining in the ZI of Lhx6-Cre line after saline (D) or CNO (E) injection. Magnified image of B is shown in F. Scale bar = 100 µm. (h) A bar graph showing the percentage cFos-immunostained neurons in hM4Di-mCherry+ Lhx6-expressing neurons in the ZI. N = 3 mice/saline, N = 3/mice/CNO. * = P < 0.05.*

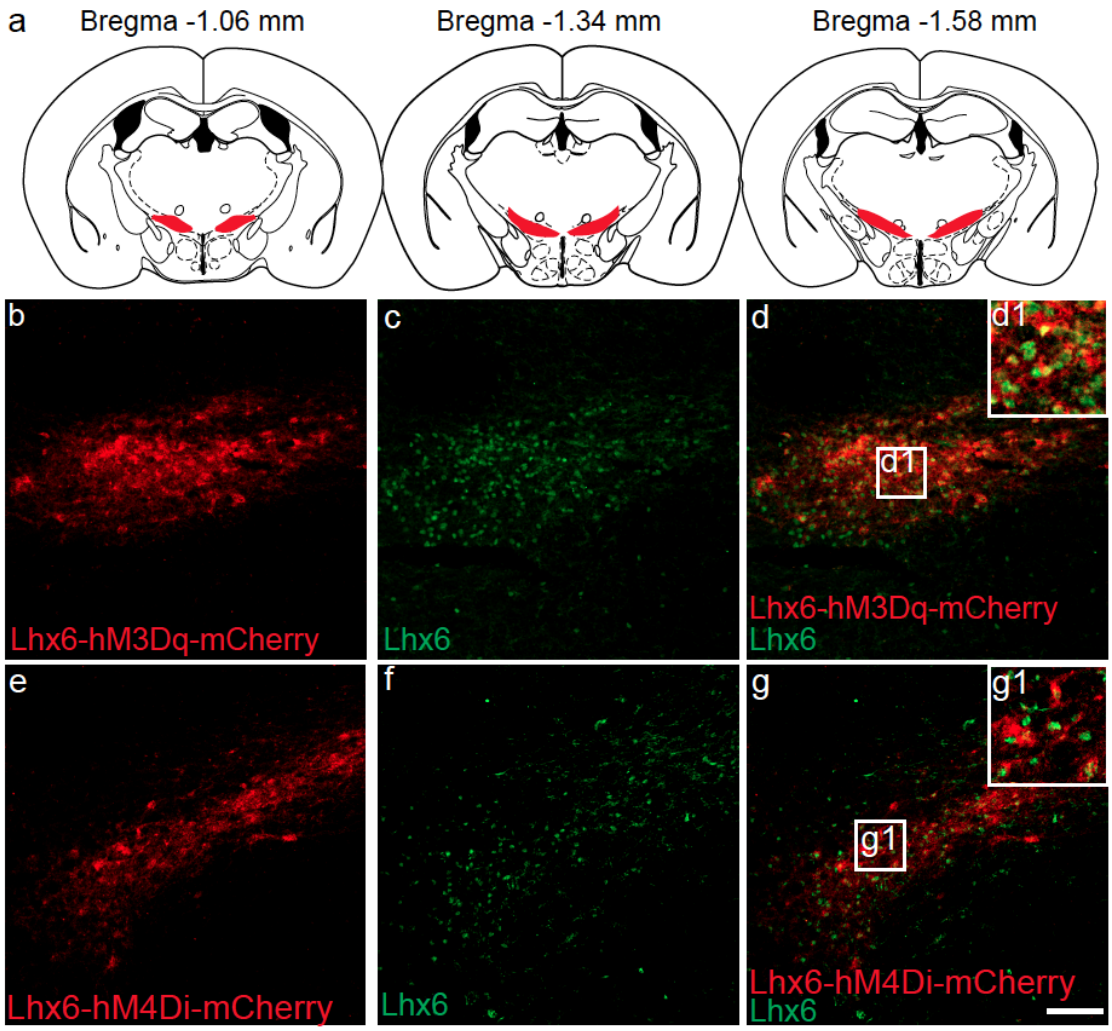

Figure 5.2.5 AAV-DREADD infection site in Lhx6-Cre mice.(a) Schematics showing the distribution of AAV-DREADD infection (red) across the full rostrocaudal extent of the ZI after AAV-DREADD was injected into the ZI of Lhx6-Cre line.(b-d) Representative images showing co-expression of hM3Dq DREADD infection in the ZI of Lhx6-Cre line (b, red) with Lhx6 immunostaining (c, green), and merged image of b and c is shown in d. Magnified image of d is shown in d1. Scale bar = 100 μm.(e-g) Representative images showing co-expression of AAV-hM4Di infection in the ZI of Lhx6-Cre line (e, red) with Lhx6 immunostaining (f, green), and merged image of e and f is shown in g. Magnified image of g is shown in g1. Scale bar = 100 μm.

5.3 Chemogenetic silencing of Zona incerta Lhx6-expressing neurons reduces both REM and non-REM sleep

After testing the effect by activation of ZI Lhx6-expressing neurons, we then examined the effect of silencing ZI Lhx6 neurons which can tell us whether Lhx6+ ZI neurons are necessary for sleep, after introducing the inhibitory Gi-coupled hM4Di DREADD to Lhx6+ ZIv neurons by bilateral stereotaxic injection (Figure 5.2.2 a,e; Figure 5.3.1).

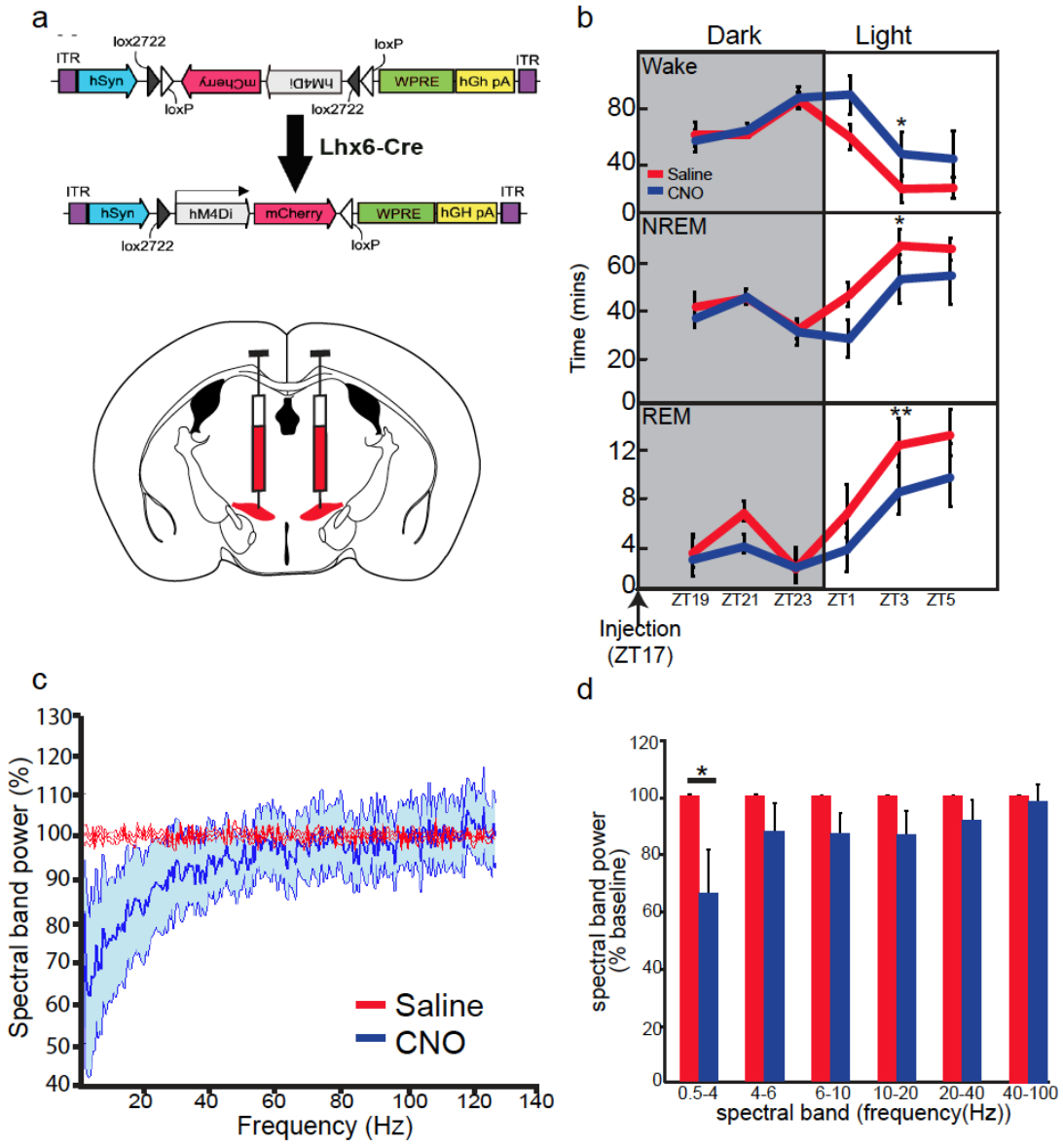

*Figure 5.3.1 Additional data from AAV-hM4Di-injected Lhx6-Cre mice (continuation from Figure 5.2.2).(a) Schematics showing the construct of AAV-hM4Di virus and the injection site of virus into the ZI of Lhx6-Cre line. (d) Graphs of EEG analysis showing amount of time spent across ZT in wake (top), NREM sleep (middle), and REM sleep (bottom) after injection of saline- or CNO-injection at ZT17 in hM4Di groups. * = P < 0.05, ** = P < 0.01, two-tailed paired t-test, Wilcoxon-Mann-Whitney test. N = 8 mice. (c-d) A graph showing fast Fourier transform (FFT) analysis of EEG power spectrum frequency of NREM stage of CNO-injected AAV-hM4Di (blue) compared to the baseline (saline-injection, red)(c), with a bar graph showing grouped EEG frequency data of spectrum band analysis between saline- (red) and CNO-injected (blue) hM4Di groups (d). * = P < 0.05, two-tailed paired t-test, Wilcoxon-Mann-Whitney test. N = 8 mice.*

Using a similar stimulation paradigm to that used for the activating DREADD, we observed a complementary sleep phenotype (Figure 5.2.2 f,g; Figure 5.3.1). Consistent with the Lhx6 conditional knockout results, CNO administration at ZT5 and ZT11 significantly reduced time spent in REM. A significant decrease in time spent in NREM, and corresponding increase in time spent awake, were also observed following CNO administration at ZT5 (Figure 5.2.2 f), with a strong decrease in the delta band during NREM sleep (Figure 5.3.1). CNO administered in the middle of the light phase at ZT5 resulted in a potent inhibition of both NREM and REM, and a corresponding increase in wake time, between 2 and 8 hours following injection (Figure 5.2.2 g). No significant change was seen in total time spent in wake, NREM or REM in the 12 hours following injection, when CNO was administered either in the middle or the end of the dark phase at ZT17 and ZT23 (Figure 5.3.1). However, when data were examined in two-hour intervals, decreases in NREM and REM and a corresponding increase in wake were observed only 8-10 hours following CNO administration, during the beginning of the light phase (Figure 5.3.1). This suggests that the sleep-promoting effects of Lhx6+ ZIv neurons may be confined to the light phase, and is consistent with our c-fos

immunostaining data demonstrating that these neurons are predominantly active during the light phase (Figure 4.2.1).

From Gq and Gi DREADDs chemogenetic experiments, we have demonstrated that ZI Lhx6 neurons are sleep-promoting. However, the mechanism by which this occurs is unclear, and is addressed in the next chapter.

5.4 Zona incerta Lhx6 neurons promote sleep by locally inhibiting hypocretin (Hcrt) neurons in the lateral hypothalamus (LH) through GABA

In Chapters 1~3, we observed that ZI Lhx6-expressing neurons are GABAergic interneurons, which can exert inhibitory action on other neuronal populations. As previously described, Hcrt neurons in the LH are adjacent to ZI Lhx6-expressing neurons. It is reasonable to hypothesize that ZI Lhx6-expressing neurons promote sleep by locally inhibiting Hcrt neurons. To demonstrate whether Lhx6+ neurons of the ZI directly inhibit Hcrt neurons, we applied optogenetics in combination with slice recordings. We generated Lhx6-Cre;Hcrt-eGFP mice, and selectively transduced ZI Lhx6-expressing neurons with AAV9 expressing FLEX-ChR2-mCherry (Figure 5.4.1 a). Using in slice electrophysiological recordings, we observed that transduced mCherry+ ZI Lhx6 neurons were efficiently activated by light pulses (Figure 5.4.1 b), and that LH Hcrt-eGFP neurons rapidly spiked in response to step current injection, making sure the slice optogenetics tool working on testing the inhibition from Lhx6 neurons to Hcrt neurons (Figure 5.4.1 c). In all of the LH Hcrt-eGFP neuron from which we recorded, we observed that light-dependent activation of transduced Lhx6 ZI neurons induced

inhibitory inward currents (Figure 5.4.1 d). The reason why we did see a depolarization-like inhibitory waveform is because the we kept a high concentration of Cl- inside the recording glass pipette. This inhibition was with an average latency of 1.5 ms, indicating probable direct inhibitory projections from the Lhx6 ZI neurons to the Hcrt LH neurons. However, all the inhibitory effects were not removed by application of ionotrophic glutamate receptor antagonists CPP and NBQX, but were completely blocked by the $GABA_A$ receptor antagonist SR95531 (Gabazine), but not by NBQX and CPP. Washout of SR95531 partially restored light-activated inhibitory inward currents (Figure 5.4.1 d-e). These experiments demonstrated that ZI Lhx6 neurons can inhibit hypocretin neurons via GABA directly.

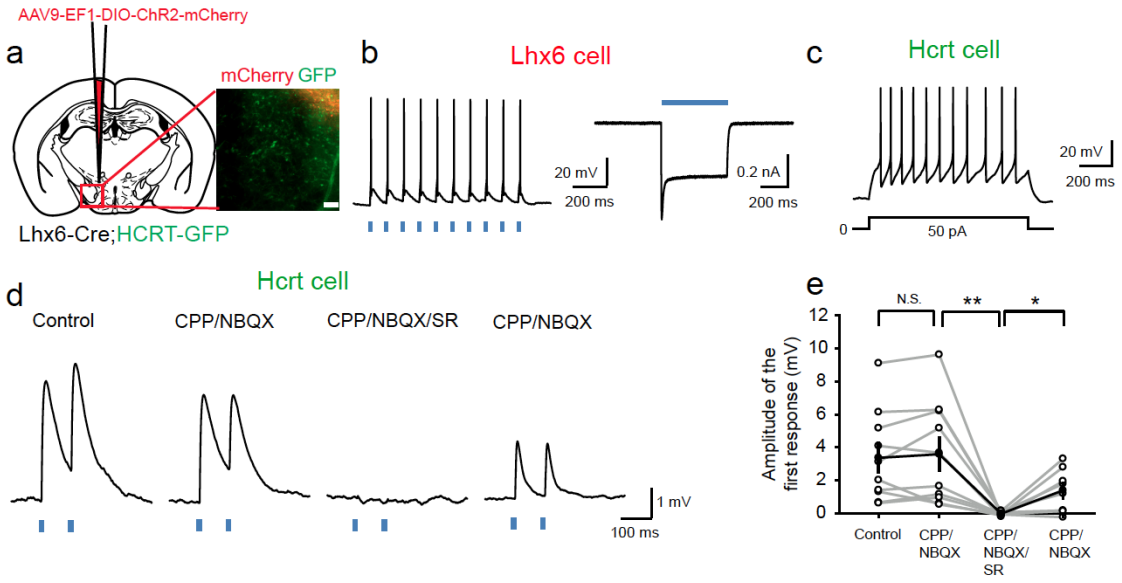

Figure 5.4.1 GABAergic Lhx6-expressing neurons in the ZI inhibit activity of HCRT-expressing neurons in the LH, and the activity of Lhx6-expressing neurons in the ZI is activated by sleep pressure.(a) Schematics showing injection of ChR2-mCherry virus into the ZI of Lhx6-Cre;HCRT-eGFP line, and a red box showing HCRT-expressing neurons (green) in the LH and ventromedial portion of the ZI with Lhx6+ neurons (red). Scale bar = 100 µm.(b) Representative images of a membrane potential (left), and current responses (right) of ChR2-mCherry-expressing, Lhx6+ neuron to blue light photostimulation (middle). Note that action potentials fire reliably to light pulses in a

current clamp mode (left) and 1s-long photostimulation results in continuous inward current in a voltage clamp mode (right).(c) Representative images of action potentials of Hcrt neurons in response to a step current injection (right).(d) Representative traces of membrane potential responses of a Hcrt neuron to photostimulation under glutamate receptor blockers (CPP/NBQX), with and without GABAAR blocker (SR95531). Note that high concentration of chloride in the internal solution evoked depolarizing responses in response to inhibitory input. (e) A summary graph of amplitudes of the first responses to photostimulation. 16 of 20 Hcrt neurons showed detectable responses to photostimulation. 10 of the 16 responding neurons were tested with GABAAR blocker (SR95531), and the responses were abolished. 8 of the 10 cells were able to be used for SR95531 washout experiment. These 8 cells were plotted in the summary graph. Paired two-tailed t-test was used to test statistical significance between different conditions (n=8 cells from 4 mice; CPP/NBQX, 3.59 ± 0.99 mV vs CPP/NBQX/SR -0.03 mV ± 0.04 mV, p=0.0051, Shapiro-Wilk Normality Test, paired t-test; CPP/NBQX/SR vs CPP/NBQX (SR washing out) 1.39 ± 0.46 mV, p=0.0194,Shapiro-Wilk Normality Test, paired t-test).

These slice electrophysiology experiments suggested that ZI Lhx6-expressing neurons promote sleep by direct inhibition of Hcrt+ neurons in the LH. To verify this finding in vivo, we performed a chemical epistasis experiment, and investigated whether there was a detectable interaction between the effects of inhibiting the activity of both ZI Lhx6-expressing neurons and blocking Hcrt signaling. To do this Gi DREADD-injected mice were treated with both suvorexant [100], a hypocretin receptor antagonist, and CNO. These experiments demonstrated that suvorexant treatment could indeed reverse the effects of CNO (Figure 5.4.2), However, these data unable to determine whether the effects of CNO and suvorexant were addititve or non-additive, and could not definitively show that inhibition of Hcrt+ neurons is the only means by which Lhx6-expressing ZI neurons .

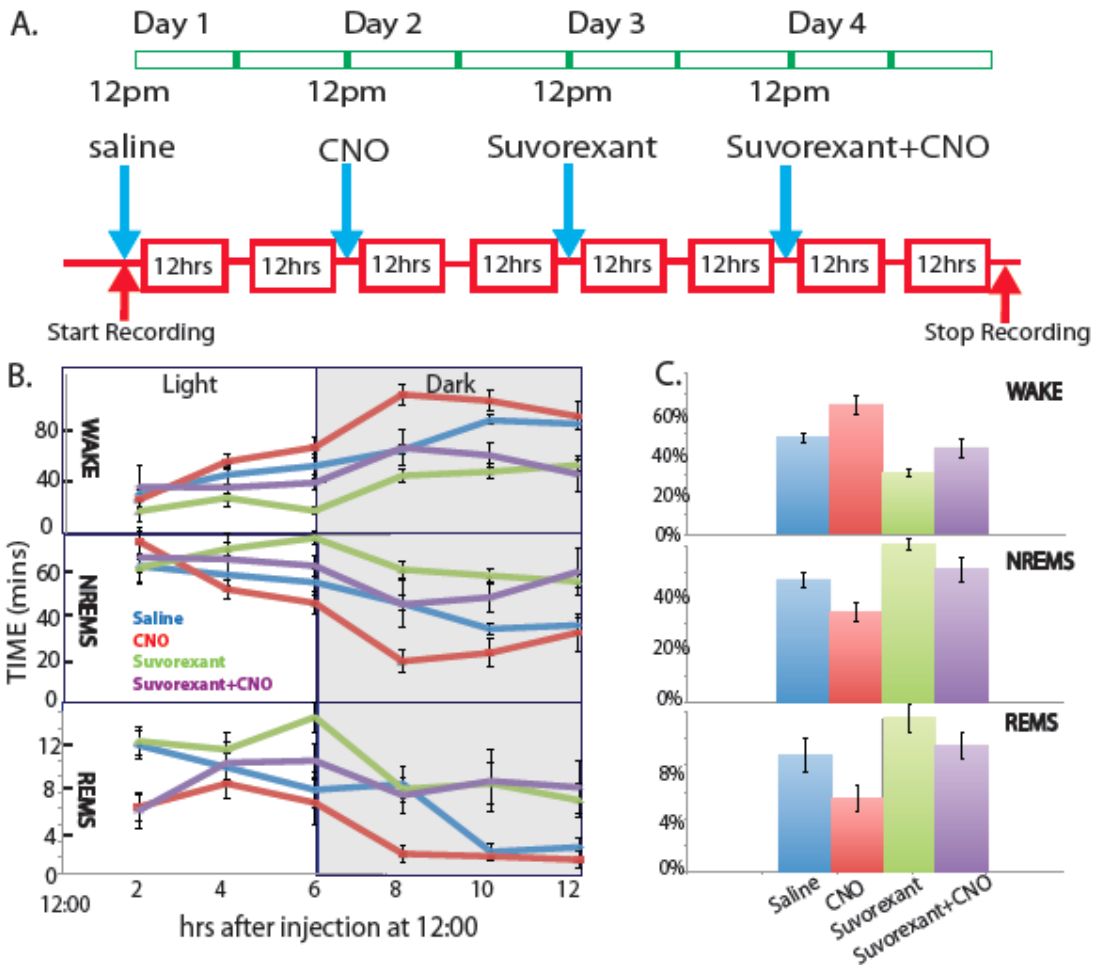

*Figure 5.4.2 Suvorexant effect on promoting sleep was canceled by DREADD-dependent inhibition of Lhx6-expressing neurons in the ZI (a) Schematics showing sleeping recording paradigm (EEG and EMG recording) with saline-, CNO, suvorexant or both-injection in hM4Di mice. Each individual mouse is assayed under the conditions indicated.(b) Schematics showing hM3Dq-mCherry virus construct and injection of virus into the ZI of Lhx6-Cre line.(c) EEG analysis showing the percentage of time spent during the 12 hour post-injection interval in wake (top), NREM sleep (middle), and REM sleep (bottom) - across ZT with saline- or CNO-injection in hM3Dq groups. * =P < 0.05, ** = P < 0.01, two-tailed paired t-test, Wilcoxon-Mann-Whitney test. N = 8 mice. (d) Graphs of EEG analysis showing amount of time in wake (top), NREM sleep (middle), and REM sleep (bottom) after injection of saline- or CNO-injection at ZT5 in hM3Dq groups. * = P < 0.05, ** = P < 0.01, two-tailed paired t-test, Wilcoxon-Mann-Whitney test. N = 8 mice. (e) Schematics showing hM4Di-mCherry virus construct and injection of virus into the ZI of Lhx6-Cre line.(f) EEG analysis showing the percentage of 12-hour interval cycle with wake (top), NREM sleep (middle), and REM sleep (bottom) with saline- or CNO-injection in hM4Di groups. * < 0.05, ** = P < 0.01, *** = P <0.001, two-tailed paired t-test, Wilcoxon-Mann-Whitney test. N = 8 mice.(g) Graphs of EEG analysis showing amount of time spent during the 12 hour post-injection interval in wake*

*(top), NREM sleep (middle), and REM sleep (bottom) after injection of saline- or CNO-injection at ZT5 in hM4Di groups. * = P < 0.05, ** = P < 0.01, two-tailed paired t-test, Wilcoxon-Mann-Whitney test. N = 8 mice.*

Chapter 6 Discussion and future work

6.1 Discussion

My thesis has focused on the study of a previously uncharacterized population of hypothalamic neurons labeled by a LIM homeodomain transcriptional factor Lhx6. Since the role of Lh6 in migration and differentiation of cortical interneurons has been extensively characterized, we started to investigate the developmental properties of Lhx6 in hypothalamus. We found substantial differences in gene expression patterns of hypothalamic and cortical Lhx6 neurons by RNA-Seq analysis. Lhx6 is essential for the development and migration of a large fraction of telencephalic interneurons [22]. In the diencephalon, however, Lhx6 is expressed in a much more restricted subset of GABAergic neurons that are not widely dispersed [76], and do not express canonical markers of telencephalic Lhx6+ interneurons, such as Pvalb and Som. Lhx6 neurons in hypothalamus do not migrate, and most importantly, Lhx6 is required for the survival of hypothalamic Lhx6 neurons, in contrast to the cortical Lhx6 is not required. The highly diverse functions of telencephalic interneurons, in contrast to the more specialized diencephalic Lhx6+ cells, are likely mediated by major differences in the organization of Lhx6-dependent transcriptional regulatory networks in both brain regions. Further characterization of the genes that guide the development and function of diencephalic Lhx6+ neurons will provide further insight into molecular pathways that can potentially be targeted for treatment of sleep disorders.

In our studies of the behavioral functions of hypothalamic Lhx6 neurons, we ultimately identified these cells as playing a central role in the promotion of sleep. We can say this is a previously unidentified subpopulation of GABAergic neurons in the ventral zona incerta (ZIv) that are distinct from previously characterized subtypes of sleep-promoting neurons. While the ZI has not previously been directly implicated in control of sleep, it is known to modulate cortical activity and behavioral arousal through direct inhibitory projections to both thalamus and cortex [76, 78]. Pvalb-expressing GABAergic neurons, the majority of neurons in the ZIv, directly inhibit sensory input to the posteromedial thalamic nucleus, and have been hypothesized to inhibit thalamocortical signaling during NREM sleep [101]. In this study, we identify GABAergic Lhx6+ ZIv neurons as a novel neuronal subtype that send descending projections to regions that contain wake-promoting neurons. Most notably, these neurons are immediately presynaptic to the wake-promoting Hcrt+ neurons of the LH, and robustly inhibit their activity. GABAergic ZIv neurons are interconnected, and receive input from wake-active neuronal populations [101, 102]. This raises the possibility that Pvalb+ and Lhx6+ ZIv neurons may coordinate their activity during wake and NREM, to separately regulate thalamocortical activity and suppress wake-active hypothalamic and midbrain neurons, respectively. Furthermore, since complete ablation of the ZI does not induce changes in sleep/wake cycles, these findings imply that other as yet unidentified wake-promoting neuronal subpopulations may exist in this structure.

6.2 Future research

Our findings demonstrate that Lhx6-expressing neurons in the hypothalamus, are GABAergic and distributed across the rostral-caudal gradient of the ZI, DMH and the PH. It is also important to note that experiments so far highlight that hypothalamic Lhx6-expressing neurons are different in both function and gene expression profile compared to cortical Lhx6-expressing neurons, as hypothalamic Lhx6-neurons do not show classical markers that define Lhx6-expressing GABAergic interneurons in the cortex. Importantly, fISH experiments highlight that there are multiple distinct subtypes of hypothalamic Lhx6-expressing neurons, even within a single structure such as the ZI, highlighting that Lhx6-expressing neurons are hypothalamus may be more heterogenous than the cortical Lhx6-expressing neurons.

To address this, it will ultimately be necessary to profile the diversity of hypothalamic Lhx6-expressing neurons using single-cell RNA-Sequencing (SC-RNA-Seq). Large-scale SC-RNASeq analysis makes it possible to profile diverse neuronal populations such as Lhx6-expressing neurons in the hypothalamus. However, given that hypothalamic Lhx6-expressing neurons only are a fraction of total number of cells in the hypothalamus, it is first important to enrich Lhx6-expressing neurons. Our Lhx6-eGFP line, which faithfully capture Lhx6-expression in the hypothalamus, will be highly useful as we can purify Lhx6-expressing neurons using FACS by enriching GFP-positive populations as previously done in bulk RNA-Seq. Although there are multiple methods of performing SC-RNASeq, our lab recently had success with using the Chromium Single Cell Solution Device (10x genomics) in the retina, and we anticipate that we will be able to apply this same method on FACS-isolated hypothalamic Lhx6-expressing neurons. Once we obtain SC-RNASeq, we could sub-categorise hypothalamic Lhx6-expressing

neurons based on its transcript expression and using specific markers [40] to identify different functional subtypes of Lhx6-expressing neurons into the ZI, DMH and PH. SC-RNASeq will not only allow us to characterize heterogeneity of Lhx6-expressing neurons but will also help us to identify molecular cues that give rises to Lhx6 neuronal diversity. With more specific markers, we can identify the potential markers which act downstream of Lhx6 in hypothalamus to control cell survival.

The presynaptic afferent to hypothalamic Lhx6 neurons are unknown. Since melanin-hormone concentrating (MCH) neurons have been reported to receive presynaptic innervation from vlPAG [103], we plan to conduct Callaway monosynaptic tracing [104] of hypothalamic Lhx6 neurons by stererotaxically injecting helper AAV genes and rabies virus into Lhx6-Cre mice. We expected to see that wake-promoting monoaminergic neurons in midbrain and brainstem send projections to hypothalamic Lhx6 neurons (HLINs), which is consistent with the mutual inhibitive "flip-flop" theory for sleep/wake circuitry.

Since we have been able to demonstrate that HLINs are necessary for initiation and/or maintenance of REM sleep, we will next determine if these effects are mediated by descending inhibitory projections to the midbrain nucleic such as the vlPAG and DR nucleus. To do this, we will take advantage of a recently developed inhibitory DREADD variant that is selectively targeted to axonal processes and synaptic terminals [105]. We will selectively induce expression of this inhibitory DREADD in HLINs using bilateral stereotactic injections of AAV9-CMV-flex-hM4Di-neurexin-HA [105]. In addition to EEG recording devices, we will also implant a cannula directly immediately dorsal to the midbrain cerebral aqueduct as described [105], allowing for direct drug delivery to both

vlPAG and DR. Following initial infection, we will then deliver either CNO or saline through the cannula during the middle of the light phase, and determine whether CNO infusion leads to a disruption of REM sleep that is comparable to that observed with conventional inhibitory DREADDs. To demonstrate the specificity of these effects, we will determine if they can be reversed by simultaneous infusion of bicuculline as described [106], which will trigger activation of postsynaptic GABAA receptors even following inhibition of HLIN activity. Infection efficiency and synaptic localization of inhibitory DREADDs will be determined by immunofluorescence for the HA epitope tag as described [105].

References:

[1] Pawson, T. & Nash, P. Assembly of cell regulatory systems through protein interaction domains. Science 300, 445–452 (2003).

[2] Schmeichel, K. L. & Beckerle, M. C. The LIM domain is a modular protein-binding interface. Cell 79, 211–219 (1994).

[3] Julie L. Kadrmas & Mary C. Beckerle. The LIM domain: from the cytoskeleton to the nucleus. Nat Rev Mol Cell Biol. 5(11):920-31 (2004).

[4] Michelsen, J. W. et al. Mutational analysis of the metal sites in an LIM domain. J. Biol. Chem. 269, 11108–11113 (1994).

[5] Zhao, Y., Flandin, P., Long, J.E., Cuesta, M.D., Westphal, H., and Rubenstein, J.L. Distinct molecular pathways for development of telencephalic interneuron subtypes revealed through analysis of Lhx6 mutants. J. Comp.Neurol. 510, 79–99 (2008).

[6] Kimura N, Ueno M, Nakashima K, Taga T. A brain region-specific gene product Lhx6.1 interacts with Ldb1 through tandem LIM-domains. J Biochem. 126:180-7. (1999)

[7] Somogyi P, Klausberger T. Defined types of cortical interneurone structure space and spike timing in the hippocampus. J Physiol. 562:9-26 (2005).

[8] Petilla Interneuron Nomenclature Group, Ascoli GA, Alonso-Nanclares L, Anderson SA, Barrionuevo G, Benavides-Piccione R, Burkhalter A, Buzsáki G, Cauli B, Defelipe J, Fairén A, Feldmeyer D, Fishell G, Fregnac Y, Freund TF, Gardner D, Gardner EP, Goldberg JH, Helmstaedter M, Hestrin S, Karube F, Kisvárday ZF, Lambolez B, Lewis

DA, Marin O, Markram H, Muñoz A, Packer A, Petersen CC, Rockland KS, Rossier J, Rudy B, Somogyi P, Staiger JF, Tamas G, Thomson AM, Toledo-Rodriguez M, Wang Y, West DC, Yuste R. Petilla terminology: nomenclature of features of GABAergic interneurons of the cerebral cortex. Nat Rev Neurosci. 9(7):557-68 (2008).

[9] Kawaguchi Y, Kubota Y . GABAergic cell subtypes and their synaptic

connections in rat frontal cortex. Cereb Cortex 7:476 –486 (1997).

[10] Markram H, Toledo-Rodriguez M, Wang Y, Gupta A, Silberberg G, Wu C,

Monyer H. Interneurons of the neocortical inhibitory system.

Nat Rev Neurosci 5:793–807 (2004).

[11] Wonders CP, Anderson SA. The origin and specification of cortical interneurons. Nat Rev Neurosci. 7:687–696 (2006).

[12] Rudy B, Fishell G, Lee S, Hjerling-Leffler J. Three groups of interneurons account for nearly 100% of neocortical GABAergic neurons. Dev Neurobiol. 71:45–61 (2011).

[13] Welagen J, Anderson S. Origins of neocortical interneurons in mice. Dev Neurobiol. 71:10–17 (2011).

[14] de Carlos JA, Lopez-Mascaraque L, Valverde F. Dynamics of cell migration

from the lateral ganglionic eminence in the rat. J Neurosci

16:6146 –6156 (1996).

[15] Anderson SA, Eisenstat DD, Shi L, Rubenstein JL.Interneuron migration

from basal forebrain to neocortex: dependence on Dlx genes.

Science 278:474 –476 (1997).

[16] Tamamaki N, Fujimori KE, Takauji R. Origin and route of tangentially

migrating neurons in the developing neocortical intermediate zone.

J Neurosci 17:8313–8323 (1997).

[17] Lavdas AA, Grigoriou M, Pachnis V, Parnavelas JG. The medial ganglionic

eminence gives rise to a population of early neurons in the developing

cerebral cortex. J Neurosci 19:7881–7888 (1999).

[18] Marin O, Rubenstein JL. Cell migration in the forebrain. Annu Rev

Neurosci 26:441–483 (2003).

[19] Pleasure SJ, Anderson S, Hevner R, Bagri A, Marin O, Lowenstein DH,

Rubenstein JL. Cell migration from the ganglionic eminences is

required for the development of hippocampal GABAergic interneurons.

Neuron 28:727–740 (2000).

[20] Valcanis H, Tan SS. Layer specification of transplanted interneurons

in developing mouse neocortex. J Neurosci 23:5113–5122 (2003).

[21] Sussel L, Marin O, Kimura S, Rubenstein JL. Loss of Nkx2.1 homeobox gene

function results in a ventral to dorsal molecular respecification within the basal

telencephalon: evidence for a transformation of the pallidum into the striatum. Development.126:3359–3370 (1999).

[22] Liodis P, Denaxa M, Grigoriou M, Akufo-Addo C, Yanagawa Y, Pachnis V. Lhx6 activity is required for the normal migration and specification of cortical interneuron subtypes. J Neurosci. 27:3078–3089 (2007).

[23] Du T, Xu Q, Ocbina PJ, Anderson SA. NKX2.1 specifies cortical interneuron fate by activating Lhx6. Development. 135:1559–1567 (2008).

[24] Kepecs A., Fishell G.,. Interneuron Cell Types: Fit to form and formed to fit. Nature. 505(7483): 318–326 (2014).

[25] Liodis P, Denaxa M, Grigoriou M, Akufo-Addo C, Yanagawa Y, Pachnis V. Lhx6 activity is required for the normal migration and specification of cortical interneuron subtypes. J Neurosci. 27(12):3078-89 (2007).

[26] Somogyi P, Klausberger T. Defined types of cortical interneurone

structure space and spike timing in the hippocampus. J Physiol (Lond)

562:9 –26 (2005).

[27] Fogarty M, Grist M, Gelman D, Marin O, Pachnis V, Kessaris N. Spatial genetic patterning of the embryonic neuroepithelium generates GABAergic interneuron diversity in the adult cortex. J Neurosci. 27:10935–10946 (2007).

[28] Rudy B, Fishell G, Lee S, Hjerling-Leffler J. Three groups of interneurons account for nearly 100% of neocortical GABAergic neurons. Dev Neurobiol. 71:45–61 (2011).

[29] Denaxa M, et al. Maturation-promoting activity of SATB1 in MGE-derived cortical interneurons. Cell Rep. 2:1351–1362 (2012).

[30] Close J, et al. Satb1 Is an Activity-Modulated Transcription Factor Required for the Terminal Differentiation and Connectivity of Medial Ganglionic Eminence-Derived Cortical Interneurons. Journal of Neuroscience. 32:17690–17705 (2012).

[31] Zhao Y, Flandin P, Long JE, Cuesta MD, Westphal H, Rubenstein JL. Distinct molecular pathways for development of telencephalic interneuron subtypes revealed through analysis of Lhx6 mutants. J Comp Neurol. 510:79–99 (2008).

[32] Alifragis P, Liapi A, Parnavelas JG. Lhx6 regulates the migration of cortical interneurons from the ventral telencephalon but does not specify their GABA phenotype. J Neurosci. 24:5643–5648 (2004).

[33] Michaud JL, Rosenquist T, May NR, Fan CM. Development of neuroendocrine lineages requires the bHLH-PAS transcription factor SIM1. Genes Dev. 12:3264–3275 (1998).

[34]. Schonemann MD, et al. Development and survival of the endocrine hypothalamus and posterior pituitary gland requires the neuronal POU domain factor Brn-2. Genes Dev. 9:3122–3135 (1995).

[35]. Labosky PA, et al. The winged helix gene, Mf3, is required for normal development of the diencephalon and midbrain, postnatal growth and the milk-ejection reflex. Development. 124:1263–1274 (1997).

[36]. Wehr R, Mansouri A, de Maeyer T, Gruss P. Fkh5-deficient mice show dysgenesis in the caudal midbrain and hypothalamic mammillary body. Development. 124:4447–4456 (1997).

[37]. Davis AM, et al. Loss of steroidogenic factor 1 alters cellular topography in the mouse ventromedial nucleus of the hypothalamus. J Neurobiol. 60:424–436 (2004).

[38]. Acampora D, et al. Progressive impairment of developing neuroendocrine cell lineages in the hypothalamus of mice lacking the Orthopedia gene. Genes Dev. 13:2787–2800 (1999).

[39]. Goshu E, et al. Sim2 contributes to neuroendocrine hormone gene expression in the anterior hypothalamus. Mol Endocrinol. 18:1251–1262 (2004).

[40] Shimogori T, Lee DA, Miranda-Angulo A, Yang Y, Wang H, Jiang L, Yoshida AC, Kataoka A, Mashiko H, Avetisyan M, Qi L, Qian J, Blackshaw S. A genomic atlas of mouse hypothalamic development. Nat Neurosci. 13(6):767-75 (2010).

[41] Dalal J, Roh JH, Maloney SE, Akuffo A, Shah S, Yuan H, Wamsley B, Jones WB, de Guzman Strong C, Gray PA, Holtzman DM, Heintz N, Dougherty JD. Translational profiling of hypocretin neurons identifies candidate molecules for sleep regulation. Genes Dev. 27(5):565-78 (2013).

[42] Liu J, Merkle FT, Gandhi AV, Gagnon JA, Woods IG, Chiu CN, Shimogori T, Schier AF, Prober DA. Evolutionarily conserved regulation of hypocretin neuron specification by Lhx9. Development. 142(6):1113-24 (2015).

[43] Bedont JL, LeGates TA, Slat EA, Byerly MS, Wang H, Hu J, Rupp AC, Qian J, Wong GW, Herzog ED, Hattar S, Blackshaw S. Lhx1 controls terminal differentiation and circadian function of the suprachiasmatic nucleus. Cell Rep. 7(3):609-22 (2014).

[44] Bedont JL, LeGates TA, Buhr E, Bathini A, Ling JP, Bell B, Wu MN, Wong PC, Van Gelder RN, Mongrain V, Hattar S, Blackshaw S. An LHX1-Regulated Transcriptional Network Controls Sleep/Wake Coupling and Thermal Resistance of the Central Circadian Clockworks. Curr Biol. 27(1):128-136 (2017).

[45] Weber, F. & Dan, Y. Circuit-based interrogation of sleep control. Nature. 538, 51-59 (2016).

[46] Aserinsky, E. & Kleitman, N. Regularly occurring periods of eye motility, and concomitant phenomena, during sleep. Science. 118, 273–274 (1953).

[47] Takahashi K, Kayama Y, Lin JS, Sakai K. Locus Coeruleus Neuronal Activity During the Sleep-Waking Cycle in Mice. Neuroscience 2010.

[48] Wright KP, Jr, Badia P, Wauquier A. Topographical and temporal patterns of brain activity during the transition from wakefulness to sleep. Sleep. 18:880–889 (1995).

[49] Saper CB, Fuller PM, Pedersen NP, Lu J, Scammell TE. Sleep state switching. Neuron. 68(6):1023-42 (2010).

[50] Hallanger AE, Levey AI, Lee HJ, Rye DB, Wainer BH. The origins of cholinergic and other subcortical afferents to the thalamus in the rat. J Comp Neurol. 262:105–124 (1987).

[51] Satoh K, Fibiger HC. Cholinergic neurons of the laterodorsal tegmental nucleus: efferent and afferent connections. J Comp Neurol. 253:277–302 (1986).

[52] El Mansari M, Sakai K, Jouvet M. Unitary characteristics of presumptive cholinergic tegmental neurons during the sleep-waking cycle in freely moving cats. Exp Brain Res. 76:519–529 (1989).

[53] Steriade M, McCormick DA, Sejnowski TJ. Thalamocortical oscillations in the sleeping and aroused brain. Science. 262:679–685 (1993).

[54] Sherin JE, Shiromani PJ, McCarley RW, Saper CB. Activation of ventrolateral preoptic neurons during sleep. Science. 271:216–219 (1996).

[55] Sherin JE, Elmquist JK, Torrealba F, Saper CB. Innervation of histaminergic tuberomammillary neurons by GABAergic and galaninergic neurons in the ventrolateral preoptic nucleus of the rat. J Neurosci. 18:4705–4721 (1998).

[56] Chou TC, Bjorkum AA, Gaus SE, Lu J, Scammell TE, Saper CB. Afferents to the ventrolateral preoptic nucleus. J Neurosci. 22:977–990 (2002).

[57] Lu J, Jhou TC, Saper CB. Identification of wake-active dopaminergic neurons in the ventral periaqueductal gray matter. J Neurosci. 26:193–202 (2006).

[58] Saper CB, Chou TC, Scammell TE. The sleep switch: hypothalamic control of sleep and wakefulness. Trends Neurosci. 24(12):726-31 (2001).

[59] Saper CB, Scammell TE, Lu J. Hypothalamic regulation of sleep and circadian rhythms. Nature. 437,1257-63 (2005).

[60] Von Economo, C. Sleep as a Problem of Localization. Journ of Nerv. and Ment. Dis., 71:249-259 (1930).

[61] Wilson, S.A.K. Modern problems in neurology (Edward Arnold, London, 1928).

[62] Sakurai T, Amemiya A, Ishii M, Matsuzaki I, Chemelli RM, Tanaka H, Williams SC, Richardson JA, Kozlowski GP, Wilson S, Arch JR, Buckingham RE, Haynes AC, Carr SA, Annan RS, McNulty DE, Liu WS, Terrett JA, Elshourbagy NA, Bergsma DJ, Yanagisawa M. Orexins and orexin receptors: a family of hypothalamic neuropeptides and G protein-coupled receptors that regulate feeding behavior. Cell. 92(4):573-85 (1998).

[63] de Lecea L, Kilduff TS, Peyron C, Gao X, Foye PE, Danielson PE, Fukuhara C, Battenberg EL, Gautvik VT, Bartlett FS 2nd, Frankel WN, van den Pol AN, Bloom FE, Gautvik KM, Sutcliffe JG. The hypocretins: hypothalamus-specific peptides with neuroexcitatory activity. Proc Natl Acad Sci U S A. 95(1):322-7 (1998).

[64] Lin L, Faraco J, Li R, Kadotani H, Rogers W, Lin X, Qiu X, de Jong PJ, Nishino S, Mignot E. The sleep disorder canine narcolepsy is caused by a mutation in the hypocretin (orexin) receptor 2 gene. Cell. 98(3):365-76 (1999).

[65] Hassani, O. K., Henny, P., Lee, M. G. & Jones, B. E. GABAergic neurons intermingled with orexin and MCH neurons in the lateral hypothalamus discharge maximally during sleep. Eur. J. Neurosci. 32, 448–457 (2010).

[66] Jego, S. et al. Optogenetic identification of a rapid eye movement sleep modulatory circuit in the hypothalamus. Nat. Neurosci. 16, 1637–1643 (2013).

[67] Chowdhury, S. & Yamanaka, A. Optogenetic activation of serotonergic terminals facilitates GABAergic inhibitory input to orexin/hypocretin neurons. Sci. Rep. 6, 36039 (2016).

[68] Saito, Y. C. et al. GABAergic neurons in the preoptic area send direct inhibitory projections to orexin neurons. Front. Neural Circuits. 7, 192 (2013).

[69] Burt J, Alberto CO, Parsons MP, Hirasawa M. Local network regulation of orexin neurons in the lateral hypothalamus. Am J Physiol Regul Integr Comp Physiol. 301(3):R572-80 (2011).

[70] Li Y, Gao XB, Sakurai T, van Den Pol AN. Hypocretin/orexin excites hypocretin neurons via a local glutamate neuron-A potential mechanism for orchestrating the hypothalamic arousal system. Neuron 36: 1169–1181 (2002).

[71] Yamanaka A, Tabuchi S, Tsunematsu T, Fukazawa Y, Tominaga M. Orexin directly excites orexin neurons through orexin 2 receptor. J Neurosci 30: 12642–12652 (2010).

[72] Hassani, O. K., Lee, M. G. & Jones, B. E. Melanin-concentrating hormone neurons discharge in a reciprocal manner to orexin neurons across the sleep-wake cycle. Proc. Natl Acad. Sci. USA 106, 2418–2422 (2009)

[73] Tsunematsu, T. et al. Optogenetic manipulation of activity and temporally controlled cell-specific ablation reveal a role for MCH neurons in sleep/wake regulation. J. Neurosci. 34, 6896–6909 (2014)

[74] Konadhode, R. R. et al. Optogenetic stimulation of MCH neurons increases sleep. J. Neurosci. 33, 10257–10263 (2013)

[75] Rao, Y. et al. Regulation of synaptic efficacy in hypocretin/orexin-containing neurons by melanin concentrating hormone in the lateral hypothalamus. J. Neurosci. 28, 9101–9110 (2008).

[76] Lin, C. S., Nicolelis, M. A., Schneider, J. S. & Chapin, J. K. A major direct GABAergic pathway from zona incerta to neocortex. Science 248, 1553-1556 (1990).

[77] Mitrofanis, J. Some certainty for the "zone of uncertainty"? Exploring the function of the zona incerta. Neuroscience 130, 1-15 (2005).

[78] Liu, J. et al. Frequency-selective control of cortical and subcortical networks by central thalamus. Elife 4, e09215 (2015).

[79] Liu, M. et al. Orexin gene transfer into zona incerta neurons suppresses muscle paralysis in narcoleptic mice. J. Neurosci. 31, 6028-6040 (2011).

[80] Jurkowlaniec, E., Trojniar, W. & Tokarski, J. The EEG activity after lesions of the diencephalic part of the zona incerta in rats. Acta Physiol. Pol. 41, 85-97 (1990).

[81] Gong, S. et al. A gene expression atlas of the central nervous system based on bacterial artificial chromosomes. Nature 425, 917-925 (2003).

[82] van den Pol, A N et al. Hypocretin (orexin) enhances neuron activity and cell synchrony in developing mouse GFP-expressing locus coeruleus. J. Physiol. 541, 169-185 (2002).

[83] Fogarty, M. et al. Spatial genetic patterning of the embryonic neuroepithelium generates GABAergic interneuron diversity in the adult cortex. J. Neurosci. 27, 10935-10946 (2007).

[84] Taniguchi, H. et al. A resource of Cre driver lines for genetic targeting of GABAergic neurons in cerebral cortex. Neuron 71, 995-1013 (2011).

[85] Humphreys, B. D. et al. Fate tracing reveals the pericyte and not epithelial origin of myofibroblasts in kidney fibrosis. Am. J. Pathol. 176, 85-97 (2010).

[86] Rodriguez, C. I. et al. High-efficiency deleter mice show that FLPe is an alternative to Cre-loxP. Nat. Genet. 25, 139-140 (2000).

[87] Lee, J. H. et al. Global and local fMRI signals driven by neurons defined optogenetically by type and wiring. Nature 465, 788-792 (2010).

[88] Armbruster, B. N., Li, X., Pausch, M. H., Herlitze, S. & Roth, B. L. Evolving the lock to fit the key to create a family of G protein-coupled receptors potently activated by an inert ligand. Proc. Natl. Acad. Sci. U. S. A. 104, 5163-5168 (2007).

[89] Lee, D. A. et al. Tanycytes of the hypothalamic median eminence form a diet-responsive neurogenic niche. Nat. Neurosci. 15, 700-702 (2012).

[90] Blackshaw, S. et al. Genomic analysis of mouse retinal development. PLoS Biol. 2, E247 (2004).

[91] Bader, C., MacLeish, P., and Schwartz, E.: Responses to Light of Solitary Rod Photoreceptors Isolated From Tiger Salamander Retina ,Proc Natl Acad Sci U S A 75, 3507 (1978).

[92] Rudy B1, Fishell G, Lee S, Hjerling-Leffler J. Three groups of interneurons account for nearly 100% of neocortical GABAergic neurons. Dev Neurobiol. 71(1):45-61 (2011).

[93] Belgorosky A, Guercio G, Pepe C, Saraco N, Rivarola MA. Genetic and clinical spectrum of aromatase deficiency in infancy, childhood and adolescence. Horm Res. 72(6):321-30 (2009).

[94] Veasey, S. C., Yeou-Jey, H., Thayer, P. & Fenik, P. Murine Multiple Sleep Latency Test: phenotyping sleep propensity in mice. Sleep 27, 388-393 (2004).

[95] Salvatierra, J. et al. The LIM homeodomain factor Lhx2 is required for hypothalamic tanycyte specification and differentiation. J. Neurosci. 34, 16809-16820 (2014).

[96] Armbruster, B. N., Li, X., Pausch, M. H., Herlitze, S. & Roth, B. L. Evolving the lock to fit the key to create a family of G protein-coupled receptors potently activated by an inert ligand. Proc. Natl. Acad. Sci. U. S. A. 104, 5163-5168 (2007).

[97] Hayashi, Y. et al. Cells of a common developmental origin regulate REM/non-REM sleep and wakefulness in mice. Science 350, 957-961 (2015).

[98] Weber, F. et al. Control of REM sleep by ventral medulla GABAergic neurons. Nature 526, 435-438 (2015).

[99] Venner, A., Anaclet, C., Broadhurst, R. Y., Saper, C. B. & Fuller, P. M. A Novel Population of Wake-Promoting GABAergic Neurons in the Ventral Lateral Hypothalamus. Curr. Biol. 26, 2137-2143 (2016).

[100] Etori K, Saito YC, Tsujino N, Sakurai T. Effects of a newly developed potent orexin-2 receptor-selective antagonist, compound 1 m, on sleep/wakefulness states in mice. Front Neurosci. 8:8 (2014).

[101] Trageser, J. C. et al. State-dependent gating of sensory inputs by zona incerta. J. Neurophysiol. 96, 1456-1463 (2006).

[102] Herbert, H., Klepper, A. & Ostwald, J. Afferent and efferent connections of the ventrolateral tegmental area in the rat. Anat. Embryol. (Berl) 196, 235-259 (1997).

[103] González JA, Iordanidou P, Strom M, Adamantidis A, Burdakov D. Awake dynamics and brain-wide direct inputs of hypothalamic MCH and orexin networks. Nat Commun. 22;7:11395 (2016).

[104] Wall NR, Wickersham IR, Cetin A, De La Parra M, Callaway EM. Monosynaptic circuit tracing in vivo through Cre-dependent targeting and complementation of modified rabies virus. Proc Natl Acad Sci U S A. 107(50):21848-53 (2010).

[105] Stachniak, T.J., A. Ghosh, and S.M. Sternson, Chemogenetic synaptic silencing of neural circuits localizes a hypothalamus-->midbrain pathway for feeding behavior. Neuron. 82(4): 797-808 (2014).

[106] Vanini, G., et al., GABAergic processes in the mesencephalic tegmentum modulate the occurrence of active (rapid eye movement) sleep in guinea pigs. Neuroscience. 145(3): p. 1157-67 (2007).

[107] Golden JA, Cepko CL. Clones in the chick diencephalon contain multiple cell types and siblings are widely dispersed. Development.122(1):65-78 (1996).

[108] Arnold-Aldea SA1, Cepko CL. Dispersion patterns of clonally related cells during development of the hypothalamus. Dev Biol. 173(1):148-61 (1996).

Curriculum Vitae

Name: Kai Liu
Date of Birth: July 21st, 1983
Place of Birth: Beijing, China
Email: vincentliuk@gmail.com

Professional Summary

PhD in **Neuroscience** and M.S.E in **Computer Science** at Johns Hopkins University.
• **neuroscience:** Intensive research experience on identifying and characterizing a novel **neuronal circuitry** (first-author paper to be published at **Nature)**
• Investigated neural decoding and encoding mechanisms on somatosensory cortex and hippocampus.
• **computational neuroscience**: Developed and applied a mathematical state space model to analyze brain activity data.
• **machine learning** expert with more than 4-years' experience on various domains, including natural language processing, image recognition, speech recognition, neural decoding and encoding and signal processing. Wrote codes to implement standard machine learning algorithms.
• Specialized in **deep learning** (Wrote a deep learning package shared on Github)

Award

2017 The 40th JHMI Mette Strand Research Young Investigator Award.

Areas of Expertise and Skills

• Neuroscience: Systems Neuroscience, Extracellular Electrophysiology, Virus Tracing of Neural Circuit, Behavior Analysis, EEG, RNA-sequencing and Biostatistics Data Analysis, Histology.
• Machine Learning: linear regression, linear discriminant analysis, support vector machine, K-means, K-nearest neighbors, gaussian mixture model, naive bayes, kalman filter, hidden markov model, PCA, sparse coding, ICA, CCA, reinforcement learning etc.
• Deep Learning: unsupervised deep InfoMax, deep belief neural nets, recurrent neural networks(RNN), LSTM, Convolutional neural networks (CNN), denoised autoencoder, deep canonical correlation analysis.
• Optimiazation: Line search (gradient descent, LBFGS), stochastic gradient descent (momentum, Adagrad, RMSprop), dropout, KKT conditions.
• Skills: Java, C++, Python, R, MATLAB, scikit, TensorFlow

Research projects

2010~current Johns Hopkins School Of Medicine, Department of Neuroscience

• Developed and engineered tools to study the function of neuronal circuitry in behaving animals

• Discovered and characterized a novel neuronal circuitry responsible for modulating sleep.

2012~current Johns Hopkins University, Department of Computer Science

• Time Series analysis- developed a state-space model with constrained kalman filter-based EM algorithm for time series analysis of whole brain activity data (contribution: coding and experiments).

• Deep Learning 1- developed a Caffe-like C++ deep learning package – DeepIntelligence, shared on Github, including modules of RNN, LSTM, CNN, RBM, AutoEncoder, Multigraph-Reinforcement Learning (contribution: coding and experiments).

• Deep Learning 2- applied and extended deep canonical correlation analysis (DCCA) and semi-CCA on a cross-lingual document classification task by learning interlingual representations for English and Spanish, improving document classification accuracy by 5~8% in F1 score. (contribution: code extending and experiments).

2010~current Johns Hopkins School of Medicine, Department of Neuroscience
• Developed and engineered tools to study the function of neuronal circuitry of animal behavior
2009 Rotation Student at Johns Hopkins System Neuroscience
• Applied a support vector machine classifier (SVM) classifier to successfully tuning populational neural decoding patterns from primates somatosentory cortex.
2007~2009 Research Assistant at Tsinghua University Neural Engieering Lab
• Conducted memory synchrony analysis in hippocampus firing patterns by phase-locking signal processing methods.

Education

2017 Ph.D in Neuroscience. Johns Hopkins School of Medicine - Baltimore, MD
2015 M.S.E in Computer Sciences. Johns Hopkins University - Baltimore, MD
2009 M.S.E of Engineering for Robotics. Institute of Automation, Chinese Academy of Sciences - Beijing, China.
2005 B.S. in Physics and Electronic Engineering (double degree) Peking University - Beijing, China.

Publications

1. **K. Liu,** S. Zhang, J. Kim, DW. Kim, M. Denaxa, HC. Bao, E. Kim, C. Liu, V. Pachinis, S. Hattar, J. Song, S. Brown, and S. Blackshaw. Lhx6-positive neurons of the zona incerta promote sleep by local inhibition of wake-promoting hypocretin neurons. (*Nature,* under review)
2. SJ. Chen**, K. Liu,** YG. Yang, YT. Xu, S. Lee, M. Lindquist, B.S. Caffo, J.T. Vogelstein. An M-Estimator for Reduced-Rank System Identification. (Accepted by *Pattern Recognition Letters*)
3. **K. Liu**, L. Song, S. Blackshaw, A novel analytic tool to detect contaminants in RNA-sequencing analysis of FACS-isolated neurons. (submitting to *bioRxiv*).
4. **K. Liu**, KN. Xie, ZM. Qiao, SK. Gao, B. Hong, Impaired neural coordination in hippocampus of diabetic rats. *Acta physiologica Sinica*. 2009,61(5): 417-423.
5. ZM. Qiao, K. Xie, **K. Liu,** G. Li, Decreased neuronal bursting and phase synchrony in the hippocampus of streptozotocin diabetic rats. *J Diabetes Res*. 2014, July.

Conference Presentations

Oral Presentation at the 2nd Annual Johns Hopkins University *Sleep and Circadian Research Conference, July 27th, 2016.*

K. Liu, S.Zhang, S.Hattar, S.Blackshaw. Hypothalamic Lhx6-positive neurons regulate REM sleep. *Janelia Conference 'hypothalamic circuits for control of survival behaviors'*, Ashburn, VA. Sep 27th~30th, 2015.

K. Liu, Applications of Semi-supervised CCA and Deep CCA in cross-lingual projection for documents classification. *2015 Amazon Graduate Research symposium.*

K. Liu, YG. Yang, SJ. Chen, J.T.Vogelstein. Functional structure analysis of whole brain activity by a sparse high dimensional state-space model. *Janelia Conference '**Big data in neuroscience:** Emerging tools for acquisition and interpretation of whole-brain functional data'*, Ashburn, VA. Nov, 1st~4th, 2015.

K. Liu, H. Wang, S. Blackshaw, Control of hypothalamic neuronal specification and survival by the LIM homeodomain factor Lhx6. *Society for Neuroscience conference*, Washington DC. Nov. 2014.

ZM.Qiao, **K.Liu**, K.Xie, S.Gao, B.Hong. In vivo study of temporal firing pattern of hippocampal neuron in diabetic rat. *Society for Neuroscience conference*, Washington DC. Nov. 2008.

Leadership

Chair on Janelia conference *'hypothalamic circuits for control of survival behaviors',* session for Circadian/Sleep-PartIII. Ashburn, VA. Sep 27th~30th, 2015.

Co-founder and Vice President, Baltimore Chinese A+ Scholar Association. Baltimore, MD. Sep 2012 – Oct 2013.

• Initiated and founded an organization for scientific and social communication among visiting scholars and physicians.

• Organized meetings and social events for over 200 visiting scholars in Baltimore and DC area.

Mentoring, Johns Hopkins School of Medicine. Sep 2009 – present.

• More than two years mentoring junior postdoc, graduate students and undergrad students for neuroscience research in the lab.

Teaching Assistant, Neuroanatomy course for Johns Hopkins medical students. Johns Hopkins University School of Medicine. Feb - Jun 2013.